NSIRC 2020 LIVE

THE ONLINE ANNUAL CONFERENCE

23 JULY 2020

nsirc

ENQUIRIES@NSIRC.CO.UK
+44 (0) 1223 899 000
NSIRC.COM

WELCOME TO NSIRC 2020 LIVE

Welcome to NSIRC 2020 Live – showcasing postgraduate study at the National Structural Integrity Research Centre

NSIRC is a postgraduate education and research centre established in 2012 to train over 500 postgraduate qualified engineers and employ 61 professionals in its first ten years.

With the world experiencing unprecedented, challenging times in the light of the Covid-19 pandemic, and the ongoing need for social distancing measures, we are delighted to still be able to bring you the NSIRC Annual Conference this year.

As you may have noticed from our pre-event communications, we took the decision quite early on to run the conference virtually for 2020, hence the new name! This means we can continue to share with you the first-class research and development being undertaken by our students, over 30 of whom will be presenting their work during the conference. In addition, I would like to thank our keynote speakers who kindly agreed to join us for this virtual experience; their support being invaluable in providing our audience with a rich and varied conference experience this year.

I am pleased to report that NSIRC continues to flourish, with all of our students now studying remotely, and is outperforming its targets to date and making significant strides towards its long-term goals. Our major achievements include:

- Providing the opportunity for 280 postgraduate research students to work at a state-of-the-art facility to enhance their knowledge and make scientific breakthroughs.
- Creating 100 new jobs in the engineering and technology sectors.
- Internationalising through partnerships with universities in Belgium, The Netherlands, Denmark, Lithuania, Malaysia, South Korea, China and Singapore.
- Increasing our network of academic partners via signed agreements with more than 40 universities.
- Promoting the inclusion of underrepresented communities in engineering. More than 30% of NSIRC PhD students are female, compared to a UK engineering workforce representation of 9%.
- The completion of five cohorts of MSc in Structural Integrity (Asset Reliability Management) students and two groups of MSc in Oil and Gas Engineering students at Brunel University London, with a further two anticipated in the summer of this year.

- The first students graduating from the MSc/Executive Apprenticeship in Engineering Leadership and Management with Aston University by the end of 2019. A further intake is planned for November 2020.
- Three additional Masters' courses commencing in January 2021: MSc in Artificial Intelligence, MSc in Lightweight Structures Impact Engineering and Masters of Business Administration (also available as an Executive Apprenticeship).
- A 100% employment rate for PhD students within one year of graduating.

NSIRC's core ambition is to advance fundamental research with real world applications in industry. It is, therefore, rewarding to see many of our students' work being developed further and contributing to higher Technology Readiness Level (TRL) applications in global safety.

Our continuous improvement and ongoing success has been assured by the effort and dedication of the NSIRC, TWI and university staff, and the support of our sponsors. I would like to express my sincere gratitude to everyone involved in developing NSIRC as the international research centre of choice for structural integrity.

Lastly, a very warm welcome to this first virtual conference: NSIRC2020 Live.

Tat-Hean

Professor Tat-Hean Gan
NSIRC Director
TWI Director, Innovation & Skills

Brunel University London

Successfully bridging the gap between research and industry

Brunel University London delivers world-leading research focused on areas in which we can integrate academic rigour with the needs of governments, industry and the not-for-profit sector, delivering creative solutions to global challenges and bringing economic, social and cultural benefit.

With world-class facilities and exceptional engineering capability Brunel has invested heavily in the development of research capability in materials and manufacturing including metal casting and processing as well as precision and additive manufacturing.

Brunel has a long history of collaboration with TWI, leading to the establishment of the Brunel Innovation Centre (BIC) in 2009. Then the National Structural Integrity Research Centre (NSIRC) in 2012, with Brunel receiving £15M of funding from HEFCE for its creation. Most recently establishing a second innovation centre, the Brunel Composite Centre (BCC), in 2016.

Research at Brunel is carried out within the Institute of Materials and Manufacturing, comprising the following area of expertise:

- Structural Integrity
- Materials Characterisation and Processing
- Liquid Metal Engineering
- Micro-Nano Manufacturing
- Design for Sustainable Manufacturing

Since 2014 over 50 Brunel PhD students have studied at NSIRC on a diverse range of topics including structural health monitoring, damage detection, ultrasound, fatigue and fracture, joining and additive manufacturing. The students are funded from different sources, including EPSRC ICASE, Lloyd's Register Foundation, BIC and other Brunel/TWI collaborations.

We also deliver unique, industry-focused MSc courses, of which every aspect is undertaken at Granta Park, the Cambridgeshire home of NSIRC.

www.brunel.ac.uk/research

THANK YOU TO OUR NSIRC 2020 LIVE SPONSORS

We would like to sincerely thank all our sponsors of NSIRC 2020 LIVE. Without their support, our annual conference would not have been possible.

Lloyd's Register Foundation · TWI · bp

University of Hertfordshire UH · University of Bedfordshire · University of Essex

INNVOTEK · Brunel University London · UNIVERSITY OF LEICESTER

Research Institute Future Transport and Cities · Coventry University · floteks

İletişim Yazılım Smart Factory Solutions · jackweld · HILTI

α e-technology · ASSIST Innovative Minds · IOM³

ETS · BUSİAD · SUNDANCE

Marshall · Malvern Panalytical

PM Life · GAIA Projects · Warsaw University of Technology

NEXT ENGINE · EXUS · CARRS WELDING TECHNOLOGIES LTD

CATAPULT Digital · nquiringminds ai · security · iot

33
Number of countries NSIRC students come from.

253
PhD research topics approved

ABOUT NSIRC

The National Structural Integrity Research Centre (NSIRC) was established in October 2012 with the aim of becoming the world centre for structural integrity research.

NSIRC is a state-of-the-art postgraduate engineering facility established and managed by structural integrity specialist TWI. It works closely with industrial partners Lloyd's Register Foundation and BP plc, and lead academic partner Brunel University London.

NSIRC collaborates with almost 40 world-leading universities, including University of Cambridge, University of Oxford and National University of Singapore, to meet industrial challenges. The collaborating partners provide academic excellence to address the need for fundamental research, as well as high-quality, industry-relevant training for the next generation of structural integrity engineers.

NSIRC advances fundamental research to:

- Support the safe operation of products and structures
- Develop innovative, fit-for-purpose technologies and design rules
- Demonstrate solutions for long-term asset management

This includes risk-based management, engineering critical assessment, non-destructive testing, structural health and condition monitoring, and health management for use in real world settings.

157
PhDs started

Analytics and Data Science

University of Essex

A world-class centre of excellence

We are at the dawn of the fourth industrial revolution – a revolution underpinned by computational technologies and massive amounts of data.

It's a revolution in how we collect, analyse and use information in every aspect of our lives. How we do business. How we deliver public and private services. And even how we relate to each other.

For over half a century, the University of Essex has been the intellectual home of the world's leading experts in analytics and data science. Our work spans the full spectrum of data science, from data storage and curation to the application of scientific knowledge to the real world.

In 2014, under the leadership of Professor Maria Fasli, the UNESCO Chair in Analytics and Data Science, we created the Institute for Analytics and Data Science.

We have created a centre of excellence that connects with scholars, businesses, institutes and authorities. We are keen to work with partners across the globe who share our commitment to using data to make the world a better place.

The Essex data eco system

- Research infrastructure
  - Internationally-acknowledged centre of expertise in acquiring, curating and providing access to data
- World-class Essex researchers
- Strategic partnerships with global business partners
  - UK Government has invested in Essex as part of a multi-million-pound national data infrastructure
- Centres of excellence
  - from Social and economic data research and Artificial Intelligence
- Training the next generation of global data scientists
  - through our award-winning Essex Summer Schools

Our innovators

Here are just some of the businesses we work with:

BT   MEDIACOM   FläktWoods   SIGNAL   FIRZA

above   ocado TECHNOLOGY   ORBITAL MEDIA   STEPHENSON HARWOOD

Get in touch

University of Essex, Wivenhoe Park
Colchester, Essex CO4 3SQ

T 01206 873333 **E** enquiries@essex.ac.uk

www.essex.ac.uk/research

The facts

TOP 3 — We are top 3 in the UK for the number of Innovate UK funded projects

TOP 20 — We are top 20 for research excellence
(Research Excellence Framework 2014)

GOLD — Rated Gold - Teaching Excellence Framework
(The UK Government's Teaching Excellence Framework 2017)

UNIVERSITY OF LEICESTER   **TWI**

MatIC at the University of Leicester

The Materials and Innovation Centre (MatIC), an international collaboration between The Welding Institute and the University of Leicester, creates a shared research and technology capability. Bringing together the expertise of the two organisations, it will specialise in small and full-scale materials testing in harsh environments, it will undertake joint research programmes and it will develop the next generation of technologies and engineers in this discipline.

Core areas:

- Materials performance in simulated service conditions
- Physical metallurgy of welding and other fusion-based processes
- Materials characterisation and analysis
- Failure mechanism of weldments and other components made by fusion-based processes
- Computational mechanics
- Digital manufacturing and materials modelling
- Thermal and cold spray coatings
- Thin films and metal matrix systems
- Electrochemistry and corrosion

www.le.ac.uk/matic

The University of Bedfordshire is a regional cornerstone of innovation, accelerating impact by embedding research into our knowledge exchange with businesses and public sector organisations.

The University has worked with over 450 SMEs in the past year as part of our multi-million pound co-ordinated knowledge exchange effort with local authorities, government, InnovateUK and other providers. It boasts an established reputation for providing practical advice, guidance and assistance to solve problems for commercial and societal benefit.

Across the different specialist Research Institutes at the University, we develop novel applications across a variety of disciplines to solve real-world problems. From researching applications of artificial intelligence in robotics, to fuel cell hybrid commercial vehicles, to nanotechniques for biomedicine and manufacturing, the University is committed to translating research into impact.

The UK needs commercially sustainable green energy systems and breakthrough technologies to solve the climate change crisis. To open up new markets and opportunities for companies that want to collaborate on research, the University of Bedfordshire and TWI Ltd established the Renewables Energy Systems Innovation Centre in Cambridge. This is a world class hub with a dedicated research partnership that focuses on renewable energy management and monitoring systems engineering.

For more information, please contact:

✉ businesspartnerships@beds.ac.uk

🌐 www.beds.ac.uk/irac

Partners from University of Bedfordshire and TWI Ltd

Materials and Structural Integrity

Coventry University's Institute for Future Transport and Cities (IFTC) is concerned with advancing powertrain electrification, future and disruptive mobility solutions, advanced manufacturing technology and next-generation materials to ensure a more sustainable future. As the Materials and Structural Integrity group, our activities are spread across IFTC's application areas.

Take our research in residual stress analysis. Our laboratories have world-leading capability for experimental stress analysis, including robot-mounted X-ray diffraction. We apply our methods to studying problems as diverse as welding, additive manufacturing and novel surface engineering techniques such as laser shock peening to improve the resistance of a component to fatigue damage.

Our relationship with the NSIRC has grown rapidly, and we are delighted to have been awarded 21 PhD studentships since 2014. We are keen to add to our existing award-winning industrial partnerships to develop innovative solutions to new challenges.

University of Bedfordshire | TWI

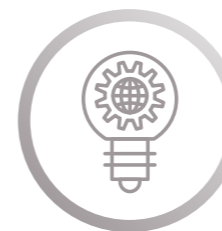**Renewable Energy Systems Innovation Centre**

INNVOTEK
INSPIRING INNOVATION

enquiries@innvotek.com
www.innvotek.com

- Grant writing and full innovation lifecycle support
- Out-of-the-box solutions for your engineering and commercial goals
- Proven R&D, boosting disruptive innovation in technology

1500+
ideas supported for
500+
clients

360° Innovation Consultancy

Data Science & Simulation

Robotics & Automation

INNOVATE. DEVELOP. COMMERCIALISE.

For more than a decade, we have helped our partners develop their ideas into disruptive, innovative solutions and transform them into viable market opportunities.

Our professionals offer 20+ years of experience in delivering innovative solutions and inspire positive change in business and technology.

With a multitude of successful projects, our engineering and project management teams have established Innvotek as a reliable and competent partner.

enquiries@innvotek.com / +44 (0) 330 223 5625

Protecting people in critical situations with world-leading applied engineering services

Marshall

marshalladg.com

f o x in ▶

AFFILIATED UNIVERSITIES

At NSIRC we combine academia with industry, working closely alongside lead academic partner Brunel University London, as well as more than 35 other affiliated universities...

Technical University of Denmark

Kaunas University of Technology

Tianjin University

UCLouvain

Delft University of Technology

KAUST

Pusan National University

Wuhan University of Technology

University of Kuala Lumpur

National University of Singapore

University of Technology Malaysia

University of Aberdeen

University of Edinburgh

University of Strathclyde

Teesside University

University of Sheffield

Sheffield Hallam University

Loughborough University

University of Nottingham

University of Leicester

De Montford University

Coventry University

University of Cambridge

Lancaster University

University of Leeds

University of Manchester

Aston University

University of Birmingham

University of Warwick

University of Essex

University of Hertfordshire

Queen Mary University of London

University of Bristol

Cranfield University

University of Greenwich

Brunel University London

University of Exeter

University of Oxford

University of Southampton

University of Surrey

London South Bank University

nsirc

University of Hertfordshire UH

ENGINEER YOUR EXPERTISE

Enhance your expertise within our Centre for Engineering Research at the University of Hertfordshire.

Find out more at
go.herts.ac.uk/cer

KEYNOTE SPEAKERS

Dr Jeremy Silver
Chief Executive Officer, Digital Catapult

Jeremy Silver, CEO of Digital Catapult, is an entrepreneur, author and angel-investor. He is a Trustee of the British Library and a member of the UK Creative industries Council. Jeremy sits on the Boards of HammerheadVR Ltd, Imaginarium Studios Ltd and FeedForward.AI.

He was previously Executive Chairman of Semetric (acquired by Apple), a strategic advisor to Shazam (acquired by Apple), and CEO of Sibelius Software (acquired by Avid). Jeremy was Worldwide Vice-President of New Media for EMI Group in Los Angeles and Head of Press at Virgin Records where he worked with Genesis, Massive Attack, Brian Eno and Bryan Ferry among others.

His history of the music industry on the internet is titled "Digital Medieval". He has spoken at TEDx, Houses of Parliament, CBI, SXSW and Midem among many trade events. His PhD in English Literature is on Ben Jonson.

Prof Andrew Curran
Chief Scientific Officer, HSE

Professor Andrew Curran is the Chief Scientific Adviser and Director of Research at the Health and Safety Executive.

He has responsibility for the professional leadership of 850 scientists, engineers and physicians, and for development and delivery of HSE's science strategy. He has oversight of HSE's Scientific Advisory Committee on Workplace Health (WHEC), is the Chair of the Sheffield Group (global network of national health and safety research organisations) and a member of the Steering Group of PEROSH (Partnership for European Research in Occupational Safety and Health).

He is a Fellow of the Royal Society of Biology, and the Chartered management Institute, and an Honorary Fellow of the Faculty of Occupational Medicine (UK). He is an Honorary Professor at two leading UK Universities, Sheffield and Manchester.

Prof Mark Gillan
Chief Technology Officer, Innovate UK

Professor Mark Gillan is responsible for leading the Strategy and Impact and Centres and Networks Governance directorates at Innovate UK.

This includes directing delivery of Innovate UK's strategy, the design and development of Innovate UK's programmes, ensuring that the organisation incentivises and drives economic growth through business-led innovation.

Mark has held engineering leadership roles in Formula One with McLaren, Jaguar/Red Bull, Toyota and as Head of the Race Team at Williams.

He was CEO of the UK renewable energy firm Wavepower and Head of Innovation and Project Lead for the ex-America's Cup team Artemis's autonomous zero emissions commercial maritime vessel programme.

A chartered engineer, Mark is also a Visiting Professor at the University of Surrey and a Fellow of the Royal Aeronautical Society.

IOT DISCOVERY PROGRAMME

CATAPULT Digital

Discover the importance of IoT for industry

Industry adoption of future IoT technologies has the potential to increase productivity, lower costs, improve product development and improve customer insights. Selecting the right products, services and solutions is essential if industries are to capitalise on the available benefits. The challenge often lies in discovering and adopting these technologies for industrial settings.

Digital Catapult's IoT Discovery Programme is designed to help industrial businesses to accelerate the understanding and adoption of IoT technologies.

Visit: bit.ly/IoTDiscovery

Digital Catapult is proud to be partners with TWI to establish a new Industrial Net Zero hub

Established as a joint initiative between two of the UK's leading innovation organisations in the engineering and digital sectors, INZIC will target asset and energy intensive industries such as aerospace, utilities and energy.

Find out more bit.ly/INZIC

DEGREES WITHIN INDUSTRY

PhD | Competitive Scholarships within Industry

During the PhD programme, students will design and carry out original experiments guided by the laboratory manager or TWI industrial supervisor.

Additionally the programme will include high-quality training and support to provide a strong foundation for future careers in engineering.

MSc | Oil & Gas Engineering

As the industry now seeks the rapid drilling and commissioning of new wells to meet energy demands, along with major investment in heavy oils and shale oil and gas, skilled engineers who can rapidly design and commission oilfield installations will be the backbone for growth in this industry.

It is precisely this type of engineer that Brunel's programme will develop. Awarded by Brunel University London.

Coming soon | Master of Business Administration (Engineering)

Accelerate your career as a senior excutive in the engineering sector and change the way you see your future and the world around your.

MSc | Structural Integrity (Asset Reliabilty Management)

This course focuses on the knowledge and skills most relevant to developing a career in technical and engineering roles where understanding and achieving structural integrity is a key component. Awarded by Brunel University London.

MSc | Engineering Leadership & Management

The course has been designed specifically to meet the needs of businesses and to develop future leaders.

Offered at NSIRC in Cambridge and awarded by Aston University, this part-time MSc can be funded from the apprenticeship levy so there are no tuition fees to pay.

For more information, visit
nsirc.com/degrees

From the Rector

The Warsaw University of Technology is achieving excellent results owing to the joint effort made by its entire academic community. Active participation of our students and scientists in projects that gain international recognition increases WUT's popularity among young people from other countries and encourages them to study at our University. The harmonious development of various fields of knowledge, represented by individual faculties, multiplies the University's achievements and makes them visible to the entire world through our excellent graduates. The skills and competences acquired at the Warsaw University of Technology enable them to fulfill their boldest dreams and often make them leaders of their communities and work environments.

PROFESSOR JAN SZMIDT, PHD, DSC
RECTOR OF THE WARSAW UNIVERSITY OF TECHNOLOGY

New fields of study are being launched, new laboratories are being established, cooperation with industry and foreign centres is constantly being developed. Our students and graduates receive the best technical education and support – they become the most sought-after specialists on the labour market.

HIGH STANDARDS are our ASSETS:
We ranked first among Polish technical universities in the Perspektywy University Ranking 2019 (14th consecutive victory in this ranking) and third among all academic universities in Poland.
First place among Polish Universities in the Perspektywy Ranking in the, Graduates in the labour market' category (2019).
Nearly 70 fields of study, including studies in English.

State-of-the-art academic research centres, including CEZAMAT, CZIiTT. Collaboration with nearly 150 foreign universities.
Over 150 student research groups, organizations, and associations.

WUT means MORE*
WUT graduates are highly sought-after specialists on the labour market. A total of 41% have received a job offer directly from an employer.
For 79.7% of second-cycle graduates have a job related to their completed studies.
62% of graduates are employed in international companies.
78.5% of second-cycle graduates are satisfied with studying at the Warsaw University of Technology.

*Results based on the Monitoring of Professional Careers of WUT Alumni 2019

www.pw.edu.pl

AGENGA

9:25
Dr Abbas Mohimi, Head of Public Funding, **TWI**
INTRODUCTION & WELCOME

9:30
Prof Tat-Hean Gan, Director, **NSIRC**
NSIRC AND ITS INDUSTRIAL IMPACT

9:40
KEYNOTE SPEAKER: **Dr Jeremy Silver**, Chief Executive Officer, **Digital Catapult**
SEND IN THE DRONES

ROOM 1: ADDITIVE MANUFACTURING CHAIR: Nenad Djordjevic	ROOM 2: COATINGS TECHNOLOGIES CHAIR: Henry Begg	ROOM 3: STANDARDS & MAINTENANCE METHODOLOGIES CHAIR: James Campbell	ROOM 4: INSPECTION & MONITORING CHAIR: Jamil Kanfoud
10:00 **Mason Rowbottom** Study of Cause and Effect of Thermal Induced Focal Shifts within the SLM Process of AlSi10Mg	**10:00** **Aamna Asad** Understanding the structure function relationships of super-omniphobic nanoparticles using magnetic resonance techniques	**10:00** **Oliver Logan** Fracture Toughness Testing of Non-sharp Defects-Assessing constraint effects in notched modified boundary layer models	**10:00** **Faris Nafiah** Pulsed Eddy Current: Signal Feature Enabling In-situ Calibration
10:20 **Mehran Shahriarifar** Effect of Build Direction and Heat-treatment on Microstructure and Tensile Properties of L-PBF 316L Stainless Steel	**10:20** **Ana Antelava** Development of Super Repellent Coatings	**10:20** **Konstantinos Kouzoumis** Biaxial loading effects on the integrity of flawed components Design of Experiments	**10:20** **Zhiyao Li** New development of spatial phase shift shearography for wind turbine blade inspection
10:40 **Emre Akgun** Porosity Defects in Additive Manufactured Titanium Ti6Al4V and their Influence on Fatigue Performance	**10:40** **Craig Melton** Corrosion Sensing Coating Viability Testing	**10:40** **Domenic Di Francesco** Improved Estimation of Fatigue Crack Growth Rate by Partial Pooling of Test Data in Bayesian Models	**10:40** **Hesham Yusuf** Semantic Feature Extraction of Defects in X-Ray Scans of Metallic Plates

11:00
BREAK

11:20
KEYNOTE SPEAKER: **Prof Mark Gillan**, Chief Technology Officer, **Innovate UK**
INNOVATE UK: INVESTING AND CONNECTING TO ACCELERATE UK INNOVATION

ROOM 1: ADDITIVE MANUFACTURING	ROOM 2: COATINGS TECHNOLOGIES	ROOM 3: STANDARDS & MAINTENANCE METHODOLOGIES	ROOM 4: INSPECTION & MONITORING
11:40 **Gowtham Soundarapandiyan** Ti6Al4V Powder Degradation in Electron beam Powder Bed Fusion Additive Manufacturing	**11:40** **Berenika Syrek** Thermally Sprayed Aluminium (TSA) Coatings for Corrosion Protection of Steel Effect of Temperature	**11:40** **Hadi Khalili** Different Bayesian Methods for Updating the Distribution of Fatigue Crack Size	**11:40** **Afnan Islam** Development of cost effective permanently installed corrosion monitoring system with permanent magnets
12:00 **Madie Allen** Numerical Modelling Methods for the Prediction of Microstructure in Metal AM	**12:00** **Rosa Grinon** Evaluation of corrosion protection offered by sacrificial Thermal Spray Coatings for offshore applications	**12:00** **Matthew Weltevreden** A Review of the Treatment of Residual Stress in BS 7910 Fracture Assessment	**12:00** **Xuening Zou** Automatic defect detection and localization in austenitic stainless steel cladding
		12:20 **Jessica Taylor** Compact Crack Arrest testing of EH47 Shipbuilding Steel	**12:20** **Han Yang** Crack growth prediction and monitoring of hydrogen induced cracking under biaxial stress conditions

12:40
LUNCH

13:40
KEYNOTE SPEAKER: **Prof Andrew Curran**, Chief Scientific Adviser and Director of Research, **HSE**
HEALTH AND SAFETY IN A POST-COVID WORLD:
UNDERSTANDING RISK, USING RESEARCH AND BUILDING RESILIENCE

ROOM 5: JOINING TECHNOLOGIES CHAIR: Paola De Bono	ROOM 6: COMPOSITES & POLYMERS CHAIR: Jasmin Stein	ROOM 7: ADDITIVE MANUFACTURING & JOINING TECHNOLOGIES CHAIR: Nick Ludford	ROOM 8: STRUCTURAL INTEGRITY CHAIR: Emily Hutchison
14:00 **Andrew Sandeman** Plasma cathode electron beam for high-integrity materials processing	**14:00** **Dimitrios Fakis** Electromagnetic Surface Waves on Fibre-reinforced Composite Substrates	**14:00** **Marie-Salome Duval-Chaneac** Effect of heat treatment on the microstructure and fatigue behaviour of 316L/IN718 layered structure made by multiple material additive manufacturing (MMAM)	**14:00** **Vishal Vats** An investigation on feasibility of using FTIR for Cr (VI) analysis in welding fumes
14:20 **Chris Nyamayaro** Underwater laser cutting in hyperbaric conditions	**14:20** **Changyi Yu** Effect of Insufficient Homogenization During the Extrusion of Polyethylene Pipes on Butt Fusion Joint Integrity	**14:20** **Stephen Cullen** Assessment of Part Geometry and Distortion in Additive Manufacturing Through Direct Energy Deposition with Laser	**14:20** **Ahmed Teyeb** Investigation of the use of ultrasonic power for the improvement of manufacturing processes

14:40
BREAK

15:00 **Bowei Li** Laser Riveting: an innovative technique for dissimilar composite to metal joining	**15:00** **Faranak Bahrami** Thermally Assisted Piercing; Manufacture and Properties of Multiply-Pierced Composites	**15:00** **Helen Elkington** Laser Beam Direct Energy Deposition– the Effect of Process Parameters on Metallurgical and Mechanical Properties	**15:00** **Alessandro Sergi** Hot Isostatic Pressing of IN625 Powder: Influence of Atomisation route on Microstructure and Mechanical Properties
15:20 **George Brooks** Investigation into the influence of Friction Stir Welding in thick section aluminium alloys			
15:40 **Pedro Santos** Influence of tool material and design on the mechanical and microstructural properties of refill friction stir spot welds			

16:00
Prof Tat-Hean Gan, Director, **NSIRC**
CLOSING WORDS

Mason Rowbottom
PhD Researcher and inventor in Additive Manufacturing technologies, Founder & CEO of Addisol and Founder of The National 3D printing Society. Mason is a strong business development professional with a extensive experience within additive manufacturing and a keen passion for future technologies and their development. Currently undertaking his PhD in powder bed fusion technologies this publication was made possible by the sponsorship and support of TWI. The work was enabled through, and undertaken at, the National Structural Integrity Research Centre (NSIRC), a postgraduate engineering facility for industry-led research into structural integrity established and managed by TWI through a network of both national and international Universities.

Development of geometric and defect characterisations within parts made via laser powder bed fusion

Dr Paul Goodwin[1], Prof Liam Blunt[2]
[1]TWI, [2]University of Huddersfield
2nd Year of PhD

Keywords: Defect characterisation, laser powder bed fusion

I. INTRODUCTION

The SLM process is a powder bed AM technology that has been around for 30 years since its invention by Fraunhofer ILT in the mid-1990s, the process has come a long way with the increase of accuracy through improved optics and an increase in productivity through multiple lasers with higher power outputs. However, these increases in laser power outputs have brought about some issues within the process, especially in regards to repeatability within weld pool depth and Volumetric Energy Distribution (VED). The variations in the weld pool depth have been shown within previous studies to be caused by "Thermal Induced Focal Shifts" these focal shifts are what cause the change in power density that is exposed on the powder bed, preliminary results within this study have shown how much these focal shifts effect the weld depth and in some cases cause the formation of "Key Hole Welds" and "Porosity". The presence of both key hole welds and porosity have shown to reduce the mechanical properties of SLM produced AlSi10Mg components, it is for reason that for further progression of this technologies production rates, the issue of "Thermal Induced Focal Shifts" needs to be addressed and investigated further for high powered lasers within the SLM process. This study shows the effects and possible solutions to "Thermal Induced Focal Shifts" through the use of COMSOL Multiphysics software. A simulation of the DREAM 1KW SLM optical system located at TWI was generated to show the alteration of VED at the point of contact on the powder layer, this was then correlated with the results of physical analysis via the production and analysis of single scan tracks of AlSi10Mg.

.

II. DESIGN/METHODOLOGY/APPROACH

In order to fully understand the characteristics and how it performs to better control the process of the SLM machine used within this project also known as the DREAM Machine (Distortion Reduction and Elimination for Additive Manufacturing), measurements of the laser source and laser system are required. This is due to "Key laser parameters which ensure a successful process include output power or energy at the work piece, spot size or beam waist size, spot location (over time) in addition to M2 or beam parameter product values." (Guttman & McCauley, 2018)[1]

Measurement of both the energy and beam waist size at varying focal offsets and power ranges can be achieved with laser beam profilers such as the Ophir BeamWatch. The Ophir BeamWatch is a good option for this part of the analysis for the following reasons:

- Min Focus spot size 55μm

- Power range 400W-100KW

- Recommended wavelengths 980-1080nm

These functionalities of the equipment provide the ability to sufficiently monitor the beam produced by the DREAM machines 1KW laser operating at a wavelength of 1070-1080nm, going below 400W will not be necessary as most to all builds performed on this machine will not be done at powers lower than 400W, Figure 12 shows the beam profiler.

In order to correlate the beam profiling results against their effects on weld pool geometry, single track scan lines will be produced for each of the parameters previously stated within the beam profiling test, the test layout is demonstrated within figure 1 below.
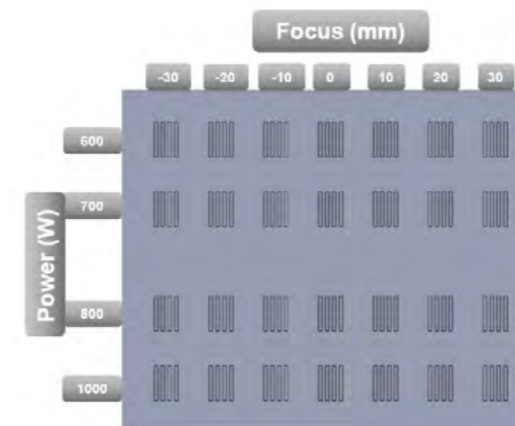

Figure 1 Single Track scan test layout

III. FINDINGS/RESULTS

The results recorded for analysis of the beam profile where the D4σX and D4σY ISO beam widths in μm, the result of the beam widths can be seen below in figure 2.
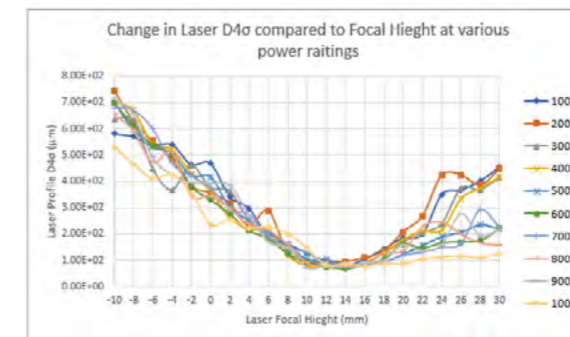

Figure 2 Graph showing beam profile results of the profile width change with varying focal offsets at various power ranges

Figure 3 below shows the effect on weld pool depth within the physical analysis of the test samples, here you can see how the weld pool depth is effect within the interaction of the Aluminium substrate at varying focal lengths and scanning speeds.
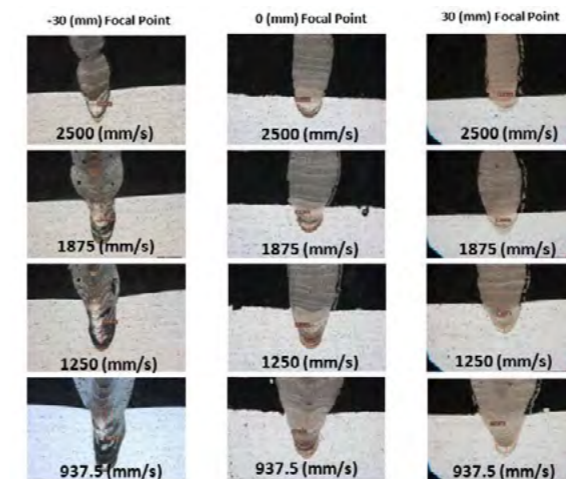

Figure 3 Optical Microscope images of cross sectioned 1KW single track scans at varying focal offsets and scanning speeds

IV. DISCUSSION/CONCLUSIONS

The initial results of the single scan track test have shown intriguing results regarding weld pool manipulation, and the possibility of increasing build rates through focal offset adjustment. However as stated previously this test will have to be reconducted after optical cleaning and coolant replumbing as to ensure that these trends remain the same, this will also provide an opportunity to improve on the last test by taking into consideration the denudation phenomenon by producing triple scan lines with a 30% overlap. This should provide the characteristics closer to that of a true component build, as the centre weld will show how over lapping beams of same parameter sets influence its formation and microstructure.

V. FUTURE PLAN/DIRECTION

After further investigation into both the results and optical system, it showed that their was contamination within the system and as such this was cleaned out. The next steps within this project will be to first deduce what alterations have occurred to the DREAM machines beam profile after cleaning, from this, new parameter sets for focal distance can be utilised within a data base upon the MCP, this will also be increased in reliability and repeatability by the use of Ophir BeamWatch profiler. Utilising the results and knowledge gained from the two previous milestones, a secound test will be conducted in order to investigate the effect of focal offsetting on porosity generation. This is required due to the presence of Key Hole porosity within this project preliminary results, as outlined and demonstrated within the presentation for the ILAS 2019 conference earlier within this project.

Finally a simulation with COMSOL Multiphysics software will be conducted as to simulate as close as possible both the optical system with the DREAM machine and the effect of altering the lens material to CVD diamond optics, this will be conducted in order to see if the thermal lensing effect at higher power ranges of 1-2KW can be mittigated to provide a more stable system.

REFERENCES

[1] Guttman, J. L., & McCauley, J. (2018). Image of laser from Rayleigh scattering directly correlated to beam waist measurements of high-power lasers, 600–603. https://doi.org/10.2351/1.5063206

Mehran Shahriarifar

After completing a BSc and MSc in Mechanical Engineering from Isfahan University of Technology, Iran, Mehran worked in academia as a Lecturer in Mechanical Engineering while also collaborating with industry. Mehran started his PhD in January 2018 with Coventry University. His research project focuses on structural integrity assessment and qualification of 316L austenitic stainless steel produced by the laser powder bed fusion (L-PBF) process, and is sponsored by Lloyd's Register Foundation, Coventry University and TWI Ltd.

Effect of build direction and heat-treatment on microstructure and tensile properties of L-PBF properties of L-PBF 316L stainless steel

Dr Matthew Doré[1] Dr Kashif Khan[2] Prof Xiang Zhang [2]
[1]TWI Ltd [2]Coventry University
3rd Year of PhD

Keywords: additive manufacturing, laser powder bed fusion, 316L, stainless steel, heat-treatment

I. INTRODUCTION

Additive manufacturing (AM), also known as rapid manufacturing or layered manufacturing, is an emerging technology that has recently gained large interest due to its potential to produce customised components [1]. Laser powder bed fusion (L-PBF) is a mainstream AM process for fabricating 3D metallic parts, where the powder bed is melted by a high energy density fibre laser according to a 2D pattern obtained by slicing the 3D CAD model with a certain layer thickness. The layer-wise production technique in L-PBF provides a high degree of freedom of design, with which to produce a wide variety of objects with complex geometries [2].

The aim of this work is to investigate the effect of build direction and heat-treatment on microstructure and tensile properties of L-PBF AISI 316L. This material is widely used in oil and gas, aerospace and medical applications due to its excellent corrosion resistance and weldability [3].

II. DESIGN/METHODOLOGY/APPROACH

Gas atomised 316L metal powder was used for production of the samples by a RenishawAM250 L-PBF machine equipped with Ytterbium 200 W fibre. The process parameters for manufacturing were selected based on previous optimisation work.

Cylindrical bars for tensile testing were printed on the build plate in vertical and horizontal directions where the loading direction is perpendicular and parallel to the additive layers respectively. The samples were then machined to the final geometry and tested as per ASTM E8/E8M standard. Half of the specimens were subjected to AMS2759 standard annealing treatment at 1066 °C for one hour followed by furnace cooling prior to machining.

Samples for microstructure characterisation were extracted from the grip section of the tensile. Two surfaces of the specimens were characterised, along the build direction and transverse to the build direction. Optical microscope, scanning electron microscope (SEM), and electron back-scattered diffraction (EBSD) were used to study the microstructure.

III. FINDINGS/RESULTS

A. Microstructure:

Figures 1 and 2 show the micrographs of the as-built and annealed specimens respectively. The samples in as-built condition present a layered microstructure typical of additive laser processes, characterized by melt pools generated by the laser beam. The scanning laser beam generated periodic melt pools in each layer that can be seen in Figure 1(a). The melting tracks can be observed from Figure 1(b). Melt pool boundaries are not existent in the build direction of the material after annealing, as can be seen from Figure 2(a). Annealing also resulted in the homogenisation of the material leading to a similar microstructure in the build and transverse directions.

EBSD maps of the as-built material show elongated grain in the build direction (Figure 3(a)) and equiaxed grain structure in the transverse direction (Figure 3(B)). The different microstructure in build and transverse directions could result in the material having anisotropic properties. Annealing resulted in more equiaxed grain morphology in both directions (Figure 4) which could be attributed to the recrystallisation of the material in the annealing process.
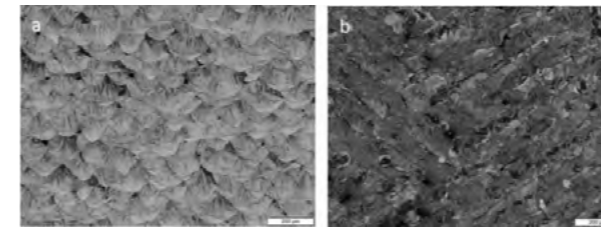

Fig. 1. Optical micrographs of as-built L-PBF 316L stainless steel (a) build direction, (b) transverse to build direction.
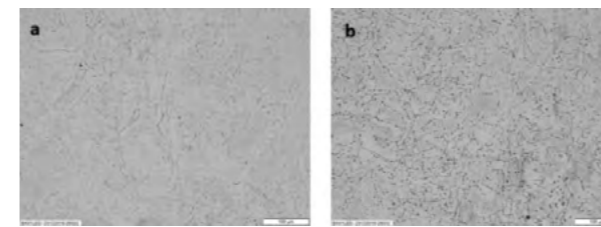

Fig. 2. Optical micrographs of annealed L-PBF 316L stainless steel (a) build direction, (b) transverse to build direction.
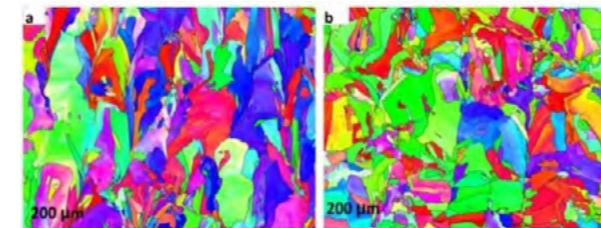

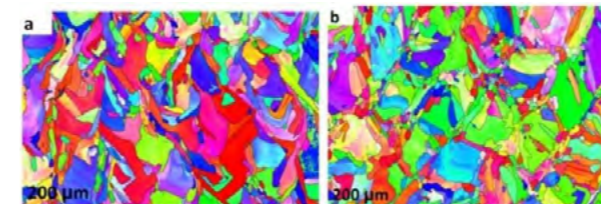**Fig. 3. EBSD maps of as-built L-PBF 316L stainless steel (a) build direction, (b) transverse to build direction.**

Fig. 4. EBSD maps of annealed L-PBF 316L stainless steel (a) build direction, (b) transverse to build direction.

B. Tensile Properties:

Figure 5 shows tensile properties of L-PBF 316L material in different build orientations and conditions. Compared to the wrought material properties [4], the L-PBF 316L has significantly higher yield strength which could possibly be due to the fine sub-grains and high dislocation network in the L-PBF material [5]. Annealing resulted in significant improvement in ductility of the material, although slightly decreased the yield strength. In both as-built and annealed conditions, horizontal samples show higher strength and ductility compared to vertical samples.

IV. CONCLUSIONS

The microstructure of L-PBF 316L material was found to have different characteristics in different orientations in the as-built condition, while annealing resulted in less inhomogeneity in the microstructure. Depending on the build orientation, the material could have different strength and elongation to failure.

Fig. 5. Tensile properties of L-PBF 316L stainless steel.
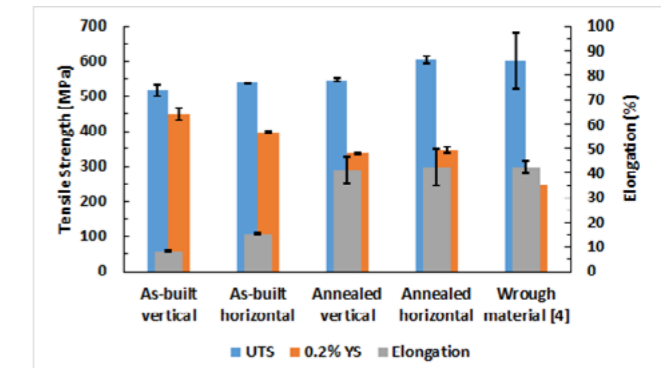
V. FUTURE PLAN/ DIRECTION

Study of the fatigue S-N curve, fatigue crack growth rate and residual stresses in L-PBF 316L stainless steel is in progress.

VI. ACKNOWLEDGEMENTS

REFERENCES

[1] W.E. Frazier, Metal additive manufacturing: A review, J. Mater. Eng. Perform. 23 (2014) 1917–1928. https://doi.org/10.1007/s11665-014-0958-z.

[2] K. Osakada, M. Shiomi, Flexible manufacturing of metallic products by selective laser melting of powder, Int. J. Mach. Tools Manuf. 46 (2006) 1188–1193. https://doi.org/10.1016/j.ijmachtools.2006.01.024.

[3] K.H. Lo, C.H. Shek, J.K.L. Lai, Recent developments in stainless steels, Mater. Sci. Eng. R Reports. 65 (2009) 39–104. https://doi.org/10.1016/j.mser.2009.03.001.

[4] I. Tolosa, F. Garciandía, F. Zubiri, F. Zapirain, A. Esnaola, Study of mechanical properties of AISI 316 stainless steel processed by "selective laser melting", following different manufacturing strategies, Int. J. Adv. Manuf. Technol. 51 (2010) 639–647. https://doi.org/10.1007/s00170-010-2631-5.

[5] L. Liu, Q. Ding, Y. Zhong, J. Zou, J. Wu, Y.L. Chiu, J. Li, Z. Zhang, Q. Yu, Z. Shen, Dislocation network in additive manufactured steel breaks strength–ductility trade-off, Mater. Today. 21 (2018) 354–361. ttps://doi.org/10.1016/j.mattod.2017.11.004.

Emre Akgun

Emre has an MSc degree in Mechanical Engineering from Bilkent University, Ankara, Turkey, obtained in 2011. Afterwards he spent more than six years in hydropower industry as a structural analysis engineer for stationary and rotating electro-mechanical components. His PhD concentrates on process-induced, porosity type defects in additive manufacturing, and their effect on fatigue performance of the popular titanium alloy Ti6Al4V. This publication was made possible by the sponsorship and support of Lloyd's Register Foundation. The work was enabled through, and undertaken at, the National Structural Integrity Research Centre (NSIRC), a postgraduate engineering facility for industry-led research into structural integrity established and managed by TWI through a network of both national and international Universities.

Porosity in additive manufacturing and its influence on fatigue performance of Ti6Al4V

Dr. Matthew Doré[1], Dr. Yanhui Zhang[1], Prof. Xiang Zhang[2]
[1]TWI, [2]Coventry University
2nd Year of PhD

Keywords: Additive Manufacturing, Fatigue, Defects, Porosity, Titanium Alloy, Ti6Al4V.

I.   INTRODUCTION

Additive manufacturing (AM) is currently in transition from prototype building to producing load-bearing components. Considering that most of the critical load-bearing components are subject to cyclic loading, fatigue failure mechanisms in AM materials need to be well understood for a successful transition. In this regard, this PhD is concerned with process-induced defects, more specifically porosity, and their influence on fatigue performance. Exploratory research in literature has shown that process-induced defects in AM materials act as an important source of failure under cyclic loading [1,2,3].

II.   APPROACH

Earlier studies in metal AM were mainly concentrated on discovering general trends by conducting experiments that have many variables. Consequently, it has been reported that fatigue properties of AM materials are influenced by feedstock quality, machine type or model, selected process-parameters, built direction and many more [1,2,3].

In order to quantify influence of porosity on fatigue performance, an experimental programme has been designed to circumvent other parameters that might influence the fatigue life. In this regard, only a single batch has been manufactured using the same build direction for all samples. Subsequently, a stress-relief heat treatment was applied to remove residual stresses. Finally, a mechanical grinding and polishing procedure was conducted to eliminate as-built surface roughness. As a result, it was expected that any variation in fatigue life among the manufactured samples, would be related to differences in defect population unique to each sample.

When possible, prior to fatigue testing, gauge volume of the test sample was scanned using the X-ray Computer Tomography (XCT) technique to quantify size and spatial location of the embedded defect population. After testing, these results were complemented with post-mortem analysis, which entailed removing the fracture surface from the sample via a precision cutter, applying ultrasonic cleaning and analysing it under scanning electron microscope (SEM) in the secondary electron mode using a 20kV accelerating voltage. Representative images of these processes are given in Figures 1 and 2.
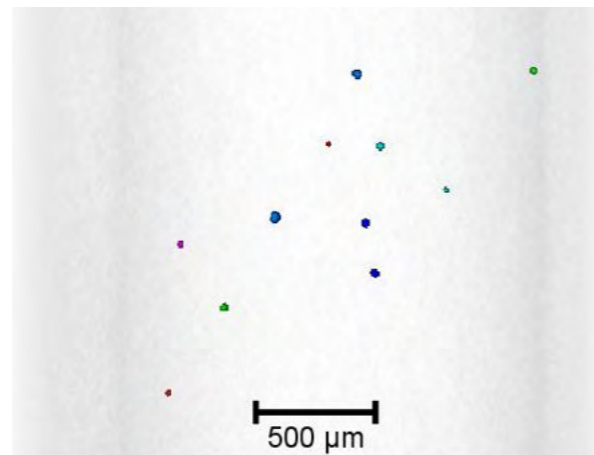

Figure 1: Part of the gauge section of a fatigue test sample captured by using XCT prior to fatigue testing, depicting embedded pores commonly seen in metal AM with spherical morphology.

Load-controlled, uniaxial fatigue testing was conducted in accordance to ASTM E466-15 [4] using a servohyrdraulic fatigue testing machine under constant amplitude (CA) loading and a stress-ratio of R=0.1. Tests were repeated at least three times per selected stress level to obtain statistically significant data.
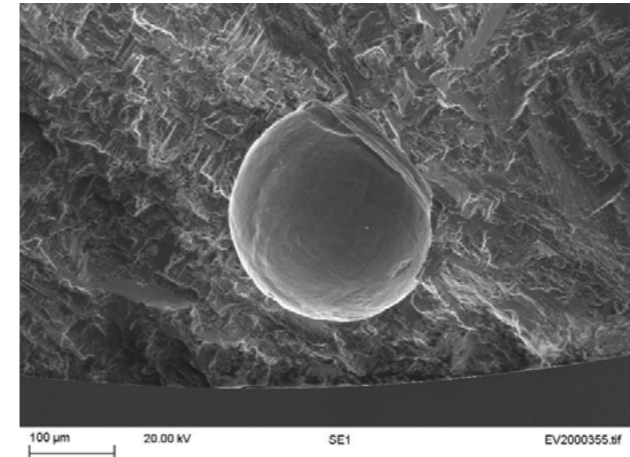

Figure 2: Fracture surface analysis of a fatigue sample showing an isolated spherical pore as the crack initiation location. Obtained via SEM.

Finally, during some of the CA load fatigue tests, crack growth rate from pores was quantified using the replica technique. Usage of optical techniques, like microscopy, was not possible due to the size and stochastic nature of the critical pore location.

III.   FINDINGS AND DISCUSSION

In metal AM, although bulk density above 99% can be regularly achieved, many micron-scale pores are present (Figure 1), and act as preferential locations for fatigue crack initiation, Figure 2. In this figure, cracking was initiated from an embedded pore, but it is in fact more common to find failure due to surface pores.

Inherent surface roughness in AM, which is between Ra=14-30 microns [5, 6], makes surface treatment a necessary post-processing step. This additional material removal results in exposing some of the embedded pores to the surface. It has been shown that surface pores are more detrimental than embedded pores [7]. Therefore, in this work, to make fatigue life predictions, attempts were made to study small crack behaviour from surface pores and quantify crack growth rate by using the replica technique, Fig. 3.

In Figure 3, it can be seen that after nucleation, cracking initially followed a tortuous path, which signifies microstructural influence on crack growth. This growth pattern continued until the crack length reached roughly the same size as the pore. The crack then propagated almost perpendicular to the loading direction, the so-called mode I crack growth.

IV.   FUTURE PLAN AND CONCLUSIONS

This abstract provides a discussion about on-going experimental work in this PhD. Controlled experiments are designed to study the effect of porosity; other parameters that might influence the fatigue performance have been circumvented. By this way, scatter in fatigue life due to porosity will be quantified by providing mean life and standard deviation for particular stress levels.

Such information has been routinely used to develop engineering design curves for mature processes, e.g. welding, but not available at the moment for the AM materials in open literature.

Furthermore, the XCT technique has been used to quantify defect population in the gauge volume prior to fatigue testing. Correlation between defect population and crack initiating defect will be important to assess the criticality of a defect discovered by non-destructive test measurements. Finally, crack growth rates from surface pores are characterised by using the replica technique. These measurements will be used to develop a model for fatigue life prediction in presence of defects.
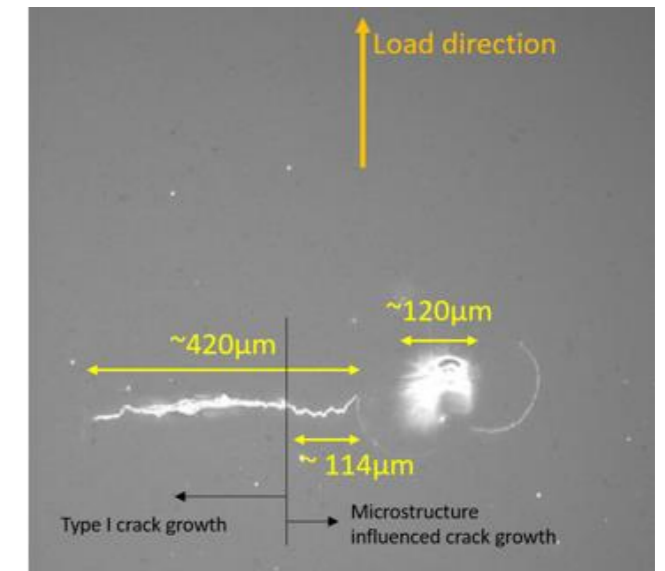

Figure 3: Crack initiating from a process-induced pore, captured by using the replica technique.

REFERENCES
[1] DebRoy, T., et al. "Additive manufacturing of metallic components–process, structure and properties." Progress in Materials Science 92 (2018): 112-224.
[2] Cao, F., et al. "A review of the fatigue properties of additively manufactured Ti-6Al-4V." JOM 70.3 (2018): 349-357.
[3] Li, P., et al. "Critical assessment of the fatigue performance of additively manufactured Ti–6Al–4V and perspective for future research." International Journal of Fatigue 85 (2016): 130-143.
[4] ASTM E466-15, Standard Practice for Conducting Force Controlled Constant Amplitude Axial Fatigue Tests of Metallic Materials, ASTM International, West Conshohocken, PA, 2015.
[5] Simonelli, M., et al. "Effect of the build orientation on the mechanical properties and fracture modes of SLM Ti–6Al–4V." Materials Science and Engineering: A 616 (2014): 1-11.
[6] Greitemeier, D., et al. "Fatigue performance of additive manufactured TiAl6V4 using electron and laser beam melting." International Journal of Fatigue 94 (2017): 211-217.
[7] Tammas-Williams, S., et al. "The influence of porosity on fatigue crack initiation in additively manufactured titanium components." Scientific reports 7.1 (2017): 1-13.

E.T.S. SISTEMI INDUSTRIALI S.r.l.

Our Expertise at your service

ETS

STRUCTURAL HEALTH MONITORING

PRESSURE TEST WITH ASSOCIATED ACOUSTIC EMISSION TEST

TANK FLOOR EVALUATION THROUGH ACOUSTIC EMISSION EVALUATION REFERED TO EN 15856:2010

PROTOTYPES AND MATERIAL TESTING. PROOF OF CONCEPT, PROCEDURES EVALUATIONS
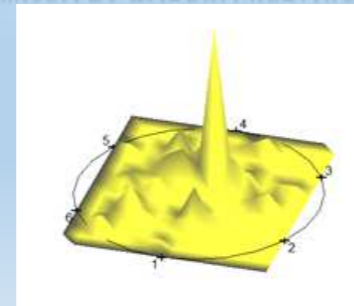
VACUUM, PRESSURE AND HELIUM LEAK TEST UNDER EN, ISO & ASME NORMATIVES

FUGITIVE EMISSION CERTIFICATION IN RESPECT TO ISO 15848 PART 1 & 2

MATERIAL GAS PERMEABILITY EVALUATION

INTENSIVE AND DEDICATED TRAININGS IN LT ED AT WITH LAST GENERATION INSTRUMENTATIONS

CERTIFICATION EXAMS IN OUR HEAD OFFICE RECOGNISED BY BUREAU VERITAS (CERT. MB-015/PND/BVI)

E.T.S. Sistemi Industriali s.r.l.

Headquarter:
Via S. Francesco 323
20861 Brugherio (MB) - Italy
Tel/Fax: +39 039 877790
Email: ets@etssistemi.it

α e-technology

The engineering service with 50 years expertise in analysis, development and design of complex electrical power and control schemes. These systems have included HV and LV converters, advanced power electronics, and electrical power systems for applications for niche markets: oil and gas, marine and renewable energy generation schemes.

This expertise covers a wide range of disciplines required to design and develop innovative solutions for systems operating in harsh environments, such as subsea. This has been achieved with an understanding of the interrelationship of the physics and the application requirements.

Computational systems analysis is used to develop the concepts, which are then correlated with data acquired from innovative monitoring techniques and controls on previous projects, to improve the qualities of the systems performance.

The equipment operators benefit from this integrated data acquisition systems, as it offers a detailed insight of the systems performance / degradation and maintenance of the equipment.

Recent projects, studies and innovations

- *Corrosion and the effects of Common Mode Currents / EMC.*
- *Development of an advanced DC-DC chopper.*
- *Development of an innovative electro-thermal de-icing system.*

Other Projects undertaken:

---
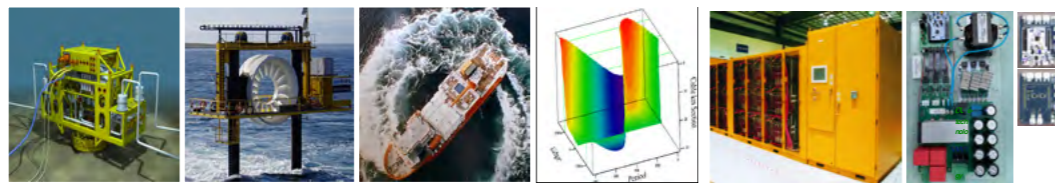
floteks ®

Engineered Plastic Products Rotomoulding Solutions

Your Experienced Partner for Product Innovation, Research and Development

EU PROJECTS:

SafeHPower

ISOPREP

LeakFree

DeICE-UT
DEICING OF WIND TURBINE BLADES

MONITANK

OHSAS 18001 — OCCUPATIONAL HEALTH & SAFETY ASSESSMENT

ISO 14001 — ENVIRONMENTAL MANAGEMENT SYSTEM

AS 9100

IATF 16949 — QUALITY MANAGEMENT SYSTEM

Exhibitions:

ARMI MEMBER

ARMO MEMBER

IAA Commercial Vehicles
Driving tomorrow

AGRI TECHNICA
THE WORLD'S No.1
2019
10-16 NOVEMBER, HANNOVER, GERMANY · PREVIEW DAYS 10/11 NOVEMBER · WHERE INNOVATION MATTERS

Floteks Plastik Sanayi ve Ticaret A.Ş
DOSAB Fulya Sk. No:7 16245 Osmangazi   **Bursa / TURKEY**   info@floteks.com.tr   www.floteks.com.tr

Gowtham Soundarapandiyan

Gowtham is a NSIRC PhD student in Material Science and Engineering from Coventry University. He has a MSc degree in Advanced Metallurgy from University of Sheffield and a BSc degree in Mechanical Engineering from VIT University, India. His PhD focusses on investigating Ti6Al4V powder degradation and its effect on component integrity in powder bed fusion additive manufacturing process.

A study on gas atomised Ti6Al4V powder degradation in electron beam powder bed fusion additive manufacturing

Carol Johnston[1], Raja Khan[1], Bo Chen[2,3], Michael Fitzpatrick[2]
[1]TWI Ltd, [2]Coventry University, [3]Leicester University
3rd Year of PhD

Keywords: Additive manufacturing, Ti6Al4V, electron beam melting, powder degradation, structural integrity

I. INTRODUCTION

Additive manufacturing (AM) processes such as electron beam powder bed fusion (EB-PBF) are widely used to produce near-net shaped components for the aerospace, dental, energy and automotive industries [1]. The powder that is left-out post-fabrication in the EB-PBF process is often recovered and recycled to improve cost-effectiveness [2]. However, the physical and chemical properties of the unconsumed powder might have changed during manufacturing or powder handling. One of the key issues in the wide-scale adoption of EB-PBF process is repeatability in part properties [3]. Therefore, ensuring the quality of the recycled powder before reusing it is one of the key parameters to maintain consistency in build properties. Previous studies conducted in this domain were mainly performed on relatively costly powders produced by plasma-based processes and powder degradation was studied with respect to the number of times the powder was reused. In this work, a relatively cheap powder was used, which was produced by the gas atomisation process. Powder degradation was investigated with respect to its location in the powder bed and number of reuse times. Powders were characterised using a range of powder characterisation techniques and the results were compared with the properties of the virgin powder. In addition, metallurgical and mechanical properties of specimens produced from virgin and recycled powder were also investigated.

II. METHODOLOGY

The work was conducted in ARCAM Q10 plus EB-PBF system using argon gas atomised Ti6Al4V extra-low interstitial powder. A controlled and simulated recycling methodology was employed to produce four test coupons following two conditions, virgin and recycled as summarised in Fig. 1. Four types of powder samples were investigated: Near-melt zone, away-melt zone, 10 times recycled and sieve residue powder and compared with the virgin powder properties. In addition, fatigue, tensile and Charpy impact tests were peformed on the specimens produced from both virgin and recycled conditions.
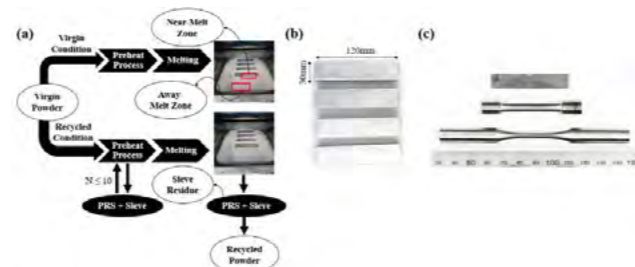
Fig. 1: (a) Build strategy and powder sampling, (b) Extracted blocks after powder recovery system (PRS), (c) Machined specimens as per ASTM standards.

III. FINDINGS/RESULTS

1. Powder Morphology
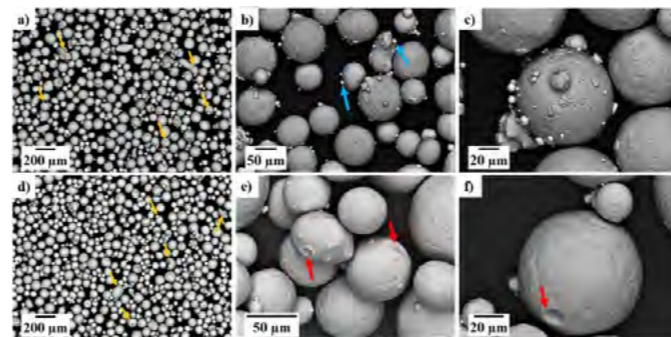
Fig. 2: Scanning electron microscopy (SEM) image of (a-c) virgin and (d-f) recycled powder mophology.

As shown in fig. 2, virgin powder consisted of fine particles bonded to coarse particles (indicated by blue arrow) while recycled powder had concave sites on its surface caused by the detachment of fine particles during powder recovery (indicated by red arrows).   Near-melt zone powder consisted of partially melted and hard sintered powder particles (Fig. 3 (a-c)) due to heat from the melt pool while away-melt zone powder consisted of soft-sintered powder particles (Fig. 3(d-f)) caused by the preheating process.
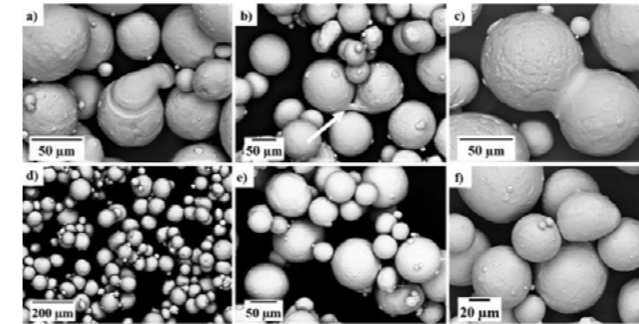

Fig. 3: SEM image of (a-c) near-melt zone and (d-f) away-melt zone powder morphology.

2. Powder Microstructure

The virgin powder consists of martensitic (α') microstructure caused by rapid cooling during the gas atomisation process. However, the near-melt zone powder, consisted of $\alpha+\beta$ microstructures. Since recycled powder consists of unconsumed particles from both the near-melt zone and away-melt zone regions, they contain particles with a mixture of α' and $\alpha+\beta$ microstructure.
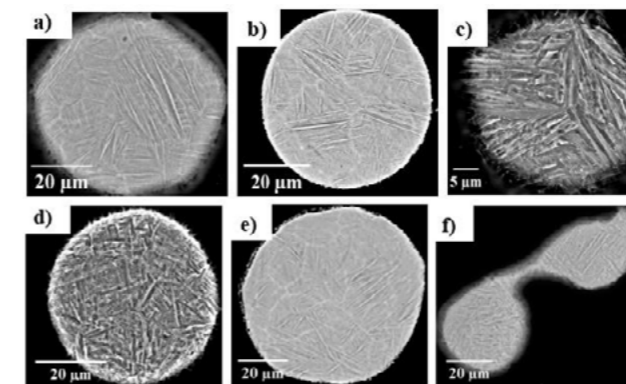

Fig. 4: SEM image of (a) virgin (b) away-melt zone, (c) near-melt zone (d and e) recycled and (f) sieve residue powder microstructure

3. Powder Oxygen Content

The interstitial oxygen content increased from 800 ppm to 1000 ppm in the away-melt zone, 1200 ppm in the near-melt zone, 1100 ppm in recycled and 1200 ppm in sieve residue powders.

4. Powder Flow, Apparent and Tap Densities

The powder flow increased from 25 s/50g to 24 s/50g with no significant change in apparent and tap densities. According to the Hausner ratio, recycled powder exhibited good flow and packing behaviour even after 10 times of recycling.

5. Mechanical Properties

The yield strength (YS) and ultimate tensile strength (UTS) of the specimen increased marginally by 12MPa and 14MPa respectively after 10 times recycling but the average fatigue life of the specimens decreased from 111384 cycles to 92827 cycles to failure after recycling. No significant change was observed in the microstructure, hardness and Charpy impact test values.

IV. CONCLUSIONS

(i) Virgin vs recycled powder: The recycled powder had better sphericity and powder flow but had 200 ppm more oxygen content than the virgin   powder
(ii) Near-melt zone vs away-melt zone powder: The near-melt zone had hard sintered particles whereas the away-melt zone powder had soft sintered particles. The near melt-zone powder had a higher oxygen content (1200 ppm) than the away-melt zone powder (1000ppm).
(iii) YS and UTS increased marginally from 845MPa and 917MPa to 857MPa and 928MPa with recycling. HCF results show a marginal reduction in the fatigue lives of specimens produced from recycled powder.

V. FUTURE DIRECTION

Quantitative investigation of defect size and population will be performed on blocks manufactured from both virgin and recycled powders to understand the reduced fatigue life of the specimens produced from recycled powder.

VI. ACKNOWLEDGEMENTS

REFERENCES

[1] S. Franchitti et al.,'Investigation on Electron Beam Melting:Dimensional accuracy and process repeatability',Vacuum,157,340–348,2018.

[2] A. T. Sutton et al.'Powders for Additive Manufacturing Processes: Characterization Techniques and Effects on Part Properties',Solid Free. Fabr. Proc.,1004–1030,2016.

[3] M. J. Heiden et al.,'Evolution of 316L stainless steel feedstock due to laser powder bed fusion process', Addit. Manuf.,25,84–103,2019.

Madie Allen

Madie is in the final year of her PhD with NSIRC. Following a summer placement within the Numerical Modelling and Optimisation (NMO) team, she decided to undertake her PhD within the same section after completing her integrated masters in Maths (MMath) at Durham University. Madie has recently joined the team as a project leader whilst completing her studies. Her PhD focuses on the development and implementation of numerical models for metal additive manufacturing processes. This work is sponsored by the Lloyd's Register Foundation.

Numerical modelling methods for the prediction of microstructure in metal AM

Tyler London[1], James Campbell[2]
[1]TWI, [2]Brunel University
3rd Year of PhD

Keywords: Numerical Modelling, Additive Manufacturing, Microstructure, Simulation

I. INTRODUCTION

Additive manufacturing (AM) is a novel manufacturing process that produces parts through the deposition of material layer by layer. There are a number of different types of AM processes from powder bed fusion (PBF) methods to direct energy deposition (DED) techniques. PBF utilises a build chamber in which a layer of powder is spread and selectively melted according to a CAD file of the desired geometry. On the other hand, DED processes deposit molten material at the position of the heat source. These include processes such as wire-arc additive manufacturing (WAAM) and laser metal deposition (LMD). AM is set to become a $21.5 billion industry by 2025 [1] due to the large range of benefits it offers, including high material usage, the development of complex geometries and

Figure 1: Laser Powder Bed Fusion. Image Courtesy of TWI Ltd.

However, as with all new technologies there are some challenges and limitations preventing the widespread implementation of this manufacturing method within industry. These challenges include manufacturing constraints, surface finish, as well as residual stress and distortion due to the rapid heating and cooling cycles. Moreover, there is a significant issue with the reliability and repeatability of additively manufactured parts.

This issue needs addressing to ensure the safety and performance of any AM part to be used within service.

In a recent additive manufacturing roadmap by the Lloyd's Register Foundation it was noted that the key to the development of safe products is through the understanding of the properties and performance of AM parts [2]. Material properties are determined by the microstructure of the part, which in turn is driven by the thermal history of the process. Thermal history can change greatly depending on the AM method implemented and the process parameters used within this technique. Therefore, it is important to be able to understand the links between process, microstructure and properties.

II. APPROACH

This project focuses on developing and implementing a numerical modelling method to help improve understanding on the links between process parameters and resultant microstructure. Numerical modelling is an efficient way of investigating the effect of process parameters, particularly when there are a large amount of variables available, as there is for AM processes.
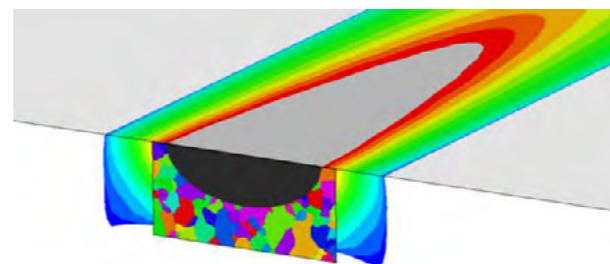
Figure 2: Overlap between FE thermal model and CA microstructure model.

The modelling approach undertaken within this work implements a Cellular Automata (CA) - Finite Element (FE) model. Finite element models are used to simulate the thermal history of the AM process on a continuum scale. This involves modelling the heat profile as well as accounting for the scanning strategy, material deposition and heat losses involved within the process. The thermal model is then imported into the CA model to drive grain growth in the microstructure simulations.

Cellular automata models make use of a grid of cells, where each cell is assigned a number of state variables. These are updated throughout the model according to a prescribed set of rules. Within this microstructure model, these state variables and rules are defined to represent the physical solidification mechanisms that take place within AM processes, and are based upon those used in the model presented by Rappaz and Gandin [3] for casting applications. Work is now being seen within literature to apply these models to additive manufacturing processes.

III. RESULTS

A 2D version of the modelling approach has been validated using open source data provided by the NIST laboratories [4]. The set up involved a single laser scan across a bare IN625 substrate. A strong level of agreement was achieved and the approach was deemed to be successful. Furthermore a statistical analysis has been undertaken to evaluate the probabilistic effects of the microstructure model.

Following this work we are now applying the model to a DED process. An extensively monitored experimental design has been undertaken, including thermocouple measurements, in order to validate FE thermal models before their implementation within the CA models.
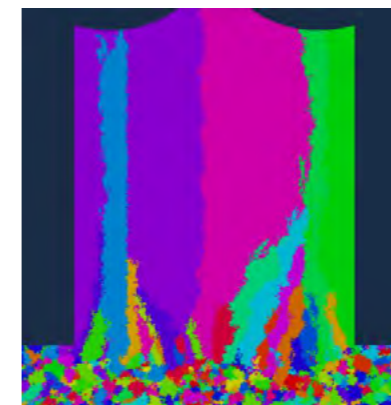

Figure 3: Example of an application of the CA model to a Wire- Arc Additive Manufacturing process.

A good level of visual agreement was achieved between experimental EBSD images and simulated microstructures. Qualitative measurements have also been undertaken.

IV. DISCUSSION

Within this work the modelling approach has been validated against a simple benchmark study. Following the success of this it has been applied to a direct energy deposition process and successfully simulated the key grain characteristics within the build part.

V. FUTURE PLANS

The modelling approach implemented here offers a wide variety of applications for the future, from the prediction of grain size to help determine the strength of a material to the prediction of microstructural transitions for the development of functionally graded materials. Future adoption of the methods will see a growth in understanding surrounding the processes involved in these complex manufacturing technologies and help accelerate the safe implementation of these parts
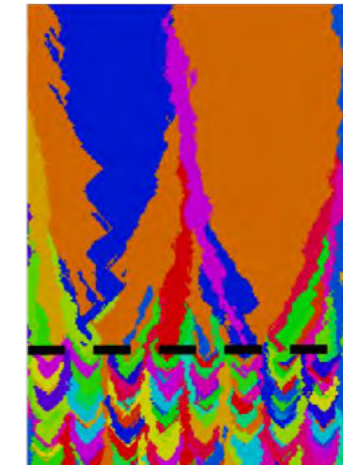
in industry.

Figure 4: Application of the model to a PBF microstructural transition.

VI. ACKNOWLEDGEMENTS

REFERENCES

[1] AM-motion, "Deliverable D5.4, Final AM Roadmap," 2018.

[2] Roadmap for additive manufacturing, Lloyd's Register Foundation Report series: FRSISP 2015.1.v2/No. 1 (2016)

[3] Probabilistic Modelling of Microstructure Formation in Solidification Processes, M. Rappaz, Ch.-A. Gandin, Acta metall. Mater., Vol. 41, No. 2, pp 345-360, 1993

[4] NIST AMB2018-02 Description - https://www.nist.gov/ambench/amb2018-02-description

Aamna Asad
Aamna graduated with a first class BEng(Hons) from Lancaster University in 2017. She later pursued an MSc in Advanced Chemical Engineering from the University of Manchester where her research focused on the determination of self-diffusivities of gases in petroleum using molecular modelling techniques. In October 2018, Aamna started an iCASE PhD with the University of Cambridge and TWI Ltd. Her work focuses on establishing a methodology to characterise, design and optimise the functionalisation process of silica nano-particles.

Understanding the structure function relationships of super-omniphobic nano-particles

Anna Wojdyla-Cieslak[1], Mick Mantle[2], Alan Taylor[1]
[1]TWI, [2]University of Cambridge
2nd Year of PhD

Keywords: type here

I. INTRODUCTION

The Stöber method makes use of the sol-gel process and creates monodispersed spherical silica particles by the hydrolysis and condensation ofalkoxysilanes. The benefit of using the Stöber method over other synthesis routes is that it produces high purity materials with narrow particle distributions, reduces energy costs and, most importantly, is able to control the surface chemistry of silica nano-particles (SNP).[1] The surface of SNPs can be made hydrophobic by functionalising or grafting with certain silanes in order to form trimethylsilyl (TMS) groups (-Si(CH3)3).[2] Surface functionalisation has different uses in a variety of applications including catalysis, biochemical sensing, biolabeling, coatings and photonics. Therefore, it is important to develop a methodology to characterise, design and optimise the functionalisation of SNPs. This research will allow for the quantification and qualification of a range of Stöber silicas with different structures and surface chemistries.

II. DESIGN/METHODOLOGY/APPROACH

As part of this research, Stöber silicas of many different sizes were synthesised using a statistically valid approach. The materials were reacted in solvent dispersions with hexamethyldisilazane (HMDS), at different concentrations and reaction times to facilitate the functionalisation process. The silica:silane ratio was varied gravimetrically and is defined as T = Stöber silica/mass of functionalised silica. In addition to primary characterisation techniques such as dynamic light scattering (DLS), thermogravimetric analysis (TGA) and particle surface area measurements, solid-state ^1H, ^{29}Si and ^{13}C nuclear magnetic resonance (NMR) techniques were used to provide chemical characterisation and quantify the extent of functionalisation/TMS coverage on the functionalised silica particles.

III. RESULTS AND DISCUSSION

The three types of Stöber SNPs and their functionalised materials were characterised and analysed using DLS and nitrogen sorption methods. The results are summarised in Table 1. With reference to surface area values, it can be seen that the three different particles exhibit different trends with respect to functionalising times. This could be due to the different geometrical and chemical structures of these particles. The surface area of SMS35 decreases when functionalising time increases, however, the opposite trend is noted for SMS310.

Table 1 Particle size and surface area measurements of parent and functionalised silica particles

Sample	Particle size (nm)	Surface area (m²/g)
SMS35 (parent silica)	63.7 ± 25	286.67 ± 5.15
SMS35 HMDS 4.0T 1HR	67.7 ± 26	230.31 ± 4.31
SMS35 HMDS 4.0T 1DAY	66.7 ± 27	246.90 ± 4.16
SMS35 HMDS 4.0T 1WEEK	66.0 ± 26	146.03 ± 2.20
SMS120 (parent silica)	131.2 ± 36	206.02 ± 4.47
SMS120 HMDS 4.0T 1HR	124.8 ± 41	206.43 ± 4.54
SMS120 HMDS 4.0T 1DAY	125.9 ± 39	195.50 ± 4.04
SMS120 HMDS 4.0T 1WEEK	126.2 ± 36	197.31 ± 4.50
SMS310 (parent silica)	407.8 ± 151	15.23 ± 0.18
SMS310 HMDS 4.0T 1HR	304.9 ± 56	14.41 ± 0.11
SMS310 HMDS 4.0T 1DAY	305.9 ± 103	56.18 ± 1.05
SMS310 HMDS 4.0T 1WEEK	309.1 ± 117	155 ± 2.18

The chemistry of silica has been studied through history by various authors, using ^1H and ^{29}Si NMR methods. The various species that are found on the surface of silica are summarised in Figure 1.

Q2 – Geminal silanol   Q3 – Isolated silanol   Q3 – Hydrogen-bonded silanol   Q4 - Siloxane   M – TMS species
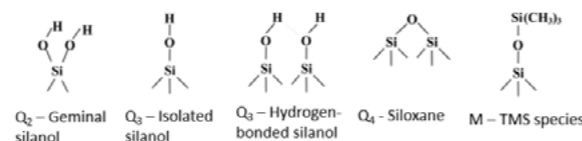
Figure 1 The various types of species present on the silica surface

Each of these species can be identified with a certain chemical shift on the NMR spectrum, considering SMS35 and its corresponding functionalised materials.

The ^1H Magic Angle Spinning (MAS) results, as depicted in Figure 2, display various regions that match to different species present on the silica surface. All the functionalised samples show an appearance of a new peak at approximately 1 ppm which is likely to be due to the HMDS functionalisation, as it is absent on the parent SMS35.
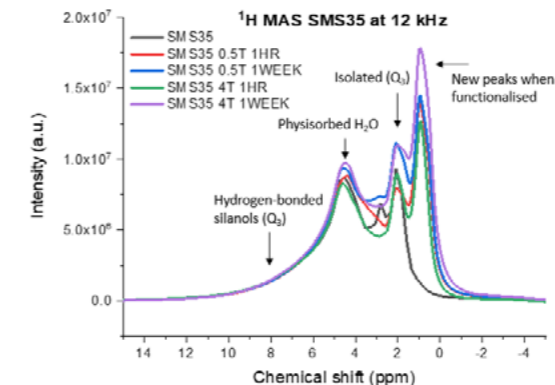

Figure 2 ^1H MAS spectra of SMS35 and HMDS SMS35

The equivalent ^{29}Si High powered ^1H-decoupled (HPDEC)-MAS spectra, Figure 3, of SMS35 and HMDS SMS35 show high intensities of structurally mature Q4nd Q3 species, but low intensities of Q2 species. A well defined M peak/region is also seen to lie on the spectrum at 14 ppm for all functionalised samples which is due to the formation of TMS species. The ^{13}C Cross polarised-MAS spectra (Figure 4) displays the different carbon species present in the silica. The peaks at 17 and 58 ppm are due to the presence of CH3 and CH2 groups from ethanol leftover from the reaction mixture which was not removed, post drying protocol (120 degree C for >24 hrs). For the higher concentrations of HMDS, i.e. 4T, the carbon intensity signal is also greater. It can be noted that for the parent SMS35, there is no TMS species at 0 ppm.
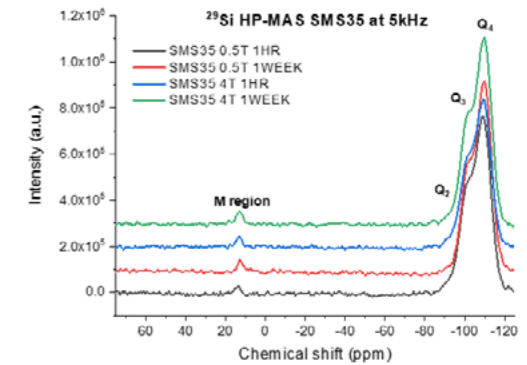

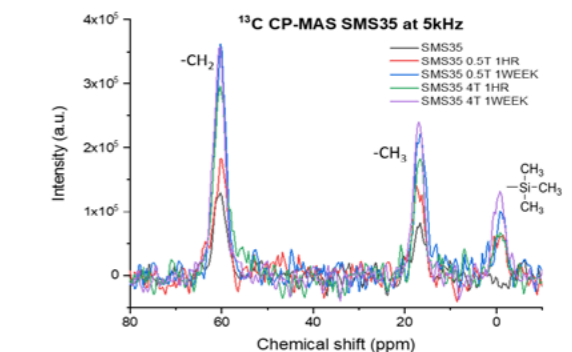**Figure 3 ^{29}Si HP - MAS spectra of SMS35 and HMDS SMS35**

Figure 4 ^{13}C CP -MAS spectra of SMS35 and HMDS SMS35

IV. CONCLUSIONS/FUTURE DIRECTION

In its current state, this research is focused in understanding and quantifying the chemistry of the silica surface and the changes made post functionalisation. Though not shown here, SMS120 displayed less functionalisation than SMS35, and SMS310 showed the least functionalisation out of all materials. Future work will consist of deuterium exchange experiments to quantify the number of surface hydroxyls present on the surface that play a part in functionalisation.

V. ACKNOWLEDGEMENTS

[1] Bourebrab, Marion A., et al. "Influence of the initial chemical conditions on the rational design of silica particles."Journal of Sol-Gel science and Technology 88.2 (2018): 430-441.
[2] Suratwala, T. I., et al. "Surface chemistry and trimethylsilyl functionalization of Stöber silica sols."Journal of Non-Crystalline Solids 316.2-3 (2003): 349-363.

Ana Antelava

Ana graduated with a BEng in Chemical and Process Engineering from London South Bank University (LSBU) in 2017, and before starting her PhD, worked as a process safety engineering challenger at BP. She also worked as an industrial trainee at GPIC in the Kingdom of Bahrain. During her BEng at LSBU Ana researched thermal and catalytic pyrolysis of plastic solid waste for energy recovery. Currently, Ana is undertaking a PhD at NSIRC with LSBU and her topic is "Development of durable super repellent coatings". Ana's PhD is sponsored by Lloyd's Register Foundation. Lloyd's Register Foundation helps to protect life and property by supporting engineering-related education, public engagement and the application of research.

Development of durable super repellent coatings

Anna Wojdyla-Cieslak[1], Geraldine Durand[1,2], Achilleas Constantinou[2] Alan Taylor[1]

[1]TWI, [2]London South Bank University

3rd Year of PhD

Keywords: super repellence, wetting, surface roughness, surface chemistry

I. INTRODUCTION

Surface contamination is an industrial problem that leads to loss of performance and increased maintenance costs. Numerous methods have been developed to prepare a super-repellent coating but the retention of high levels of repellence has not been achieved yet[1]. The development of surfaces that repel liquids has attracted lots of interest due to a wide variety of possible applications in industry. A deeper understanding of the key chemical and topographic characteristics that dictate this behaviour would provide the enabler for the engineering of anti-contamination, anti-sticking and self-cleaning materials[2]. The purpose of this research is to better understand the conditions that dictate very high levels of repellence, specifically to decouple the effect of surface chemistry from surface roughness and to develop a new methodology for assessing wettability.

II. DESIGN/METHODOLOGY/APPROACH

To decouple the effects of surface chemistry from topographic contributions, substrates with micro-scale, nano-scale and minimum surface roughness were used. The substrates were treated with commercially available coatings as well as a range of chemical functionalities known to promote low surface energies[3]. This included fluorinated and non-fluorinated silane treatments with long and short alkyl chains.

For the minimal surface roughness, glass slides and stainless steel 304 slides polished to mirror finish were used. To achieve micro-scale topography, stainless steel 304 slides were used as received and were also blasted with grit of various sizes; 36, 60, 100 at 70 PSI, 50 PSI and 40 PSI respectively.

To achieve nanoscale roughness, 35nm silica nanoparticles functionalised with trimethylsilyl ligands were deposited on the smooth substrates to build up topography[4].

To assess the repellence of fabricated samples, the drop shape analyser (DSA) was used. Contact angle measurements were undertaken with water, diiodomethane and ethanol/water blend probe liquids. To provide a more discriminating assessment to enable the selection of the most repellent surface chemistry and topography, an examination of advancing-receding contact angle as a function of tilt was undertaken. In addition, an evaluation of the droplet location as a function of tilt was carried out to determine whether it exhibits film-forming behavior.

The achieved topographic roughness was assessed using atomic force microscopy (AFM), Alicona confocal microscopy and white light interferometry (WLI).

III. FINDINGS/RESULTS

Planar substrates with minimal roughness showed little difference in the degree of repellence between fluorinated, non-fluorinated silane treatments and commercial coatings. It was also demonstrated that the maximum static water contact angle achievable on a smooth surface was around 110°. In order to pass this limititation of surface chemistry, the surface has to exhibit the correct degree of surface roughness (Figure 1).
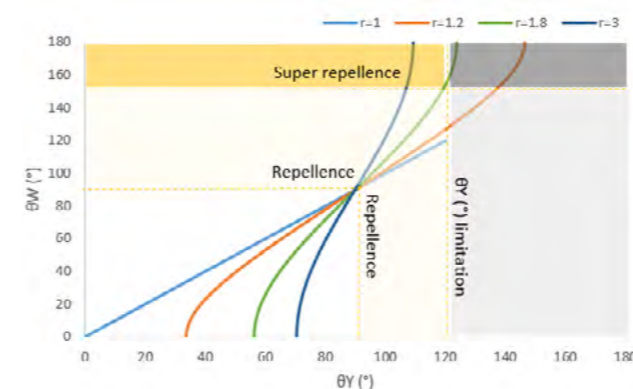

Figure 1 effect of roughness on apparent contact angle values

The grit blasted stainless steel 304 exhibited roughness in the range from 0.16 to 4.08 microns (Figure 2. a and b). While, the subtstrate coated with the layer of SMS35 silica nanoparticles showed roughness of 35 nm. (Figure 2. c)
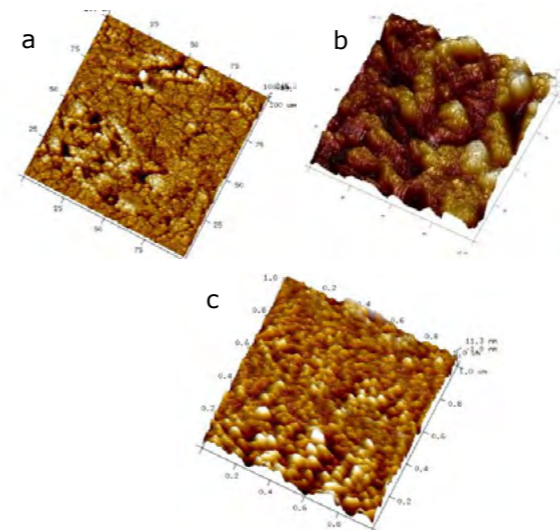

Figure 2 a) AFM image of Stainless steel 304 slide as received. b) blasted with 100 grit at 40 PSI. c) layer of SMS35 silica nanoparticles deposited on glass slide

The substrates with micro-scale roughness displayed an increase in static water contact angle to ~125° but the dynamic contact angle measurments revealed that samples were exhibiting the petal effect - the deposited droplets had contact angle hysteresis (CAH) of 30° and did not roll off even at a 80° tilt.

The samples with nanoscale topography showed an increase of static contact angle to 140° (Figure 3). Dynamic contact angle measurments as a function of tilt showed that the surface exhibited low contact angle hysteresis of 3°and the roll off angle of 8°.
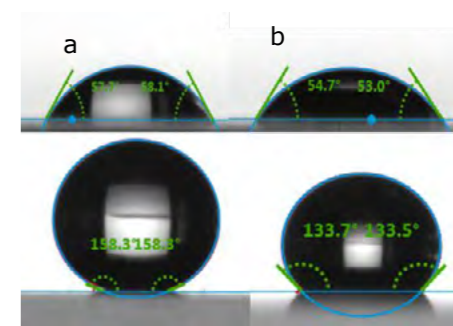

Figure 3 Water (a) and diiodo-methane (b) droplets on the planar glass slide without any treatment (top) and on the layer of trimethylsilyl treated silica nanoparticles (bottom)

IV. DISCUSSION/CONCLUSIONS

To decouple the effects of surface chemistry from topographic contributions, substrates with various degree of surface roughness were studied together with fluorinated and non-fluorinated silane treatments with long and short alkyl chains.

Planar substrates with minimal roughness showed the maximum static water contact angle achievable on a smooth surface was around 110°. Substrates with micro-scale roughness showed increased static contact angle but exhibited petal effect. The nano-scale topography showed the highest static contact angles and also lowest CAH and roll-off angle.

V. FUTURE PLAN/DIRECTION

- Assessment of additional surface chemistry/roughness profiles
- Durability assessment
- The roughness parameters will be investigated to determine those that enhance repellence without increasing CAH.

REFERENCES

[1] A. Wojdyła, G. Durand, A. Taylor, and I. Boyd, Advanced low-energy durable coatings. International Journal of Energy Research, 39(2), pp.165-171 (2014).

[2] C. Hsieh, F. Wu, and W. Chen, Super water- and oil-repellencies from silica-based nanocoatings. Surface and Coatings Technology, 203(22), pp.3377-3384 (2009).

[3] L. Li, B. Li, J. Dong, and J. Zhang, Roles of silanes and silicones in forming superhydrophobic and superoleophobic materials. Journal of Materials Chemistry A, 4(36), pp.13677-13725 (2016).

[4] Feng C, Zhang Z, Li j, Qu Y, Xing D, Gao X, Zhang Z, wen Y, Ma Y, Ye j and Sun R, A bioinspired, highly transparent surface with dry-style anti-fogging, anti-frosting, anti-fouling and moisture cleaning properties. Macromel. Rapid Commun (2019) 40, 180078

Craig Melton
Craig began his university education by studying a B.Sc. in chemistry from Newcastle University, graduating in 2011. After which, he spent a year as laboratory technician and went on to study an M.Sc. in Corrosion Control Engineering at The University of Manchester, graduating 2013. He then spent 4 years working in the oil and gas industry as a Corrosion, Materials and Integrity Engineer for Wood (PLC). And finally started his PhD in 2017 with the IMPaCT Centre at the University of Leicester and is conducting research in to smart polymer coatings for marine environments. This research is sponsored, in addition to TWI, by the Lloyds Register Foundation. Lloyd's Register Foundation helps to protect life and property by supporting engineering-related education, public engagement and the application of research www.lrfoundation.org.uk.

Corrosion sensing coating viability testing

Dr Shiladitya Paul[1], Dr Simon Gill[2]
[1]TWI, [2]Leicester
3rd Year of PhD

Keywords: Corrosion, Organic Coatings, Smart Coatings, & Polymer Coatings.

I. INTRODUCTION
Steels used in offshore constructions corrode, and one of the most common corrosion mitigation techniques is the application of polymer coatings.

Epoxy coatings, protect the steel by functioning as a physical barrier to the environment and by providing a high resistance, thereby preventing current exchange between cathode and anode [1][2]. However, coatings degrade overtime, allowing corrosive species to permeate through and corrode the underlying substrate.

Inspection is carried out to ascertain the coating condition and to find out if corrosion beneath the coating has occurred. One concept to simplify the inspection is to incorporate chromophore-containing molecules (CCM) which change colour when in contact with products of corrosion[3].

$$Fe \longrightarrow Fe^{2+} + 2e^- \qquad (1)$$
$$O_2 + 2H_2O + 4e^- \longrightarrow 4OH^- \qquad (2)$$
$$Chromo + OH^- \longrightarrow Chromo^- + H_2O \qquad (3)$$
$$\text{(Original Colour)} \qquad \text{(Different colour)}$$
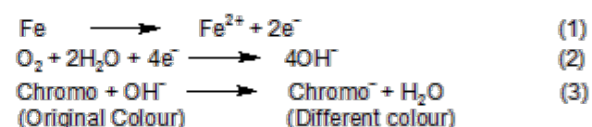
As the steel corrodes, hydroxide ions are formed at cathode. These ions deprotonate the CCM, bring about structural conjugation and a colour change which an engineer can inspect (see equations 1-3).

The aim of this study is to investigate the viability of two CCMs (phenolphthalein (phph) and thymol blue (TB)) with two epoxy coatings (liquid and powder).

II. EXPERIMENTAL APPROACH
The experimental approach was to firstly check compatibilty between phph and TB and the coatings. To do this, glass slides were coated in CCM and in epoxy coatings (either liquid or powder).

The details of phph and TB are given in table 1.

	Colour change	pH range of colour change
Phenolphthalein (phph)	Colourless to pink	<8.2 - >10.0
Thymol Blue (TB)	Yellow to Blue	<8.0 - >9.6

Table 1: Selected CCMs, their respective colour changes and the pH ranges of said colour changes.

The ability for the TB and phph to change colour in the coating was then investigated by utilising the epoxy powder glass samples and immersing them in 0.1M NaOH solution for 35 days.

Following this, S355 steel plates and S355 plates thermally sprayed with 85% Zn & 15% Al (TSZA) were taken and coated in either phph or TB then coated with epoxy powder. These plates were then exposed to synthetic seawater (adjusted to pH 7.2) for 35 days.

III. RESULTS
The results of each stage of coating viability test are given below, note than unsuccessful coating/CCM combinations did not receive further evaluation.

Figure 1 phph (left) and TB (right) coated glass coated in liquid epoxy.
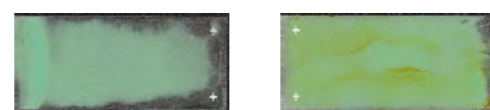
Figure 2 phph (left) and TB (right) coated glass coated in powder epoxy.

Figure 3 phph and epoxy powder coated glass immersed in 0.1M of NaOH for: 0 days (left), 2 days (centre) and 35 days (right).

Figure 4 TB and epoxy powder coated glass immersed in 0.1M of NaOH for: 0 days (left), 2 days (centre) and 35 days (right).

Figure 5 phph and epoxy powder coated S355 plates exposed to seawater for: 0 days (left), 7 days (centre) and 35 days (right).
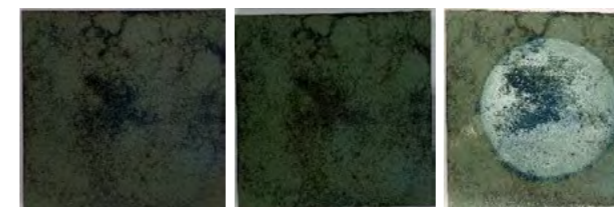

Figure 6 Thymol Blue and powder epoxy coat S355 plates exposed to seawater for: 0 days left, 7 days (centre) and 35 days (right)

Figure 7 phph and epoxy powder coated TSZA S355 plates exposed to seawater for: 0 days left, and 35 days (right)
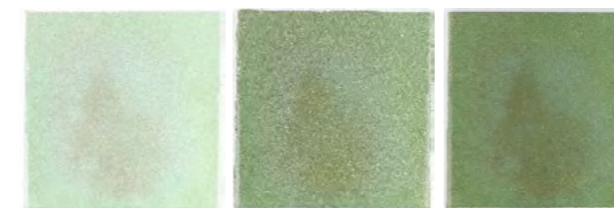

Figure 8 TB and epoxy powder coated TSZA S355 plates exposed to seawater for: 0 days (left), 10 days (centre) and 35 days (right)

IV. DISCUSSION/CONCLUSIONS
It can be seen that the liquid epoxy coating system is incompatible with the two CCMs utilised. This is due to the use of amine-containing hardening agents to cure the polymer. Amines increase the pH, this results in the CCM colour change.

Epoxy powders 'cure' mechanism does not utilise amine hardeners but involves heating to 232°C which, as the results on glass show, prevents the activation of the CCM and does not result in colour change. After the epoxy powder samples were immersed in NaOH the colour change of phph and TB was observed. Immersion in NaOH imitates corrosion at the cathode and showed that the chromphore-containing molecules post cure are still available for activation.

Viability of this coating system is further demonstrated with the seawater exposure tests of the coated S355 plates. After 7 days a colour change is visible, this colour change is more obvious for thymol blue samples, and is sustained through to the end of the test at day 35.The results of the TSZA S355 plates exposured to seawater in a 35 day time frame demonstrated no colour change on the phph samples and little on the TB samples, this may be due to the reduced corrosion rate of the Zn/Al coating in comparison to steel. It may also be due to readiness of Zn or Al to form slightly soluble complexes with hydroxide ions, meaning that there are less hydroxide ions available for increasing the pH and therefore CCM colour changes. Perhaps with an extended exposure the corrosion sensing capability and coating viability will become more apparent on TSZA.

V. FUTURE PLAN/DIRECTION
Future investigations will include, but are not limited to, quantifying any possible alterations in anti-corrosion barrier properties of the epoxy powder coating by evaluating the system via electrochemical impedance spectroscopy, pull-off strength, defect propensity and salt spray corrosion testing. Currently, real world environmental testing is being carried out on test plates in a coastal environment and a marine environment. The results of these tests are due in September 2020.

VI. ACKNOWLEDGEMENT

REFERENCES
[1] S.B.Lyon, R.Bingham & D.J.Mills, Advances in Corrosion Protection by Organic Coatings: What We Know and What We Would Like to Know, Progress in Organic Coatings (102), 2017, pp 2-7.
[2] J.M.Sykes, E.P.Whyte, X.Yu, & Sharer Sahir, Does "Coating Resistance" Control Corrosion?, Progress in Organic Coatings (102), 2017, pp 82-87.
[3] J.Zhang & G.S.Frankel, An Investigation of the Corrosion-Sensing Behavior of an Acrylic-Based Coating System, Corrosion (55), 1999, pp 957-967.

Berenika Syrek-Gerstenkorn

Berenika is a third year PhD student at the University of Birmingham. She is currently carrying out her project on thermally sprayed coatings for corrosion protection of steel operating in marine environments. Before starting her PhD, Berenika completed an undergraduate degree in Mechanical and Medical Engineering at Gdansk University of Technology in Poland, an MSc in Mechanics and Machine Design at the same university as well as an MSc degree in Structural Integrity at Brunel University in London.

TSA coatings for corrosion protection of steel - effect of temperature

Prof Alison J Davenport[1], Dr Shiladitya Paul[2]

[1]University of Birmingham, [2]TWI

3rd Year of PhD

Keywords: Thermally sprayed coatings, thermally sprayed aluminium, TSA, cathodic protection, sacrificial coatings.

I. INTRODUCTION

The most commonly used corrosion mitigation methods for structures operating in seawater include a combination of protective coatings and cathodic protection (CP) provided by sacrificial anodes, but the use of such systems is not without limitations. In the absence of an effective CP system, organic coatings can provide protection to steel only when they remain intact. In subsea where the CP is effective, sacrificial anodes can considerably increase the overall mass of the structure.

An alternative method is application of thermally sprayed aluminium (TSA) coatings. TSA offers long-term, maintenance-free protection to steel substrate, working as a barrier to the corrosive environment when intact, and acting as an evenly distributed anode which sacrificially protects steel when damaged. Furthermore, high resistance to mechanical damage, large operating temperature range, and low corrosion rate makes it an excellent corrosion mitigation coating for offshore applications.

In this work, the behaviour of arc-sprayed aluminium coatings deposited on carbon steel is investigated under full artificial seawater immersion. Effectiveness of TSA coatings is evaluated using electrochemical techniques.

II. METHODOLOGY

Carbon steel plates (S355) were used as substrate materials. Before spraying, steel coupons were prepared by blasting with 80 mesh alumina abrasive blasting grit. The substrates were then sprayed with commercially pure aluminium (99.5wt%) using twin wire arc spraying method. After spraying 5% of the coating was removed to simulate a defect in the coating.

For electrochemical measurements a typical 3 electrodes systems consisting of Ag/AgCl reference electrode, Pt/Ti counter electrode, and a sample as a working electrode. Electrochemical measurements were performed using a Biologic VMP-300 potentiostat. Linear Polarization Resistance (LPR) method was used to determine polarisation resistance of the samples. Samples were polarised ±10 mV from the open circuit potential (OCP).

III. RESULTS AND DISCUSSION

The OCP of TSA coatings containing defects was monitored during the 32-day immersion in artificial seawater at 4ºC and 15ºC. The results are shown in Fig. 1. Noticeably, the potential of the sample exposed to the lower temperature was significantly higher during the whole duration of the test.

The TSA coating exposed at 4ºC, did not polarise the steel substrate to the protection potential of -
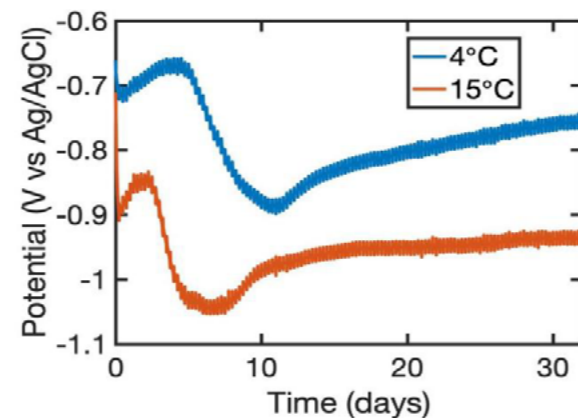
Figure 1 Evolution of the open circuit potential of TSA coatings with defects on steel during immersion in artificial seawater at 4 and 15ºC.

0.8 mV (Ag/AgCl/seawater) specified by the DNV- RP-B401 standard.

However, both of the samples exhibited similar evolution of the potential as a function of time: initial increase of the potential, followed by its sharp drop and another gradual rise. The initial increase of the potential is most probably associated with formation of oxides and hydroxides layers on the aluminium coatings. The sudden potential drop could be due to the dissolution of aluminium layer accompanied by the formation of calcareous deposits (such as CaCO3 and/or MgOH) on the exposed steel. The gradual rise of the potential is most likely associated with the formation of corrosion products on the coating.
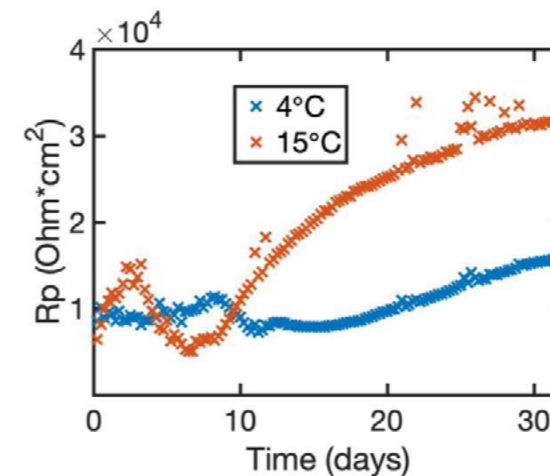

Figure 2 Evolution of the polarisation resistance of TSA coatings with defects on steel during immersion in artificial seawater at 4 and 15ºC.
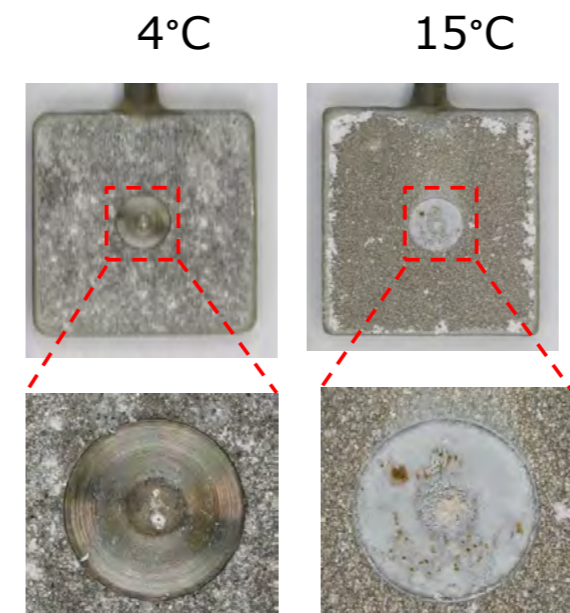

Figure 3 Images of the samples after the 32-day immersion in artificial seawater at 4 and 15ºC.

Worse performance of TSA at lower temperature can also be seen from the results of the LPR measurements (Fig. 2). Higher Rp values at 15ºC indicate higher resistance to corrosion and lower corrosion rate. Moreover, as can be seen in Fig.3, at 15ºC, exposed steel is covered with calcareous deposits, whereas at 4ºC, not much products have formed.

II. CONCLUSIONS

1. Temperature has an effect on the performance on TSA coatings in seawater.

2. TSA coatings with defects showed better corrosion performance at 15ºC as compared to 4ºC.

3. It is important to evaluate corrosion performance of Al-coatings at temperatures of intended service.

III. FUTURE PLAN

Investigation of the reasons for the worse performance of TSA coatings at lower temperatures using several techniques such as zero resistance ammetry (ZRA), electrochemical impedance spectroscopy (EIS), X-ray photoelectron spectroscopy (XPS), Raman spectroscopy.

III. ACKNOWLEDGEMENTS

Rosa Grinon Echaniz
Rosa graduated with a Chemistry degree and an MSc in Nanomaterials at the University of Zaragoza (Spain) before starting at NSIRC. She is part of the Innovative Metal Processing Centre for Doctoral Training (IMPaCT) at the University of Leicester, as well as supported by Lloyd's Register Foundation. The aim of her PhD is to provide fundamental knowledge of the corrosion protection offered by thermal spray coatings in marine environments by a combination of laboratory and field tests. This will contribute to the design of thermal spray coatings for offshore applications in order to mitigate corrosion of carbon steel structures, aiming to reduce the high costs and risks associated with marine environments.

Evaluation of corrosion protection offered by sacrificial thermal spray coatings for offshore applications

Shiladitya Paul[1], Rob Thornton[2]
[1]TWI, [2]University of Leicester
4th Year of PhD

Keywords: marine corrosion, thermal spray coatings, cathodic protection

I. INTRODUCTION

Marine environments are highly corrosive for offshore structures made of carbon steel such as oil and gas platforms, pipelines or wind farms. Corrosion mitigation in this environment can be achieved by metallic coatings, such as Thermal Spray Aluminium (TSA). These coatings consist of finely dispersed molten or semi-molten aluminium particles deposited onto the steel substrate by a high temperature and high velocity gas stream.

TSA acts as a physical barrier against the harsh environment, and also provides cathodic protection in case of coating damage [1]. In addition, due to cathodic polarisation, chemical reactions on the surface occur on exposed steel and calcareous deposits precipitate on top of the steel acting as an additional barrier against the environment.

With the UK as one of the world leaders in offshore wind power, corrosion of these structures could cause loss of assets and concerns about safety. Therefore, this work aims to provide a better understanding of the long-term offshore corrosion performance of TSA coatings by means of electrochemical measurements and surface characterization of the deposits formed both in laboratory and real marine environments.

II. METHODOLOGY

Low carbon steel (S355) coupons (40 x 40 x 6 mm) were coated with 250 ± 50 μm of commercially pure aluminium (Al 1050, 99.5 % Al) by Twin Wire Arc Spray (TWAS).

Circular defects were machined post-spray at the centre of each sample (covering 5 % of sample surface area), in order to simulate coating damage or failure.

All electrochemical measurements were carried out using a three-electrode cell configuration; TSA samples as working electrode, Ag/AgCl (KCl sat.) as reference electrode and platinum/titanium wire as counter electrode. Artificial seawater (ASTM D1141) was used as electrolyte in individual cells maintained at 25 ± 2 °C. Electrochemical techniques used to study the corrosion protection mechanism of TSA coatings:

- Polarization curves
- Open Circuit Potential (OCP)
- Linear Polarization Resistance (LPR)
- Voltammetry Around OCP (VAOCP)
- Electrochemical Impedance Spectroscopy (EIS)

Samples were also exposed to a real marine environment at Les Minimes (La Rochelle, France) in collaboration with the "Laboratoire des Sciences de l'Ingénieur pour l'Environnement (LaSIE)". Electrochemical measurements and post-exposure surface characterization was performed following same procedures as laboratory exposed samples.

Corrosion products on the surface of the of the specimens were characterised by Scanning Electron Microscopy and Energy Dispersive X-Ray spectroscopy (SEM/EDX), Raman spectroscopy and X-Ray Diffraction (XRD).

III. RESULTS AND DISCUSSION

Aluminium coatings are used to protect carbon steel structures in marine environments due to two main factors:

- Aluminium is less noble than steel in the galvanic series, therefore providing cathodic polarisation in case of coating damage

Due to the pH of seawater, aluminium pseudo-passivates reducing its self-corrosion rateThe long-term behaviour of TSA in marine environments is commonly studied through LPR measurements. It is a non-invasive method that provides instant corrosion rates (CR). However, it presents some limitations as it requires an active general corrosion mechanism. As aluminium pseudo-pasivates and can present localised corrosion in seawater, TSA samples with defects were also studied by VAOCP and EIS measurements. The results from these techniques provided a better understanding of the corrosion protection mechanism offered by TSA coatings to protect offshore structures. With these techniques, the pseudopassivation behaviour of Al was taking into account to calculate more
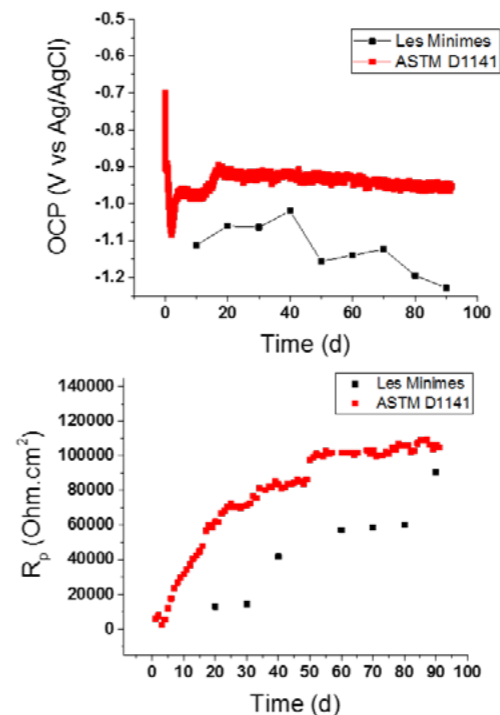
accurate CR, which correlate well with the ones obtained through LPR.

Figure 1. OCP and Rp comparative of TSA samples with 5 % of surface area defect to laboratory (ASTM D1141) and real marine environments (Les Minimes).

In order to observe the influence of the environment and evaluate how laboratory tests can predict the long term performance of TSA coatings, electrochemical measurements were recorded in situ at a real marine environment (Les Minimes, France) and compared to the ones obtained through controlled laboratory tests with artificial seawater. Potential values (OCP) and polarization resistance (Rp) data of TSA samples were collected over 90 days of exposure (Figure 1).

From these graphs, a good correlation can be observed between artificial and real

environments. In both cases, TSA samples with defects show cathodic polarization of the steel substrate with OCP values below -0.8 V.

Polarization resistance measurements recorded by LPR increase over time in both cases, showing values over 100 kΩ cm2 on the sample tested in a controlled environment and final value of over 90 kΩ cm2 on the sample exposed at Les Minimes. These values would translate into corrosion rates of less than 20 μm/year, therefore TSA coatings can protect offshore structures over 20 years.
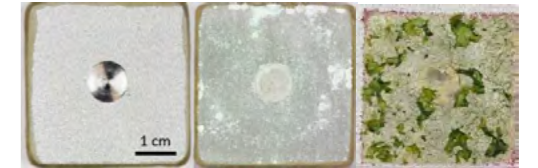

Figure 2. Photographs of TSA samples with 5 % of surface area defect before (left), after exposure to artificial seawater for 90 days (centre) and after exposure at a real marine site for 90 days (right).

Figure 2 shows images of TSA samples with defects before and after exposure to laboratory and real marine environments, showing the formation of deposits on top of coating and defect areas. In addition, the sample exposed at Les Minimes presents algae coming from the environment.

Surface characterization by SEM/EDX, Raman and XRD revealed same compouds independently of exposure to laboratory or real marine environments. On top of the TSA coatings, aluminium oxides/hydroxides were identified as a result of corrosion protection offered. On top of the defects, a bilayer of brucite and aragonite was identified. These are the so called calcareous deposits that precipitate as a result of the cathodic polarization provided to the steel substrate.

IV. CONCLUSIONS

From a combination of electrochemical techniques and exposure to laboratory and real marine environments, it has been shown that TSA coatings can provide corrosion protection to carbon steel offshore structures for over 20 years.

V. ACKNOWLEDGEMENTS

VI. REFERENCES

[1] H. S. Lee, A. Mohamed, B. C. Hong, "Arc thermal metal spray for the protection of steel structures: An overview." Corrosion Reviews 33.1-2 (2015): pp. 31-61

Oliver Logan

Oliver studied his Masters in Mechanical Engineering at the University of Bristol, graduating in June 2018. He started his PhD in September 2018 at the University of Bristol and TWI Ltd. He is a member of NSIRC and the Solid Mechanics Research Group. His PhD investigates the effects notch tip radius of non-sharp defects has on fracture toughness assessments. This work was co-funded by the Industrial Members of TWI as part of the Core Research Programme and the University of Bristol via a PhD programme. The work was enabled through, and undertaken at, the National Structural Integrity Research Centre (NSIRC), a postgraduate engineering facility for industry-led research into structural integrity established and managed by TWI through a network of both national and international Universities.

Assessing constraint effects in notched modified boundary layer models

Isabel Hadley[1], Nicolas Larrosa[2]
[1]TWI Ltd, [2]University of Bristol
2nd Year of PhD

Keywords: Notch Effect, Constraint, Two-parameter Fracture Mechanics, Modified Boundary Layer Models

I. INTRODUCTION

Structural integrity assessment procedures conventionally categorise flaws either as infinitely sharp cracks or local thinned areas (LTAs) [1], [2]. Defects failing an LTA geometry check are assumed to be sharp cracks and are assessed using a fracture mechanics-based approach.
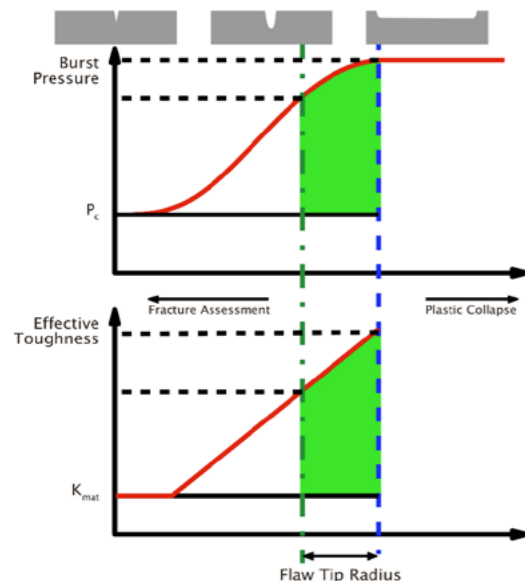
Figure 1: Effect of flaw tip acuity on plastic collapse load and apparent fracture toughness. The black line shows the current value used and the red line shows the expected behaviour.

Although real world defects are often sharp defects or LTAs, they can lie somewhere in between - a non-sharp defect. Figure 1 shows the expected behaviour as defects transition between sharp defects and LTAs, highlighting the excessive conservatism that might be added to an assessment by simplifying a non-sharp defect into a sharp crack. As a result, there is the need to develop procedures that assess non-sharp defects more realistically [3]–[5]. This change in defect severity from sharp to non-sharp can be considered an in-plane constraint loss.

It was also recently observed that specimens that would satisfy minimum thickness requirements for a fatigue pre-cracked test in typical fracture toughness tests (e.g. ASTM E1820-18 [6]) may not be appropriate for non-sharp defects [7], [8]. The change of the defect from sharp to non-sharp also influences the out-of-plane constraint.

This work seeks to unify the procedures by which non-sharp defects and constraint effect are addressed in fracture assessments by means of applying a two-parameter fracture mechanics approach based on J and Q.
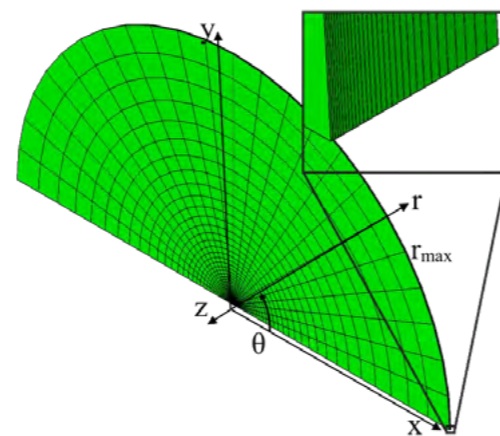
Figure 2: 3D modified boundary layer model.

II. DESIGN

In this work, 3D modified boundary layer (MBL) models (see, Figure 2) have been used to assess the effects of notch tip radius and in-plane and out-of-plane constraint effects on stresses ahead of the crack tip, measured halfway through the thickness.

The loadings were applied uniformly across the disc thickness at $r = r_{max}$ using displacement boundary conditions defined by the stress intensity factor, K_I, and far field T-stress, T. These were defined by:

$$u_x = \frac{K_I}{2\mu}\sqrt{\frac{r}{2\pi}}\cos\left(\frac{\theta}{2}\right)\left[\kappa - 1 + 2\sin^2\left(\frac{\theta}{2}\right)\right] + \frac{1-v}{2\mu}Tr\cos\theta \quad (1)$$

$$u_y = \frac{K_I}{2\mu}\sqrt{\frac{r}{2\pi}}\sin\left(\frac{\theta}{2}\right)\left[\kappa + 1 - 2\cos^2\left(\frac{\theta}{2}\right)\right] + \frac{(-v)}{2\mu}Tr\sin\theta \quad (2)$$

and $u_z = 0$ to simulate plane-strain conditions, where μ is the shear modulus, v is the Poisson's ratio and $\kappa = 3 - 4v$. A wide range of analyses for loadings of the same K_I (and J) and varying T/σ_0 ratios were carried out.

Two-parameter fracture mechanics (J-Q) was used to characterise the in-plane stress fields under different levels of constraint and for various notch tip radius. This is a unique framework to quantify the level of deviation of the stress/strain fields from high crack tip constraint conditions - a 2D plane-strain MBL model with a crack (T=0) - for both types of effects.

III. FINDINGS

The results of the MBL models have shown effects of changing the levels of constraint. Figure 3 shows the relationship between Q and T/σ_0 for the high constraint 2D model compared to 3D models. As thickness increases, Q also increases. But the change to non-sharp defect causes Q to decrease.

IV. DISCUSSION

The results showed a plane constraint level increase in the MBL models as the thickness increased; achieving plane strain conditions at $T/\sigma_0 < 0.6$ (i.e. a less constrained specimen design could represent plane strain conditions if a thicker specimen was used). These results also showed the effects of the increasing notch radius, what could potentially be considered a loss of constraint.

It has been shown that the in-plane effects of the notch tip radius could be combined with an overall constraint level. This would allow a blunt notch to be assessed as a sharp defect by modifying the level of constraint. Therefore, the current R6 [2] constraint approach, equation $III.7.6$:

$$K_{mat}^c = K_{mat}[1 + \alpha(-\beta L_r)^m]; \quad (3)$$

where K_{mat} and K_{mat}^c are the fracture toughness and the constraint dependent fracture toughness respectively, α and m are material and temperature dependant constraints and $\beta = Q/L_r$; and similar approach from BS 7910:2020 Annex N [1], could be used to assess specimens containing non-sharp defects by applying a modification to the constraint applied to assessments based on sharp defects.
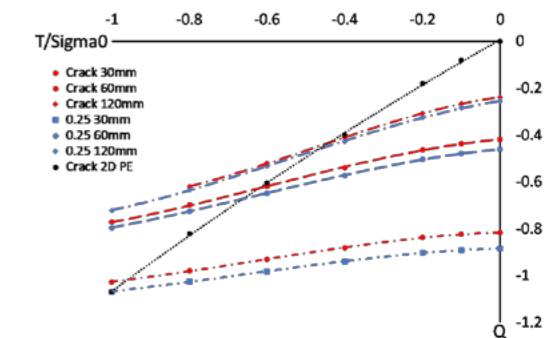

Figure 3: The effects on constraint caused by changing specimen thickness and defect radius.

V. FUTURE PLAN

The next steps for the project will be to investigate these effects with a large experimental testing programme of single edge notch bend (SEN(B)) specimens to demonstrate the effects of specimen thickness on notch fracture toughness. These results could be used to validate numerical models. References:

[1] BSI, "BS 7910:2019 Guide to methods for assessing the acceptability of flaws in metallic structures." BSI, p. 535, 2019.

[2] British Energy Generation Limited, "R6: Assessment of the Integrity of Structures Containing Defects, Revision 4 (Incl. Amendments to November 2011)," EDF Energy Nuclear Generation Ltd. Barnwood, Gloucester, 2013.Some text here.

[3] J.-J. Han, N. O. Larrosa, Y.-J. Kima, and R. A. Ainsworth, "Blunt defect assessment in the framework of the failure assessment diagram," Int. J. Press. Vessel. Pip., vol. 146, pp. 39–54, 2016.

[4] J. S. Kim, N. O. Larrosa, A. J. Horn, Y. J. Kim, and R. A. Ainsworth, "Notch bluntness effects on fracture toughness of a modified S690 steel at 150 °C," Eng. Fract. Mech., vol. 188, pp. 250–267, 2018.

[5] A. J. Horn, S. Cicero, A. Bannister, and P. J. Budden, "Validation of the Proposed R6 Method for Assessing Non-Sharp Defects," Vol. 6B Mater. Fabr., p. V06BT06A010, 2017.

[6] American Society for Testing and Materials, "ASTM E1820-18. Standard test method for measurement of fracture toughness," ASTM, Annu. B. Stand., vol. 3, 2006.

[7] A. J. Horn, A. H. Sherry, and P. J. Budden, "Size and geometry effects in notched compact tension specimens," Int. J. Press. Vessel. Pip., vol. 154, pp. 29–40, 2017.

[8] A. J. Horn, S. Cicero, and D. Andrés, "Out-of-plane constraint loss in three point bend specimens with notches," Int. J. Press. Vessel. Pip., vol. 180, p. 104025, Jan. 2020.

Konstantinos Kouzoumis

Kostas is currently in the third year of his PhD at the University of Bristol and TWI Ltd. His research focuses on investigating the effect of load biaxiality on the integrity of cracked components and the current capabilities of fitness for service standards in addressing it. He is sponsored by the UK Engineering and Physical Sciences Research Council and TWI Ltd and conducts his research in both facilities. Prior to starting his PhD in July 2017, Kostas completed his diploma in Marine Engineering and Naval Architecture at the National Technical University of Athens. Kostas believes this research will contribute towards the more accurate assessment of components under complex loading, and ensure safety of such components whilst saving time and reducing costs.

Capturing the effect of biaxiality on upper and lower shelf

Isabel Hadley[1,2], Mahmoud Mostafavi[2]
[1]TWI, [2]University of Bristol
3rd Year of PhD

Keywords: biaxiality, upper-shelf, lower-shelf, Experiment

I. INTRODUCTION

Engineering components such as pressure vessels are usually subject to pressure, residual stresses generated from welds during manufacturing and thermal stresses. Such complex loading often creates a multiaxial stress state.

Substantive research has been conducted to address the effect of load biaxiality on integrity [1]. On the lower shelf, load biaxiality increases the crack tip multi-axiality and thus increases plastic constraint, or in other words, it suppresses the flow of plasticity. It has been shown that there is a decrease in the critical value of the energy release rate (Jc) at fracture with increasing plastic constraint. Even though this effect has been quantified, very few and specific component-loading cases are currently included in fitness-for-service (FFS)) procedures.

On the upper shelf of fracture toughness, there has been an observed trend of biaxiality affecting the plastic collapse load [2] which is also supported by limited existing experimental work that attempts to address this behavior [3].

II. METHODOLOGY

To capture the effect of biaxiality on constraint/fracture toughness and plastic collapse, an experimental programme is currently underway. Test specimens are extracted from a BS1501- 224 28B mild ferritic steel plate (Young's Modulus= 191 GPa, Yield Stress = 307 MPa, Ultimate Tensile Strength = 471MPa) and will be tested at three different temperatures ranging from lower shelf to upper shelf.

The specimens are of cruciform or rectangular shape, shown in Figure 1 and Figure 2

respectively, and contain through thickness sharp cracks developed with fatigue pre-cracking. They are loaded in uniaxial or equibiaxial bending with respect to their geometry. The test setup of a biaxially loaded specimen can be seen in Figure 3, where a semispherical punch will be pushed downwards creating a 5-point bend. Test setup limitations allow only for load – crack mouth opening displacement curves (CMOD) to be recorded during testing.
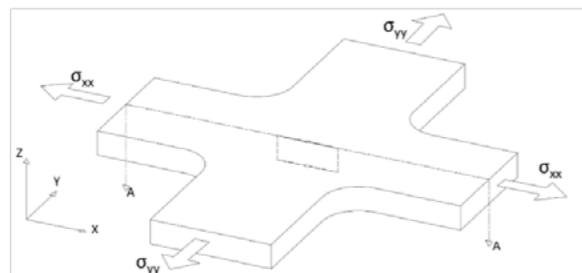
Figure 1. Cruciform ppecimen–biaxially loaded
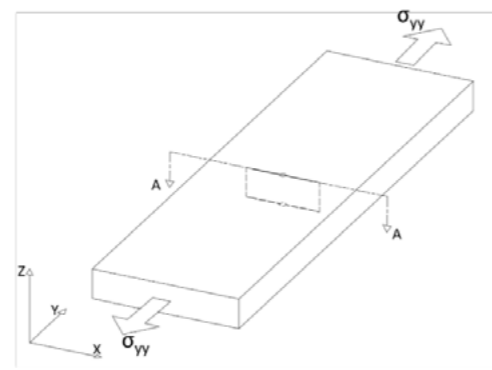
Figure 2. Rectangular ppecimen–uniaxially loaded

In order to test whether the experimental setup does capture, biaxiality PMMA samples were initially used. These had the same geometry as

the steel samples; however the cracks were sawn instead of fatigue pre-cracked. PMMA tests were executed at room temperature, in displacment control (0.2 mm/min).
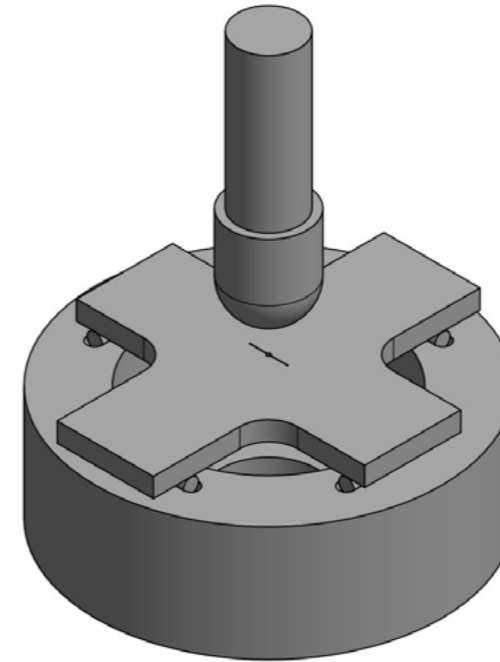

Figure 3. Setup of a 5-point bend test

III. FINDINGS

Post fracture PMMA samples can be seen in Figure 4 for a uniaxial specimen, and Figure 5 for a biaxial specimen. It is observed in the latter that the fracture trajectory has an "S" shape. This effect of the curved crack has been noted in literature [4] as an effect of biaxiality. Hence, the trajectory of the crack observed in these specimens provides confidence that the current setup captures biaxiality.
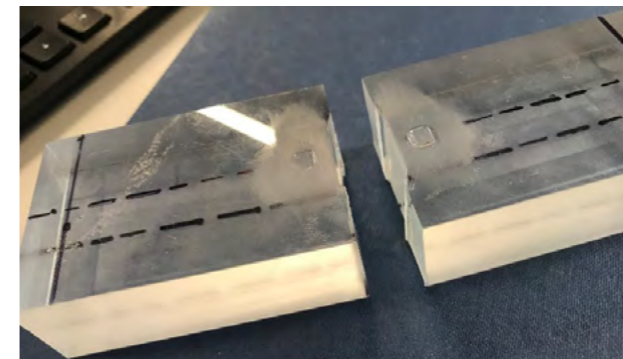

Figure 4. PMMA Uniaxial specimen - post fracture

IV. DISCUSSION

An experimental programe is currently under development to capture the effect of biaxiality on fracture toughness and plastic collapse throughout the ductile to brittle transition region. The setup proposed has been tested with the use of PMMA samples for its capability to do so. The

current results give confidence on the setup since the crack trajectory of the tested samples has the characteristic "S" shape, found when loads are applied simultaneously perpendicularly and parallel to the crack.

Figure 5: PMMA biaxial specimen - post fracture

V. FUTURE PLAN

The final step to validate the current test setup is to conduct finite element analyses (FEAs), from which the fracture toughness of each specimen geometry will be calculated. Once a lower fracture toughness is confirmed for the biaxially loaded specimens, testing of the steel specimens will commence.

Steel samples will be initially tested at -160oC with the use of a cooling chamber and liquid nitrogen gas as a coolant. Additional tests will be conducted at room temperature as well as a third temperature that will be decided based on the results of the previous testing.

REFERENCES

[1] Lidbury, D. P. G. et al. 2006. "Validation of Constraint-Based Methodology in Structural Integrity of Ferritic Steels for Nuclear Reactor Pressure Vessels." Fatigue & Fracture of Engineering Materials & Structures 29(9–10): 829–49.

[2] Hadley, I. 2018. Validation of BS 7910:2013 and R6 Fracture Assessment Procedures: Uniaxial and Biaxial Wide Plate Tests on A533B Steel. TWI Ltd. Industrial Member Report 1107/2018.

[3] Østby, Erling, and Asle O. Hellesvik. 2008. "Large-Scale Experimental Investigation of the Effect of Biaxial Loading on the Deformation Capacity of Pipes with Defects." International Journal of Pressure Vessels and Piping 85(11): 814–24.

[4] P. S. Leevers, J. C. Radon, and L. E. Culver, 'Fracture trajectories in a biaxially stressed plate', Journal of the Mechanics and Physics of Solids, vol. 24, no. 6, pp. 381–395, Dec. 1976, doi: 10.1016/0022-5096(76)90010-7.

Domenic Di Francesco
Domenic graduated from Durham University in 2012 with an MEng in mechanical engineering. He has since worked for consultancies providing structural integrity engineering services, predominantly in the oil and gas industry. He is a chartered engineer and member of the Institution of Mechanical Engineers. His research is sponsored by Lloyd's Register Foundation and focuses on Bayesian methods of modelling fatigue crack growth and quantification of the value of imperfect inspection information. This presentation will describe how Bayesian methods can account for the variability and commonality between multiple sets of fatigue tests and how the out of sample predictive accuracy of alternative / competing models can be quantified. This is based on a piece of work that has been submitted for possible publication [1]

Improved estimation of fatigue crack growth rate by partial pooling of test data in Bayesian models

Dr Ujjwal Bharadwaj[1], Professor Marios Chryssanthopoulos[2], Professor Michael Havbro Faber[3]
[1]TWI, [2]University of Surrey, [3]Aalborg University
3rd Year of PhD

Keywords: Bayesian modelling, dependency, fatigue crack growth, Markov chain Monte Carlo (MCMC) sampling, information theory

I. INTRODUCTION
Probabilistic methods can allow engineers to quantify the epistemic and aleatoric uncertainty associated with degradation models, and propagate this uncertainty so that it can be accounted for in predictions and decision analysis.

Modern Bayesian computation, based on a family of algorithms known as Markov Chain Monte Carlo (MCMC) samplers, can be used to estimate high-dimensional, joint posterior distributions of model parameters, conditional on a model structure, test data, and priors [2].

This work is an application of Bayesian statistics to the data that is used to inform the recommendations for predicting fatigue crack growth rates in BS 7910 [3].

II. BAYESIAN DATA ANALYSIS
The current guidance in BS 7910 is based on a spreadsheet analysis of data aggregated from multiple studies [4]. The model described in Equation 1 was proposed based on qualitative justification.

$$\frac{da}{dN} = \begin{cases} A_1 \cdot \Delta K^{m_1}, \ \Delta K < \Delta K_{TR} \\ A_2 \cdot \Delta K^{m_2}, \Delta K \geq \Delta K_{TR} \end{cases}$$

Equation 1: Bi-Linear Crack Growth Model

A Bayesian approach to fitting this model, based on data associated with a 'high' stress ratio and a freely corroding environment is fully detailed in [1]. Note that this includes a model uncertainty parameter, σ. MCMC samples from the posterior distribution are presented in Figure 1. This shows the uncertainty within, and the dependency between all model parameters. Both features are accounted for in Bayesian models.
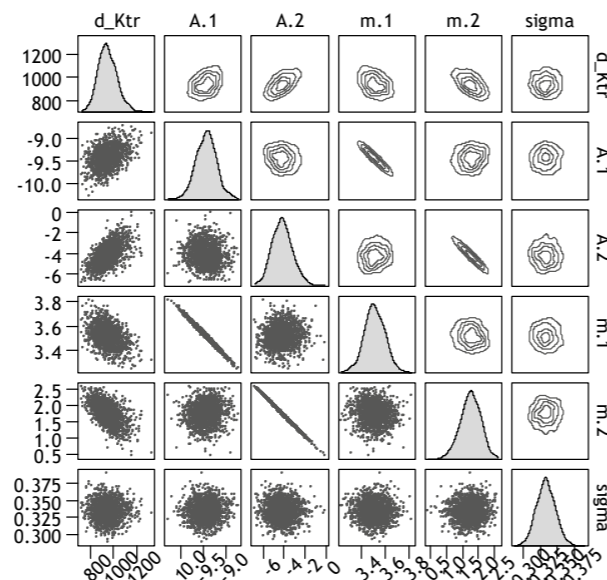
Figure 1: Posterior Distribution of Fully Pooled Bayesian Model.

III. POOLING OF INFORMATION
The 'high' stress ratio, freely corroding fatigue crack growth rate dataset is, itself comprised of 11 constituent tests. Differences between these tests include material strength, (exact) stress ratio and loading frequency. When data from non-identical tests are aggregated (or 'pooled'), the resulting model will not account for any variability between them. Such a model is described in Figure 2(a). Fully pooled models can only be used to make predictions at the population level.

Alternatively, separate models could be fit to each test, as described by the structure in Figure 2(b). A challenge associated with this approach is the reduced amount of data available for each model. Independent models can only be used to make predictions at the test level.

A solution in between these two extremes can be achieved by structuring a model as shown in Figure 2(c). A regression analysis is performed to simultaneously estimate the model parameters and the parameters of global prior models, which determine the extent of regularisation. This results in partial pooling of information between the tests, the extent of which is estimated from the data. Partial pooling models can be used to make predictions at the population and test levels.
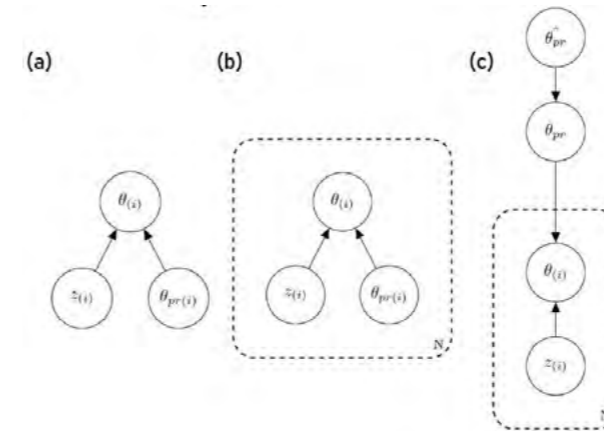

Figure 2: Structure of Alternative Bayesian Models:

(a) Fully Pooled Bayesian Model for Estimating Parameters, θ, from data, z, and Priors, θ_{pr}

(b) N Independent Bayesian Models

(c) Partial Pooling Bayesian Model for Estimating Parameters, θ, from data, z, Priors Models, θ_{pr}, and Hyperpriors $\widehat{\theta_{pr}}$

IV. FINDINGS/RESULTS
For each of the model structures described in Figure 2, a total of $10{,}000$ (post warm-up) samples of the joint posterior distribution were collected from each of 4 separate Markov chains. There were no indications of a lack of convergence, or excessive autocorrelation in any of the chains. This analysis was completed using the probabilistic programming language, Stan [5, 6].

The results of these models are shown in Figure 3, alongside the test data. There is more uncertainty associated with the partial pooling model than the fully pooled model and this reflects the additional source of variability that it incorporates.

In general, partial pooling of information is expected to result in improved performance because predictions will only be informed by other tests to the extent that the data suggest they should. The out of sample predictive accuracy (as characterised by the Watanabe Akaike Information Criterion [7]) is higher for the multi-level (partial pooling) models than for the equivalent fully pooled models. This work also shows that all of the Bayesian models considered,

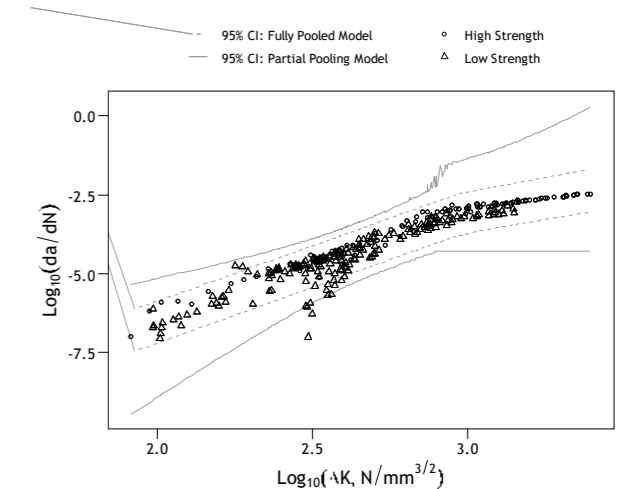performed better than the existing guidance in BS 7910.

Figure 3: Bayesian Credible Intervals (CI's) of Posterior Predictive Distributions of Alternative Fatigue Crack Growth Rate Models for a Freely Corroding Environment and a High Stress Ratio.

V. ACKNOWLEDGEMENTS

REFERENCES
[1] D. Di Francesco, M. Chryssanthopoulos, M. H. Faber, and Ujjwal Bharadwaj, "Consistent Treatment of Uncertainties and Dependencies in Fatigue Crack Growth Calculations Using Multi-Level Bayesian Models," Reliab. Eng. Syst. Saf, [SUBMITTED FOR POSSIBLE PUBLICATION].
[2] M. Betancourt, "The Convergence of Markov Chain Monte Carlo Methods: From the Metropolis Method to Hamiltonian Monte Carlo," Ann. Phys., vol. 1700214, pp. 1–6, 2018.
[3] BSI, "BS 7910:2019 Guide to methods for assessing the acceptability of flaws in metallic structures," London, 2019.
[4] R. N. King, "HSE Offshore Technology Report OTH 511: A Review of Fatigue Crack Growth Rates in Air and Seawater," 1998.
[5] B. Carpenter et al., "Stan : A Probabilistic Programming Language," J. Stat. Softw., vol. 76, no. 1, 2017.
[6] [1] Stan Development Team, "RStan: the R interface to Stan," 2018.
[7] S. Watanabe, "Asymptotic Equivalence of Bayes Cross Validation and Widely Applicable Information Criterion in Singular Learning Theory," J. Mach. Learn. Res., vol. 11, pp. 3571–3594, 2010..

Hadi Khalili

Hadi received his education in Civil Engineering from the Sharif University of Technology (BSc) and Tarbiat Modares University (MSc) in Iran. Sponsored by Lloyd's Register Foundation, his PhD study focuses on improving the reliability assessment of offshore structures. The improvement in reliability assessment is by using Bayesian methods to the uncertain parameters distribution (crack size) using real inspection data, thereby establishing more realistic assumptions for future reliability assessments.

Bayesian updating of the fatigue crack size distribution

Dr. Selda Oterkus[1] Prof. Nigel Barltrop[1] Dr. Ujjwal Bharadwaj[2]
[1]University of Strathclyde, [2]TWI
3rd Year of PhD

Keywords: Fatigue, Crack size distribution, Inspection, Bayesian updating

I. INTRODUCTION

Offshore structures are likely to be fatigue damaged due to high-stress concentration and random cyclic wave loading. To assess the state of fatigue damage, offshore platforms are periodically inspected. Inspection results can be used to update the probability distribution of crack size in a tubular joint in offshore platforms. The Bayesian framework is used to update the probability distributions of the fatigue uncertainties such as crack size in tubular joints.

II. APPROACH

A. Fatigue Reliability Analysis

In the Fracture Mechanics approach, the relationship between the crack growth rate and stress intensity factor can be developed using the Paris law:

$$da/dN = C \times (\Delta K)^m \quad (1)$$

$$\Delta K = Y \times \Delta S \times \sqrt{\pi a} \quad (2)$$

Where a represents the crack size, N is the number of load cycles, C and m are the crack growth parameters and ΔK represents the stress intensity range.

By plugging Eq.(2) into Eq.(1), and integrating from the initial crack size to the crack size at time t, the crack size can be obtained as:

$$a_t = \left\{ a_0^{1-\frac{m}{2}} + \left(1 - \frac{m}{2}\right) Y^m \times \pi^{\frac{m}{2}} \times C \times N \times \Delta S^m \right\}^{\frac{1}{1-\frac{m}{2}}} \quad (3)$$

The probability of failure can be calculated by using a limit state function. It is assumed that failure occurs when the crack size is bigger than its critical value:

$$g = a_c - a_t \quad (4)$$

Where a_c represents the critical crack size. In this study, the critical crack size is taken as the wall thickness of the tubular joint [1]. The considered uncertainties in this study are:

- Initial crack size (a_0); $Exp\,(0.11\,mm)$

- Material property (C): $LN\,(1.8 \times 10^{-12}, COV = 0.35)$

- Stress range (ΔS^m): $LN\,(300\,MPa, COV = 0.1)$

B. Bayesian Framework

When additional information becomes available, the obtained information can be used to improve the previous estimate of uncertain parameters. The framework for updating the distribution of the uncertain parameter is called the Bayesian framework. The distributions that describe our knowledge before and after incorporating new data are called Prior and Posterior distributions, respectively. The posterior distribution of the uncertain parameter (θ), given new information, is available (x), can be obtained by using Bayes' theorem as [2]:

$$f(\theta|x) = \frac{f(x|\theta) \times f(\theta)}{f(x)} \quad (5)$$

Where $f(\theta|x)$ is posterior distribution, $f(x|\theta)$ is likelihood function, $f(\theta)$ is prior distribution and $f(x)$ is a normalisation factor that makes the area under posterior distribution equal to one. In general, numerical integration is required to obtain the posterior distribution.

(a) Prior Distribution

In this study, a sampling method is used to obtain the prior distribution of the crack size. To obtain the prior distribution for crack size, a large number of samples (e.g.10^5) is generated from the probability density function of each uncertain parameter (i.e. a_0, C and ΔS^m). For each set of random samples, the crack size is calculated based on Eq.(3). The histogram of the simulated crack size is then used as a prior distribution.
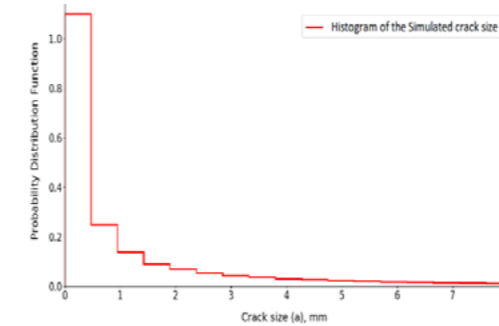

Figure 1- Prior crack size distribution

(b) Likelihood Function

The likelihood function is defined based on the expert's belief to take into account the involved uncertainties. The likelihood function can be represented as a non-normalised normal distribution as:

$$L = \exp\left(-\frac{(a - a_m)^2}{2\sigma^2}\right) \quad (6)$$

Where a_m represents the measured crack size, a is the crack size and σ is the standard deviation of crack size. In this study, a standard deviation of 0.5mm is considered for a likelihood function.
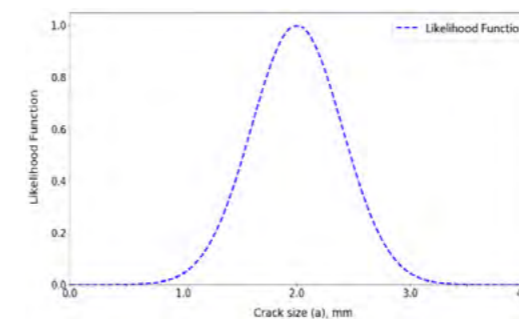

Figure 2- Likelihood function

It is assumed that ten observations ($N_{ins} = 10$) of crack sizes are available. A normal distribution with a mean value of 2mm and a standard deviation of 0.2mm is assigned to the inspection results. It is also assumed that these inspections are independent of each other.

In the Bayesian updating approach, the posterior distribution needs to be updated for each observed crack size. Therefore, the probability distribution function of crack size is updated N_{ins} times sequentially by using Eq.(5). The obtained posterior is assumed as the prior distribution for the next updating process. Therefore, the updating procedure is a computationally expensive process.

Figure 3 illustrates that the posterior distribution shifts towards the observations, i.e. the observed data dominate the posterior distributions.
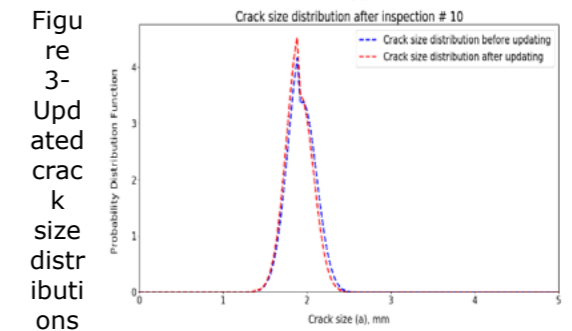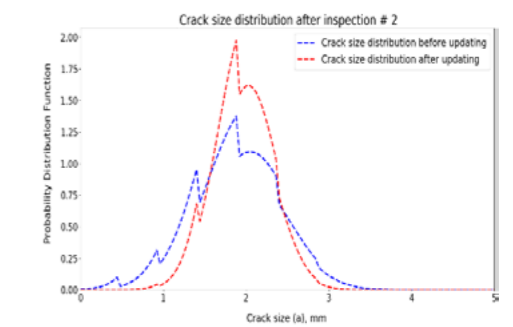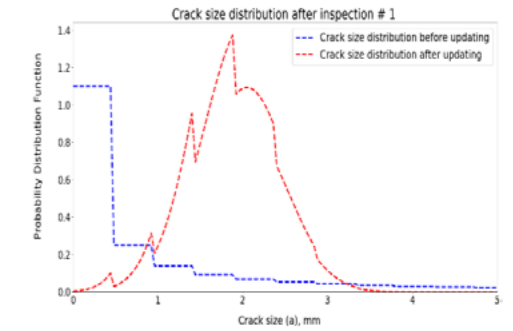

Figure 3- Updated crack size distributions

C. Conclusion

The Bayesian approach is used to update the distribution of the crack size when new information is available. In this approach, the posterior distribution is obtained by multiplying likelihood function and prior distribution.

III. ACKNOWLEDGEMENTS

REFERENCES
[1] Wang W., Shi Y., Wang C. "New method for system fatigue reliability analysis of offshore steel jacket," Advances in Structural Engineering, Vol. 9, 2006
[2] K.-V. Yuen, "Bayesian Methods for Structural Dynamics", John Wiley & Sons, 2010

Matthew Weltevreden
Matthew is in the second year of his PhD with the University of Bristol and is currently based in the Fracture Integrity Management section of TWI. He graduated from the University of Hull with a BEng in Mechanical Engineering and from the University of Bath with an MSc in Automotive Engineering. Matthew's PhD focuses on weld residual stress with specific application of probabilistic methods for pipeline girth welds.

Review of the treatment of weld residual stress in BS 7910 fracture assessment

Isabel Hadley[1], Harry Coules[2]
[1]TWI, [2]University of Bristol
2nd Year of PhD

Keywords: BS 7910, Annex Q, probabilistic assessment

I. INTRODUCTION

The procedure provided in BS 7910 [1] 'Guide to methods for assessing the acceptability of flaws in metallic structures' regarding weld residual stress is outlined in Annex Q. Annex Q is used for investigating serviceability and the failure likelihood of welded structures of varying joint types. The non-uniform residual stress profiles have been part the annex since the first publication of BS 7910 in 1999, based on a compendium of experimental data available at the time. One of its key purposes is to provide the user with simple measures to estimate the non-uniform residual stress distribution. For pipe girth welds, this can be estimated using two key parameters (1) the material type (austenitic or ferritic) and (2) the weld heat input. This assessment can be applied to cases that occur outside controlled environments, where in most of these cases, performing residual stress measurements can be costly and time consuming. The current upper bound distributions in Annex Q have remained unchanged since first publication, despite new information and measurement techniques becoming available. This paper aims to provide an overview of the literature relevant to the upper bound residual stress distributions, and present possible avenues of improving and updating them.

II. LITERATURE REVIEW

The key studies referenced in the BS 7910 1999 edition will be briefly analysed to give an overview of the residual stress knowledge accepted at the time. Scaramangas [2] and Leggatt [3] were significant contributors in the creation of the upper bound distributions given in Annex Q. Each study consisted of bringing together known data to capture general trends. Though they used similar techniques, the conclusions drawn by Leggatt, to partition residual stress distributions centred on heat input, were implemented into the 1999 edition of BS 7910 (Figure 1). The results were formulated based on 10 individual experiments with differing welding parameters.
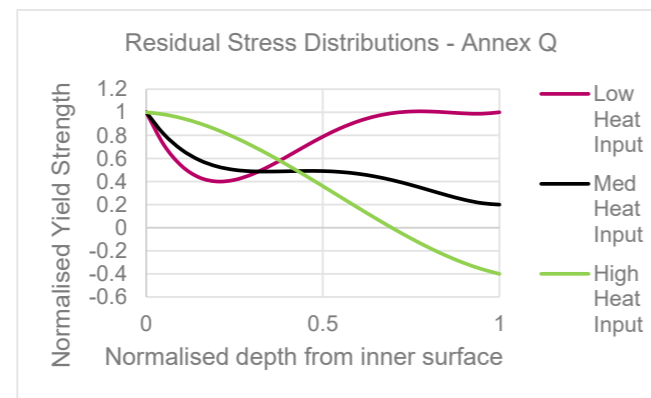
Figure 1. Residual stress distributions as presented in Annex Q

In 2012, the Health and Safety Executive [4] commissioned TWI to collect, analyse and update residual stress information regarding low heat input pipe girth welds. Excluding non-destructive methods, the data was combined and compared with the current upper bound distributions. Using an expanded database (of 9 datasets), the report proposed a new upper bound based on a 90% upper confidence limit. This recommendation however was not implemented into the 2013 or 2019 edition of BS 7910 due to lack of information regarding the original data sources outlined by Scaramangas. In addition, the document recorded significant presence of experimental variability (scatter) in results when combining the datasets. From the point of view of the standards, this is important as it makes it difficult to suggest a reliable upper bound which can apply to all cases with confidence. More recent studies which have addressed this include Mirzaee-Sisan and Wu [5] and Cathcart et al [6]. Mirzaee-Sisan and Wu analysed advances in measurement and modelling techniques between 2009 and 2019. The study highlighted some issues regarding the Annex Q distributions, stating that averaging the heat input across the entire weld is not sufficient to describe the non-uniform residual stress distribution at any location. It continues to report on the general variability of residual stresses, suggesting more specific consideration of underlying parameters (such as joint type) supported by further experiments is required. Importantly, the paper aimed to produce results which could not only be applied to specimens produced in controlled laboratory conditions but also to those in less closely controlled factory environments. Cathcart et al statistically examined the variability of residual stress in austenitic steel pipe girth welds using a Bayesian approach. Although the dataset in the study was small, there was potential to further develop the technique using additional measurements. One of the advantages of a Bayesian approach is the ability to quantify experimental scatter for use in a probabilistic framework, whereby a healthy level of conservatism can be maintained despite large weld-to-weld variability.

III. UPDATED DATABASE

This PhD project involves the development of a residual stress database which documents all relevant residual stress measurements in literature alongside their welding parameters (Table 1). This provides an overview of the available data and a basis for further statistical analysis.

No.	Outer Diameter, mm	Wall Thickness, mm	Weld Process	Base metal	Base metal yield strength, MPa	Heat Input, kJ/mm	Techniques
1	508	25.4	GMAW	X65	478	0.77	ND
2	400	50	TIG	CF8M	251 - 274	1.2	BRSL
⋮							
23	323.9	24.3	GMAW	X60	449 - 451	1.7	CHD & DHD
24	795	15.9	SAW	316L	338	2.2	ND, CHD, BRSL

Table 1. Database extract containing residual stress measurements on pipe girth welds

Partitioning data, based on similar parameters such as the base metal or measurement technique, will help develop a better understanding of variation regarding residual stress while highlighting the effect of different welding and measurement parameters.

IV. DISCUSSION

The literature analysed gives clear evidence of where the current BS 7910 upper bound distributions originate, however, the datasets used, although useful at the time, do not depict the scattering behaviour seen from the gathering of much larger data sources today. In addition, the methods for obtaining through-thickness residual stress data have improved significantly over the past 20 years, and introducing an extensive database can help shed light on the current issues regarding residual stress, especially concerning uncertainty and variability. Furthermore, this can be used to update BS 7910 based on experimental evidence and potentially offer advice for their treatment, either in deterministic or probabilistic assessments.

V. FUTURE WORK

There are several possibilities for updating our current procedures regarding the treatment of residual stress in failure assessments. One approach, as part of a wider industrial effort, is the development of a probabilistic framework to help quantify uncertainty in industry, ensuring that an appropriate level of conservatism can be met without becoming overly excessive. This framework can be reinforced through use of a database, encompassing the relevant information while identifying influential parameters which affect the resultant residual stress distribution. In addition, statistical methods such as a Bayesian approach could be used to manage datasets when partitioning information is based on these parameters. The purpose of this work is to improve the treatment of residual stress in Annex Q and help provide users with more reliable tools for assessing pipe girth welds in industry.

REFERENCES
[1] BS 7910 (2019) 'BSI Standards Publication Guide to methods for assessing the acceptability of flaws in metallic structures', BSI Standards Publication, (UK), p. 490.
[2] Scaramangas, A., Porter Goff, R.F.D. Residual stresses in cylinder girth butt welds. (1985) Proceedings of the Annual Offshore Technology Conference, 1985-May, pp. 25-30.
[3] Leggatt RH. Welding residual stresses. In: Proceedings of the fifth international conference on residual stresses, Linkoping, Sweden, 16–18 June 1997.
[4] Zhang, Y.-H. et al. (2012) 'Health and Safety Executive Residual stress measurements and modelling'.
[5] Mirzaee-Sisan, A. and Wu, G. (2019) 'Residual stress in pipeline girth welds- A review of recent data and modelling', International Journal of Pressure Vessels and Piping, 169, pp. 142–152. doi: 10.1016/j.ijpvp.2018.12.004.
[6] Cathcart, H., Horne, G., Moffat, A. The variability in weld residual stress. (2019) American Society of Mechanical Engineers, Pressure Vessels and Piping Division (Publication) PVP, 6B-2019.

Jessica Taylor
Jessica is a structural engineer with a special interest in fracture mechanics. She attained a BSc in Physics at Warwick University before joining Cranfield in 2015 for an MSc in Offshore Technology with Offshore Renewable Energy. For her thesis, she is investigating crack arrest as a method of fracture prevention in thick steel sheets, with applications in shipping and wind industries. Small scale testing will be correlated against large scale testing to predict the crack arrest properties of a range of structural steels. Jessica has presented at the 14th International Conference on Fracture (ICF14), the 38th International Conference on Ocean, Offshore & Arctic Engineering (OMAE2019) and participated in the Lloyds Register Foundation student competition 2018 and the STEM for Britain poster competition in 2019.

Correlation between initiation toughness and crack arrest toughness of steels predicted from small-scale testing.

Rob Kulka[1], Ali Mehmanparast[2]
[1]TWI, [2]Cranfield University
4th Year of PhD

Keywords: crack arrest; structral steel; small-scale testing

I. INTRODUCTION

The ability of a material to arrest a fast-running brittle crack is vital in various industries such as offshore wind, oil and gas, and shipbuilding in order to ensure the safety of the structure and the employees.

Some modern steels show a high Charpy toughness, but low resistance to crack propagation – i.e. low crack arrest toughness [1-3].

In this work, the relationship between initiation and arrest toughness is investigated in six different steels, including S355 structural steel, X65 pipeline steel, two high strength reactor pressure vessel (RPV) steels and EH47 shipbuilding steel.

II. DESIGN/METHODOLOGY/APPROACH

Small scale mechanical testing was carried out to determine the material properties, which were correlated against the microstructural characteristics of the materials.

The test program included instrumented Charpy, drop weight Pellini, fracture toughness, tensile testing, and optical and electron microscopy. Nil ductility transition temperature (NDTT) is used as a measure of arrestibility.

III. FINDINGS/RESULTS

Initiation fracture toughness (from CTOD testing) showed strong correlation with upper shelf Charpy and grain size measurements, which is shown in figure 1. These are accepted relationships [4,5] for modern steels and this agreement provides an additional level of confidence in the other results presented here. In this way, the steels behave as expected, with a small grain size providing high toughness (measured through both upper shelf Charpy and CTOD testing).
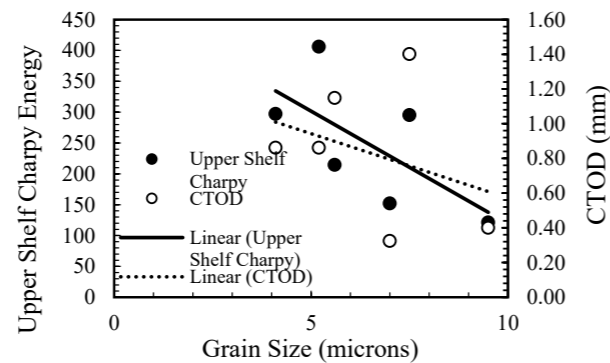
Figure 1: Correlation between grain size, upper shelf Charpy energy and CTOD.

However, figure 2 shows that there was no correlation between the initiation fracture toughness and the crack arrest toughness of the steels. This is concerning for modern steels, as upper shelf Charpy energy is commonly used as a design criterion for both fracture initiation and crack arrest performance.
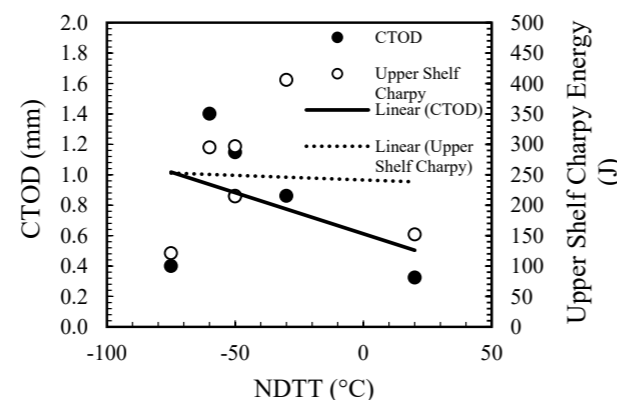
Figure 2: Correlation between NDTT (arrest parameter) and upper shelf Charpy energy (initiation parameter).

Figure 3 demonstrates that the arrest toughness is better correlated against the T(27J) temperature – i.e. the onset of the lower shelf. This relationship is valid even for steels where the NDTT lies on the upper shelf of the Charpy curve.
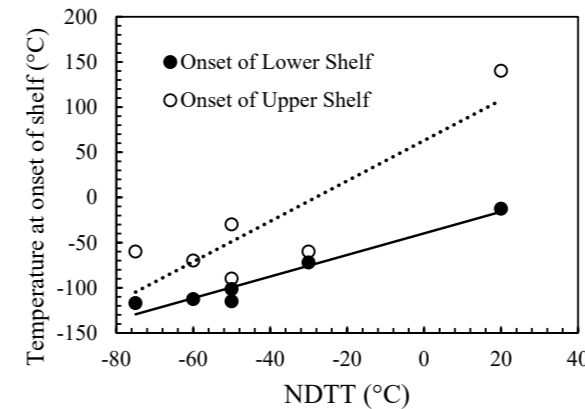
Figure 3: Correlation between lower and upper shelf Charpy temperature and NDTT

IV. DISCUSSION/CONCLUSIONS

The arrest properties cannot be correlated strongly to the materials' microstructure or initiation fracture toughness. It was expected that the NDTT would follow a similar trend as the upper shelf Charpy energy, with the fine-grained steel arresting crack propagation at a lower temperature, however this is not the case.

It is not recommended to use upper shelf CTOD or upper shelf Charpy energy as measures of crack arrestibilty in a material as there is no correlation between the two. However, there is some potential to using T(4kN) from instrumented Charpy tests, suggesting that the crack arrest behaviour is affected more by lower shelf or transition properties.

This work has shown that:

• The parameters which influence the crack arrest behaviour of modern structural steels are independent of those which provide these steels with upper-shelf fracture toughness.

• The crack arrest behaviour is more closely linked to the ductile to brittle transition temperature of the steel, such as T(27J) from Charpy testing.

• When steels are characterized only in terms of three fracture toughness tests, that is not sufficient to determine whether the steel could be at risk of unstable fracture from a localized brittle event, due to poor crack arrest toughness.

V. FUTURE PLAN/ DIRECTION

This test program will be continued in future work. Quantitative crack arrest testing in the form of "compact crack arrest" tests will be carried out on the EH47 shipbuilding steel to validate the predictions made from small-scale test methods.

These results will be further validated against the results of large-scale wide-plate crack arrest tests which have been carried out by researchers in Japan.

EBSD will be used to characterize fully the texture of the materials by including the grain orientation and correlating the materials' texture to their small-scale mechanical properties. Further correlations between mechanical and microstructural properties will be investigated for each of the materials to determine the relationship between microstructure and arrest.

If there remains no correlation, it is advised that an energy based approach is investigated to predict the arrest behaviour of the materials i.e. K(ca).

VI. ACKNOWLEDGEMENTS

REFERENCES
[1] X.K. Zhu, & B. Leis. 'Ductile-fracture arrest methods for gas-transmission pipelines using Charpy impact energy or DWTT energy.' Journal of Pipeline Engineering, 12 (3). (2013).
[2] A. Fonzo, G. Mannucci, J. M. Gray & S Mishel, 'Assuring safety against propagating cracking in gas pipelines made from modern steels with high upper shelf energy', JTM, Sydney Australia, 29th April - 3rd May, (2013).
[3] P. Moore, G. Duncan, N. Singh, and B. Bakthavathsalam, "Comparing Small-Scale Testing Approaches to Determine Crack Arrest in High Strength Steel," in Proceedings Structural Integrity 2018, (2018).
[4] Sandström, R., and Y. Bergström. "Relationship between Charpy V transition temperature in mild steel and various material parameters." Metal science 18 (4) (1984): 177-186.
[5] Armstrong, R. W. "The influence of polycrystal grain size on several mechanical properties of materials." Metallurgical and Materials Transactions B 1 (5) (1970): 1169-1176.

Faris Nafiah
Faris attained his Bachelor's degree in Electrical Engineering from the University of Auckland, New Zealand before joining International Islamic University Malaysia where he completed his Msc in Mechatronics Engineering in eddy current NDT. Sponsored by Lloyd's Register Foundation, his PhD with London South Bank University aims at developing a pulsed eddy current instrument that is capable of carrying out inspections for corrosion under insulation in pipelines. The key interest is to establish methods for fast pipe scanning while compensating the variations in various parameters variations during inspection.

Pulsed Eddy Current: Signal feature enabling in-situ calibration

Prof M. Osman Tokhi[1] Dr Duan Fang[1] Dr Zhanfang Zhao[1] Dr Shiva Majidnia[2]
[1]London South Bank University, [2]TWI
2nd Year of PhD

Keywords: pulsed eddy current, corrosion under insulation, signal feature

I. INTRODUCTION

Steel pipes in process plant applications are often covered with insulation or weather protection that make structural inspection difficult because the additional layers need to be penetrated. The pulsed eddy current (PEC) method was devised as a means of inspection through the surface layers. However, the performance of a PEC system is dependent on the electrical and magnetic properties of the pipe material, which are generally unknown. Therefore, the use of a calibration block from a different steel will give inaccurate results. The concept of calibrating using measurements obtained during inspection has not been discussed in the literature, which is the main contribution of this research. The functional behaviour of the novel feature, notated as $|\nabla|^{-1}$, with the level of corrosion, d^2, is first established using analytical solution. This allows the calibration curve of a specific pipe to be done using only two measurements; the reference measurement and the measurement without the presence of pipe. The performance of this technique is analysed.

II. METHODOLOGY/APPROACH

A. DERIVATION OF $|\nabla|^{-1}$ FEATURE

The extraction of $|\nabla|^{-1}$ starts by representing the time-dependent induced voltage in the detector coil, $V(t)$ as [1]

$$V(t)|_{t \gg 0} \approx b_1 exp \frac{-\pi^2 t}{\sigma \mu d^2} \qquad (1)$$

where σ, μ, and d are the conductivity, the permeability and the thickness of the pipe wall, respectively. The term b_1 is the fitted coefficients. Note that this equation only applies during the eddy current decay phase. Expressing this in its natural logarithmic form, the exponential term can be reduced to

$$\ln[V(t)]|_{t \gg 0} \approx \ln b_1 + \frac{-\pi^2}{\sigma \mu d^2} \qquad (2)$$

To further reduce the variables, differentiation of the whole equation gives

$$\left| \frac{d \ln[V(t)]|_{t \gg 0}}{d t} \right|_{t \gg 0} \approx \frac{-\pi^2}{\sigma \mu d^2} \qquad (3)$$

which proves the proportionality of the inverse graident with the squared of the pipe wall thickness as

$$d^2 \propto \left| \frac{d t}{d \ln[V(t)]|_{t \gg 0}} \right|_{t \gg 0} \qquad (4)$$

$$d^2 \propto |\nabla|^{-1} \qquad (5)$$

With the known relationship of the proposed feature, $|\nabla|^{-1}$, with the squared of the sample thickness, d^2, the calibration curve can be established by taking one (or multiple) reference signals from the inspected area. This can later be compared with the signals taken in air (without the presence of any pipe), and a straight line can be drawn crossing the $|\nabla|^{-1}$ values obtained from these measurements. This slope of the straight line indicates the functional relationship of $|\nabla|^{-1}$ with d^2.

B. EXPERIMENTAL SETUP

For validation purposes, a PEC system has been developed consisting of a transmit-receive coil, excitation circuit and a LabVIEW data acquisition program. Carbon steel plates of S275 grade were used, with thicknesses of 4 mm to 12 mm, at increments of 2 mm. Plastic plates were used as a non-conductive insulation of 40 mm. The excitation voltage was 10 V with 8 Hz excitation frequency. Data was acquired at the rising edge, and 16 pulse signals were averaged for each test for the purpose of white noise reduction. Experimental setup is presented in Figure 1.

Figure 1 PEC experimental setup

III. RESULTS/DISCUSSIONS

Received PEC signals show strong correlation with the sample thickness, especially during the diffusion phase of the eddy current, as shown in Figure 2. These are accepted relationships [2,3], and this agreement provides an additional level of confidence in the results presented. In this way, the PEC signals behave as expected, with the thinner sample possessing earlier eddy current diffusion time as compared to thicker samples.
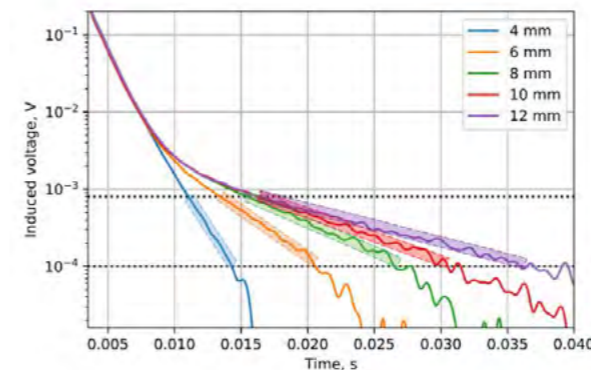

Figure 2 PEC signals corresponding to different thicknesses

The extraction of $|\nabla|^{-1}$ was carried out at the later parts of the signals, as notated in the figure. The inverse slope of these excerpted PEC signals were extracted using linear fitting in logarithmic domain, and were then compared with d^2, shown in Figure 3.
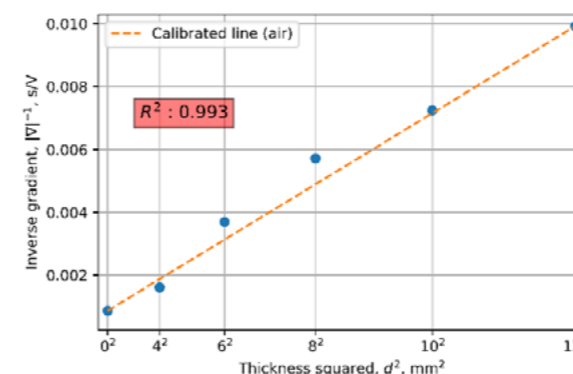

Figure 3 Plot of extracted $|\nabla|^{-1}$ against d^2

At first glance, the extracted $|\nabla|^{-1}$ can be claimed to have an approximately linear functional relationship with d^2. A straight line is drawn crossing $|\nabla|^{-1}_{air}$ and $|\nabla|^{-1}_{12\,mm}$, which represents the established calibration curve. Although discrepencies in the measurements can be seen, especially for 6 mm and 8 mm, this is still acceptable considering the practicality of a PEC technique as an estimation and screening technique.

In real life practice, reference signal (in this case, PEC signal for 12 mm plate thickness, 40 mm lift-off) can be obtained by choosing single or multiple signals in the inspected area which possess the highest feature measurement as well as having the least variations in the C-scan. Having the PEC signal in air stored in the computational memory, the calibration curve can easily be established once the reference signal is chosen.

IV. FUTURE PLAN/ DIRECTION

Current work considers the variation in the pipe wall thickness, without considering other factors that might contribute signal variations, such as lift-off, shielding effects contributed by cladding and variations in insulation thickness. Future works will see how these influences can be compensated, while still aiming to develop a PEC screening system that requires no prior calibration. Modifications in the PEC probe designs will be considered, as well as analysing different signal processing approaches.

V. ACKNOWLEDGEMENTS

REFERENCES

[1] Ulapane, N., Alempijevic, A., Miro, J. V., and Vidal-Calleja, T. (2018a). Non-destructive evaluation of ferromagnetic material thickness using pulsed eddy current sensor detector coil voltage decay rate. NDT & E International, 100:108-114.

[2] Ulapane, N., Alempijevic, A., Vidal Calleja, T., and Valls Miro, J. (2017a). Pulsed eddy current sensing for critical pipe condition assessment. Sensors, 17(10):2208.

[3] Huang, C., Wu, X., Xu, Z., and Kang, Y. (2011). Ferromagnetic material pulsed eddy current testing signal modeling by equivalent multiple-coil-coupling approach. NDT & E International, 44(2):163-168.
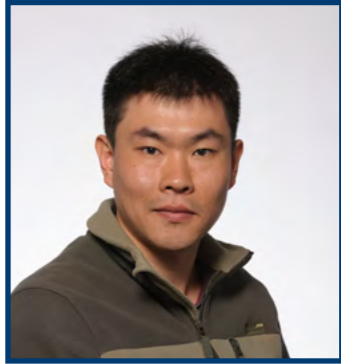
Zhiyao Li

Zhiyao Li is currently starting his third year of PhD in London South Bank University and is based at NSIRC and TWI. After his BEng of Mechanical design and manufacturing and automation at Wuhan University of Technology, he joined industry for two years and continued his MSc of Mechanical Engineering with energy system in the Department of Mechanical and Aerospace Engineering at University of Strathclyde Glasgow. He is now focusing on the work of shearography optimisation and its roboticised application.

Shearography system for wind turbine blade inspection optimisation

Prof. M. Osman Tokhi[1]; Dr. Jianxin Gao[2]
[1]London South Bank University, [2]TWI
3rd Year of PhD

Keywords: NDE, shearography, composites, wind turbine blade, interferometry

I. INTRODUCTION

Wind energy nowadays is one of the most important green electric power sources, generated from wind turbines. As wind turbines are expected to generate electricity 90% of the time during a typical lifetime of 20 years, structural flaws in wind turbine blades (WTB) are of great concern. WTB is a critical component in a wind energy installation, as its structural failure could cause a catastrophic accident.

Cracks in the blades sometimes appear soon after manufacture. Defects can also be produced during transportation. Repairing or replacing a WTB is always difficult, especially for large wind turbines. The downtime of a wind turbine installation due to a blade failure usually lasts 4-6 days, which is longer than for repairs due to electrical or mechanical failure within the nacelle.

Numerous NDE techniques have been widely used in industry, but few can be applied to the inspection of in-situ WTBs. Ultrasonic testing is a point-wise contact inspection technique and is usually only suitable for homogeneous materials, not composite materials. Radiography, especially computer tomography, is a powerful technique widely used in industry. However, its deployment to the wind tower is difficult. Thermography is a promising NDE technique, but its application to on-site WTB inspection has yet to be proven, given the environmental temperature change due to wind flow which will add considerable noise to the captured thermal images.

Compared to other optical techniques such as holography interferometry, moiré interferometry, and electronic speckle pattern interferometry (ESPI), shearography has a relatively large tolerance to vibrations, enabling it to operate beyond an optical lab. However, existing shearography techniques were designed to operate on the ground or in a test facility; their applications for on-site inspection of a WTB has not been demonstrated.

Since the WTB is in constant vibration due to wind, even when it is parked on a tower at low-speed wind, we believe that the only solution for shearography to work on a wind tower is to enable the shearography to be attached on the WTB surface during inspection when the WTB is parked, so that the relative motion between the shearography and the WTB is minimised to be within the tolerance of the shearography system. In fact, for application to WTBs, there are various choices of on-the-shelf robotic systems which can carry simple monitoring equipment such as visual inspection [1]. However, there are no reports showing a practical robot-assisted shearography for on-site WTB inspection. In this paper, we report our research surrounding the shearography that is designed for integration with a robotic climber for on-site WTB inspection. A specific robotic climber which has a high payload and was developed by ICM (International Climbing Machines, USA) was selected for integration. The climber was further adapted by our project partners.

II. DESIGN/METHODOLOGY/APPROACH

The schematic explanation of shearography system has been shown in Figure 1 (a). The sample surface to be tested is illuminated by an expanded laser beam with sole wavelength. The light scattered from the object surface passes through a Michelson interferometric prism and is split into two beams (see Figure 1(b)).
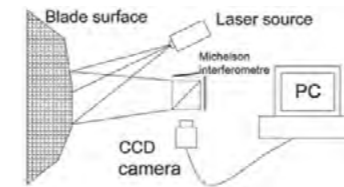

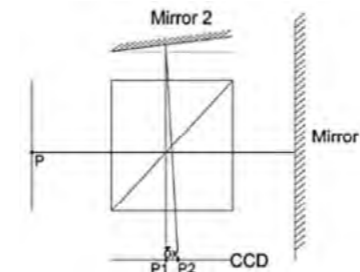Figure 1(a) Shearography set-up schematic diagram

Figure 1(b) A modified Michelson interferometer as the image shearing device

Our shearography system is specifically designed for integration with a robotic climber that it can work on a WTB on-site. The shearography unit uses an external mirror to reflect the laser from the window of the main unit. This design is to let the main body of the shearography stay on the robotic climber. The shearography set-up is intuitively shown in Figure 2 (a). The light path is shown in the Figure 2 (b). The external mirror installed over the window of the shearography unit will increase the light path for the purpose of enlarging the field of view in order to enhance the efficiency of the whole inspection process.
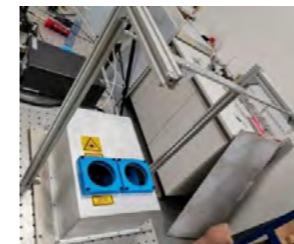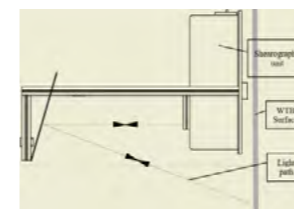

Figure 2(a) Shearography unit

Figure 2(b) Shearography light path

Figure 2 Set up of pneumatic system for suction cup

III. FINGDING/ RESULTS

Phase shift technique [2,3] is useful in result quantification of shearography fringe pattern. Below is the verification of the feasibility of the phase shift applied on the existing system using 4-steps phase shift analysis.
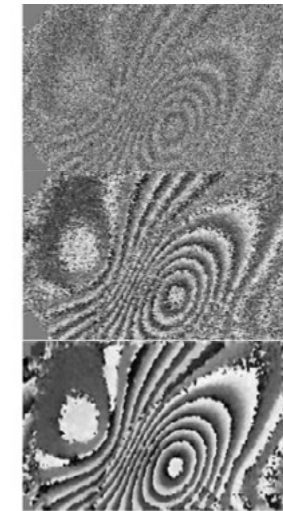

Figure 3 Phase shift result for fringe pattern

IV. DISCUSSION/CONCLUSIONS

Shearography is an effective NDE technique for inspecting WTBs for subsurface defects. Through integration with a robotic climber and associated post processing algortihms for quantitive phase analysis, a remotely controlled shearography system will become practial for the wind energy sector to adopt in the near future.

V. FUTURE PLAN/ DIRECTION

1. Further signal processing with the aid of phasing shift using PTZ transducer and spatial phase shift techniques.

2. Laser heating for lock-in shearography development.

4. Adopt further possible initiation methods on WTBs.

VI. ACKNOWLEDGEMENTS

REFERENCES

[1] Shang, Jianzhong, et al. "Design of a Climbing Robot for Inspecting Aircraft Wings and Fuselage." Industrial Robot: An International Journal, 34(6): p. 495–502, 2007

[2] Bi, Hongbo, et al. "Class of 4 + 1-Phase Algorithms with Error Compensation." Applied Optics, vol. 43, no. 21, 20 July 2004, p. 4199

[3] Zhu, Lianqing, et al. "Real-Time Monitoring of Phase Maps of Digital Shearography." Optical Engineering, vol. 52, no. 10, 8 Apr. 2013, p. 101902

Hesham Yusuf
During his BEng course in Systems and Control Engineering at The University of Sheffield, Hesham acquired an interest machine learning in his final year project that involved modelling lung air volume using neuro-fuzzy modelling. His other interests included robotics with involvement in the university's annual robotics competition for three years. After graduation, Hesham joined the Bahrain Petroleum Company towards the end of 2014 as a systems support engineer. Subsequently, Hesham decided to move back to academia, completing an MSc in Advanced Control and Systems Engineering from the University of Sheffield in 2018 and starting a PhD thereafter in Automatic Control & Systems Engineering at the University of Sheffield.

Semantic feature extraction of defects in x-ray scans of metallic plates

Kai Yang[1], George Panoutsos[2]
[1]TWI, [2]University of Sheffield
2nd Year of PhD

Keywords: feature extraction, image processing, segmentation

I. INTRODUCTION

Feature extraction (FE) is a process by which data of higher dimension is reduced to remove any redundant information that can increase processing time required without adding any significant performance benefit [1]. FE is also applicable to obtaining a dimension of data a simple model is capable of processing.

There are two types of features that can be generated as part of FE: semantic and non-semantic. The former are features that are human-understandable i.e. with a quantity that a human can reason with or understand the consequence of its changing value. In contrast, non-semantic features are numbers that are extracted from the original dataset by mathematical operations resulting in values that are not human-understandable in nature [2]. The abstract investigates the calculation of semantic features for two testing samples.

II. APPROACH

The case study for semantic feature extraction was for X-Ray images of metallic surfaces. The data includes a set of images for a surface with/without an artificial crack from different angles, the size and shape of which differs in each image.

In order to extract semantic features from the images, a two step process was used: segmentation and pattern recognition to select the crack. Segmentation is a technique by which pixels of similar intensity are grouped to form a segment. It is an approach utilised to divide image data into different regions of interest. A segmentation of a typical X-Ray image generally results in a segment for the background (air) and the rest of the segments for the varying densities in the object. For X-Ray of cracks, segmentation is likely to add the cracks to the background segment. Therefore it becomes a matter of removing the background before or after performing the segmentation.

Following the isolation of the cracks from the background pixels, calculations can be made on the crack pixels to extract semantic features such as crack dimensions and more advanced crack information such as dendrites or pits.

III. FINDINGS

The crack space contains air therefore shows up as very low intensity (near to black pixels) on the X-Ray image while the object shows up as grey to dark-grey. Hence segmentation results in dividing the cracks into their own segment. However, since the background is also air, the object has a black background. A second-step algorithm was designed to trim out the background using some basic signal processing. For images with no background, it is simpler, as no trimming is required. The FE process was able to select the crack in a majority of the images.
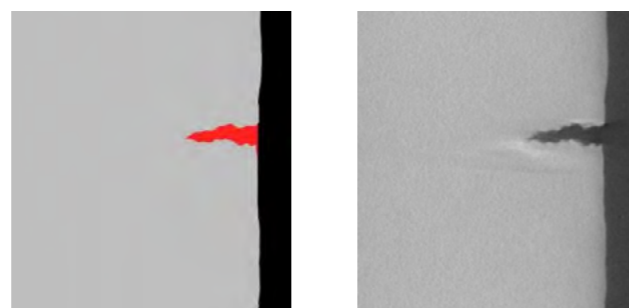

Figure 1: CT scan (left) and the result of the image segmentation (right) on metallic plate #1

Figure 1 illustrates the result of dividing of the image into three different segments: crack, object and background, which are in red, grey and black, respectively. The image on the left is the original (before processing) and the one of the right is following segmentation. Figure 2 shows metallic plate #1 from a different angle which reveals the pit.
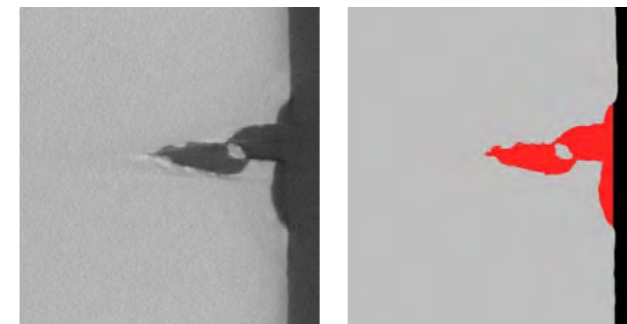

Figure 2: CT scan (left) and the result of the image segmentation (right) on metallic plate #1

Figure 3 shows the same process applied to a different set of images for metallic plate #2. Despite the images having different colours for the background. Plate #1 had a black background while #2 had a more greyish background. There was a possibility the segmentation algorithm would have grouped the background as part of the object pixels due to the similarity, however, that was not the case as shown in the Figure 3.

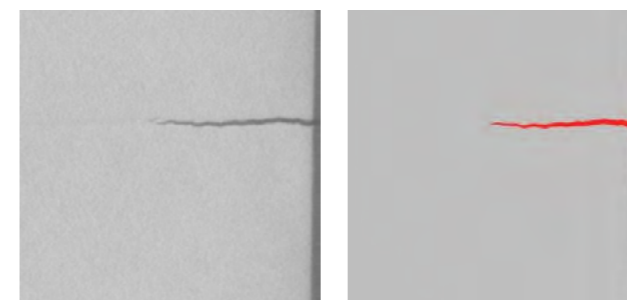Once the crack pixels were selected, the dimensions of the defect can be calculated.

Figure 3: CT scan (left) and the result of the image segmentation (right) on metallic plate #2

IV. DISCUSSION

The method developed was effective at highlighting crack pixels in two different sets of images for two different plates. The model relies on the plate being placed in a horizontal orientation, hence selecting a column to stop highlighting crack pixels results in a reasonably accurate representation of where the crack opening is in the majority of images. However, for images of objects that have edges that are not aligned with the x or y axes, this method is likely not suitable.

V. FUTURE PLAN

The future plan is to extend this method for more complex images such as UT, which contain a greater deal of features. Naturally, it is more challenging to effectively extract features from images which are more complex in structure.

Machine Learning models often rely on non-semantic features hence explaining the decisions at the end of the classification becomes less direct. However, if semantic features are used for image-based classification, it can pave the way for more explainable decisions which are more dependable and reliable for real-world applications.

REFERENCES
[1] DeepAI. 2020. Feature Extraction. [online] Available at: https://deepai.org/machine-learning-glossary-and-terms/feature-extraction [Accessed 11 March 2020].
[2] G. Plumb, M. Al-Shedivat, E. Xing, and A. Talwalkar, "Regularizing Black-box Models for Improved Interpretability," Cornell Univ., Feb. 2019.

Afnan Islam
Afnan attained his BEng in Electrical and Electronics Engineering from Brunel University, London, before joining University College London where he completed his MSc in Nanotechnology. Sponsored by Lloyd's Register Foundation, his PhD with London South Bank University aims at developing a cost effective sensor using permanent magnets, for long term condition monitoring of ferromagnetic structures. The system aims to provide a predictive analysis of defects, obtained from accurate real time data for changes observed in the geometry appearing within the structures, due to defects.

Development of cost-effective, permanently installed condition monitoring system, using permanent magnets

Prof M. Osman Tokhi[1] Dr Duan Fang[1] Dr Zhanfang Zhao[1] Dr Shiva Majidnia[2]
[1]London South Bank University, [2]TWI
2nd Year of PhD

Keywords: Magnetic Flux Leakage, Non-Destructive Testing, Condition Monitoring, Signal analysis, Finite Element Modeling.

I. INTRODUCTION

Corrosion is one of the leading causes of failure or premature deterioration of steel structures. Monitoring of critical areas of structures is often carried out at intervals using various Non-Destructive Testing (NDT) and Condition Monitoring (CM) techniques, which is not always possible in extreme conditions [1]. Sometimes, the process requires access during operation, halting primary workflow for long time periods for expensive setup for measurements. Still, these processes are unable to meet the expectations of the clients, as the data provided is inadequate. Researchers have therefore been exploring cost effective methods to provide a sound solution that are established based on the combination of the autonomous fault detection, diagnosis of the collected data from the defects, prognostics of the data for real time visibility, and, predictability of possible failures arising from the said defect. During this research a variant of the Magnetic Flux Leakage (MFL) technique is being used primarily to develop a cost effective, remote, condition monitoring system using permanent magnets for measurement of corrosion in steel.

II. METHODOLOGY/APPROACH

Ferromagnetic structures upon magnetization by an external magnetic field, will constrain magnetic flux, almost entirely, in the interior of the material. The prototype sensors are systematically placed along the outer surface of the specimen as shown in Figure 1a. A snippet of the working methodology of a single detection unit is shown in Figure 1b. Upon development of a defect on the surface or inside of the ferromagnetic material, the uniform magnetic flux is disrupted. The disruption causes changes in the permeability and magnetic resistance of the material arising from the defect, changing the magnetic field lines, causing MFL from the defect into the surrounding medium. The flux density of the leakage fields can be separated into axial, radial and tangential components, along the x, y and z planes as shown in Figure 1b and 1c, and are picked up by sensors, which interprets flux changes observed in voltage units [1].
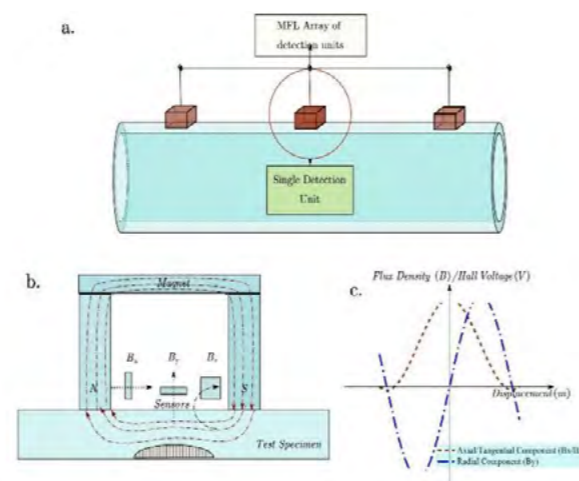

Figure 1: a) MFL array of detection units b) Single detection unit c) Leakage field components

The process is governed by the equation:

$$V_H = K_H \times I \times B \times \cos\alpha \tag{1}$$

Where VH refers to the Hall electromotive force; KH is the Hall coefficient; I is the electric current; B refers to the magnetic flux intensity; $\cos\alpha$ refers to the normal angle between B and Hall components. The magnitude of the MFL is directly proportional to the magnetic field strength of ferromagnetic material.

B. EXPERIMENTAL SETUP

A prototype system has been developed which consists of horse-shoe shaped AlNiCo magnets, hall sensors of sensitivity 4.5 mV/G in a 2 cm separated array, axial to the flux density, transmitting collected data wirelessly at 9600 Baudrate. Experiments are being carried on Low Carbon Steel plates (S275 grade) from 2-12 mm thicknesses at increments of 2 mm. The data is being analysed using Python. The experimental setup is shown in Figure 2.
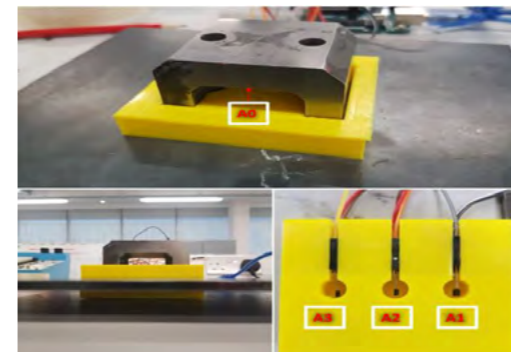

Figure 2: Sensing unit experimental setup. A0, A1, A2 and A3 are hall sensors placed systematically to observe Flux changes.

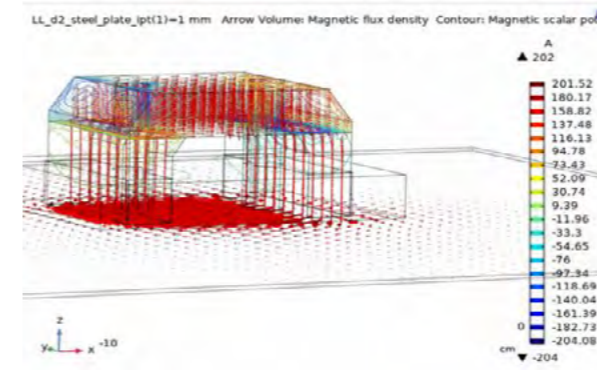3D Finite Element Modelling has been performed

Figure 3 Simulation using COMSOL Multiphysics

using COMSOL Multiphysics to validate experimental results. The model has been generated using 'Magnetic Flux, No current' module and the Geometry has been designed using AutoCAD Inventor. Exact parameters have been used from experiments to simulate the model showing results based on thickness changes.

RESULTS/DISCUSSIONS

Experimental data collected have been averaged with 1000 units of sampling over 12 hours, for each thickness measurements. The ambient temperature drifts from electronics, offset readings around 1.5-2%, after 7-8 hours of reading which is being compensated in Python, comparing to the initial data observed from the first ~3-4 hours. Figure 4a shows the drop of Voltage observed for each thickness arising from sensors A1, A2 and A3, placed under plates. A sharp fall of 2.85 to 2.60 V from A2 can be observed for thicknesses 2-6 mm. From 6-10 mm intervals the change of voltage from for the sensors overlaps, which happens due plates not reaching magnetic saturation, sensitivity limit/noise from the sensors and electronics [1].
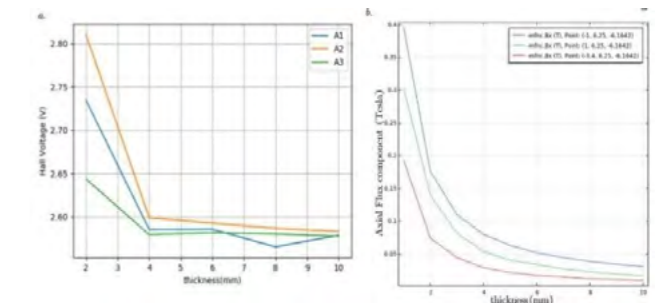

Figure 2: a) Experimental results using AlNiCo magnets b) Results obtained from FEA.

Results are still premature and needs much more investigation before conclusion can be drawn.

III. FUTURE PLAN/ DIRECTION

Currently, a basic sensing unit has been developed that observes the variation in plate thicknesses using AlNiCo horseshoe magnets. In addition, the aspect of arising defects of different geometry and chemistry has not been looked into. Future work will establish usage of Neodymium Magnets of different shapes, sizes and strengths that will be able to saturate plates and other structures of more thickness, while accelerated defects are being generated on them. Defect shapes and sizes at different positions, including their partial chemical compositions will be analysed using COMSOL and multiple sensing units will also be used with more sensitive sensors that will be fed into the predictive analysis model.

IV. ACKNOWLEDGEMENTS

REFERENCES

[1] ASM Handbook Committee, ASM Handbook Volume 17: Non-destructive Eval-uation and Quality Control. 1989, vol. 17, p. 795,ISBN: 978-0-87170-023-0.[Online]. Available:www.asminternational.org.

Xuening Zou
I graduated from Loughborough University with a BEng degree and am now continuing my studies in the Material department of Loughborough University and working towards a PhD. My project is about inspection of austenitic steel and I have been focused on the defect simulation modelling for automatic defect detection and localisation.

Automatic defect detection in austenitic steel cladding

Channa Nageswaran[1], YauYau Tse[2]
[1]TWI, [2]Loughborough University
2nd Year of PhD

Keywords: FEM, austenitic steel, CNN

I. INTRODUCTION

The difficulties associated with austenitic steel is due to the coarse textured grain structure. This makes ultrasonic beams subject to deviation, distortions and sometime ghost echoes. Consequently, the noise due to the grain scattering lowers the signal-to-noise (SNR) and skewing leads to false information, i.e. position and sizing errors. A lot of effort has been put into overcome the difficulties.

Convolution neural network (CNN) has recently shown good performance for both classification and localization tasks. We examine how several different CNN architectures can be used to localise defects in ultrasonic signals. We use full matrix capture (FMC) data acquired from a finite element simulation of inspecting austenitic cladding as a training dataset. And experimental FMC data collected from the cladding block are used as validation dataset.

II. DESIGN/METHODOLOGY/APPROACH

In our approach, metallurgical structure and grain texture are taken into consideration through electron backscatter diffraction (EBSD). The EBSD map contains grain orientation information which determines the wave transmission and reflection in the material. Then EBSD map is introduced into a FEM simulation software called OnScale to represent the austenitic steel. Ultrasonic data from simulation is subsequently fed into convolution neural network (CNN) to train detection algorithm. Experimental ultrasonic dataset from austenitic steel block with equally spaced defects was collected to validate the CNN model.

III. FINDINGS/RESULTS

Importing EBSD map into simulation software enables the simulation of phased array ultrasonic inspection. Equally spaced defects are inserted into the simulation model. The model was run long enough for the wave to be transmitted from the element of the array probe, travel into the component, interact with the flaw and then return to the probe. The received signals from simulation indicates that the material properties in the EBSD map was imported successfully to represent the austenitic steel.

IV. DISCUSSION/CONCLUSIONS

EBSD map can represent the metallurgical structure. It significantly reduces the cost of building and scanning real steel blocks to acquire enough dataset for CNN model.

V. FUTURE PLAN/DIRECTION

Building CNN model to automate detection and localize defects in austenitic steel. It is expected that the results will give accurate localization of defects even for noisy signals.

VI. ACKNOWLEDGEMENTS

REFERENCES
[1] C. Nageswaran, C. R. Bird, and A. Whittle, "Immersion transmit-receive longitudinal phased array probe for stainless steel," Insight - Non-Destr. Test. Cond. Monit., vol. 50, no. 12, pp. 673–678, Dec. 2008.
[2] N. Munir, H.-J. Kim, J. Park, S.-J. Song, and S.-S. Kang, "Convolutional neural network for ultrasonic weldment flaw classification in noisy conditions," Ultrasonics, vol. 94, pp. 74–81, Apr. 2019.

Non-Destructive Testing techniques used across industries such as aerospace, oil and gas, amedical, rail and general manufacturing to name a few. It is a crucial aspect of quality control and ultimately health and safety. Photo: TWI Ltd

Han Yang
Han is a second-year PhD student studying with Brunel University London, sponsored by Lloyd's Register Foundation. He has a Bachelor of Engineering in Navel architechture and Marine Engineering from Wuhan University of Technnogy. He had worked in the the University as a Research Assistant before his PhD study with Brunel University London from October 2018. He is currently based in CSM section of TWI, working on crack growth prediction and monitoring of hydrogen induced cracking under biaxal stress coditions.

Crack growth prediction and monitoring of hydrogen induced cracking under biaxal stress conditions

Dr Bin Wang[1]
[1]Brunel University of London
2nd Year of PhD

Keywords: Hydrogen induced cracking (HIC), Biaxal loading, Crack growth, Finite element anaysis, Acoustic emission

I. INTRODUCTION

In oil and gas production environments, acid gases and fluids can induce severe corrosion (Figure 1) in carbon and low-alloy steels. In the presence of hydrogen sulphide, hydrogen embrittlement phenomena can occur, where hydrogen atoms originating from electrochemical reduction of protons can diffuse into the steel and induce cracking [1].

Figure 1 Pipes with severe corrosion

During HIC, acoustic emission (AE) signals of high amplitude have been observed in previous research [2]. When steel is exposed to H2S for extended periods of time, hydrogen can penetrate the surface of the metal and diffuse inside the material. At an initial stage, hydrogen accumulates at weaker interfaces. Once the hydrogen reaches a critical level of pressure, the de-cohesion of weak interfaces occurs to form a crack, and the cumulative energy of AE events shows a sharp increase, depending on the size of the initial crack. After the crack initiation, the gaseous hydrogen continues to accumulate in the blisters until the pressure is sufficient to make the crack grow. Cumulative energy shows continuous increase during the stable crack growth stage. At the final stage, the crack ceases to grow and no AE related to HIC can be observed [3].

Although crack propagation in uniaxial conditions has been widely studied, crack development under biaxial loading, which often better representing the loading scenarios in practice, such as pressure vessels and pipelines, are to be considered in this research. The capability of AE techniques in monitoring crack growths with different loading routes under biaxial stress conditions is also of great interest.

II. METHODOLOGY

The traditional way of using finite element method to model crack propagation comes with a considerable computational cost as the mesh needs to be regenerated along with the crack increment. Considering this limitation, several approaches based on the concept of partition of unity had been proposed, including the extended finite element method (XFEM) [4]. XFEM has been applied in modelling material discontinuities, and will be used in this study for crack propagation.

Once the mechanism of the above-mentioned dynamic crack growth process is clarified, during which the AE waves are generated, it is necessary to study the propagation and attenuation of the elastic waves emitted with a replaced smplified AE source to build the modelling capacity.

In the first method of simplified AE source , to save computational time, the stress field is calculated with a tensile load applied to the un-cracked plate using a static analysis, and then imported as a predefined field in the dynamic analysis. The boundary condition of the crack surface is defined as symmetry in the static analysis. In the dynamic analysis, the boundary condition of the crack surface is deleted. The idea of such a first approach is to release the node of the crack to simultae the instantaneous crack surface growth and generate elastic waves [5, 6]. Anthoer method, in which the stiffness of elements of the propagating crack are reduced, can also be tried in [7].
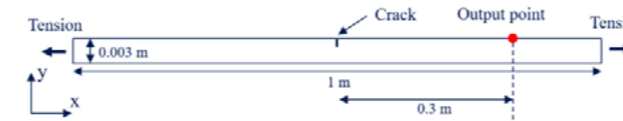

Figure 2 The model used in the first method

III. RESULTS

The time vs vertical displacement curve of the output points are plotted and shown in Figure 3. The distance between output point (AE sensor) and the crack is 0.3m. As AE sensors used in experiments have frequency responses, in order to compare results obtained from finite element modelling and those from experiments, numerical filters are applied to the signal resulted from modelling. First the time domain signal is converted to frequency domain using Fast Fourier Transform (FFT), which is a commonly used tool for obtaining frequency contents of a signal. Then a Gaussian filter is applied to modify the signal's spectrum, in the end the data is converted back to the time domain (Figure 3).
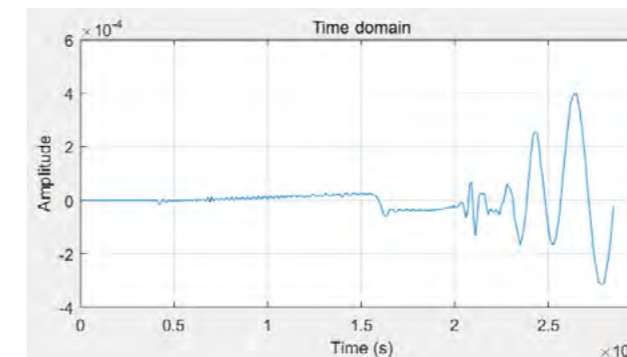

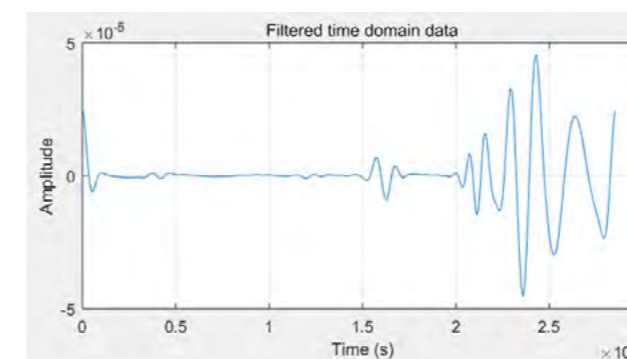**Figure 3 The time versus vertical displacement curve of output point**

Figure 4 Time domain of vertical displacement signal of output point after filtering

IV. DISCUSSION AND FUTURE PLAN

An FEA model is being developed to simulate the instantaneous crack growth and generate different models of waves. With initial simulation results available, further experiments need to be done to verify the present numerical model.

The FE modelling work will be continued using XFEM to model the crack propagation under biaxal stress conditions. Then the acostic emission generated by crack propagation can be modelled based on the crack propagation information from XFEM results. Experiments of crack propagation under biaxial stress conditions will be conducted to characterise the AE signatures. In comparison of the experiment results, the effective numerical model for the prediction of the dynamic crack growth under biaxial stress condition can be obtained, and the capability of AE technology in monitoring crack growths with different loading routes in biaxial loading conditions can be further employed.

V. ACKNOWLEDGEMENTS

REFERENCES

[1] F. Huang, P. Cheng, X. Y. Zhao, J. Liu, Q. Hu, and Y. F. Cheng, "Effect of sulfide films formed on X65 steel surface on hydrogen permeation in H2S environments," Int. J. Hydrogen Energy, vol. 42, no. 7, pp. 4561–4570, 2017.

[2] C. E. Hartbower, W. W. Gerberich, and H. Liebowitz, "Investigation of crack-growth stress-wave relationships," Eng. Fract. Mech., vol. 1, no. 2, pp. 291–304, 1968.

[3] V. Smanio, J. Kittel, M. Fregonese, T. Cassagne, B. Normand, and F. Ropital, "Acoustic emission monitoring of wet H2S cracking of linepipe steels: application to hydrogen-induced cracking and stress-oriented hydrogen-Induced cracking," Corrosion, vol. 67, no. 6, pp. 65001–65002, 2011.

[4] T. Belytschko and T. Black, "Elastic crack growth in finite elements with minimal remeshing," Int. J. Numer. Methods Eng., vol. 45, no. 5, pp. 601–620, 1999.

[5] C. K. Lee, P. D. Wilcox, B. W. Drinkwater, J. J. Scholey, M. R. Wisnom, and M. I. Friswell, "Acoustic emission during fatigue crack growth in aluminium plates," Proc. ECNDT, Berlin, Ger., pp. 25–29, 2006.

[6] J. Tang, "Characterization of fatigue damage types in fibre reinforced composites utilizing pattern recognition techniques applied to acoustic emission signals." Brunel University London, 2019.

[7] Á. Angulo, H. Yang, J. Tang, A. Khadimallah, and S. Soua, "Structural Health Monitoring of Crack Initiation and Growth in Mooring Chains using FEA Methods for Acoustic Emission Characterisation.," J. Acoust. Emiss., vol. 36, 2019.

Andrew Sandeman
Andrew graduated from the University of Manchester with a 2.1 in MPhys (Hons) Physics with Theoretical Physics in 2017. His Master's research project was on "Simulating Maxwell's Demon", where he coded various models based on the Kinetic Monte Carlo method, and obtained a first-class grade. During his undergraduate degree he enjoyed coding physics simulations. These projects ranged from an agent-based model of a fire evacuation, to a GPU-accelerated particle-track finding algorithm (during a STFC Rutherford Appleton Laboratory summer studentship). His PhD is about using particle-in-cell simulation to understand and optimise the design of a plasma electron source for electron beam guns.

Plasma cathode electron beam for high-integrity materials processing

Mr. Andrew Sandeman[1,2], Dr. Sofia del Pozo[1], Dr. Felipe Iza[2]
[1]TWI, [2]Loughborough University
3rd Year of PhD

Keywords: low temperature plasma, plasma cathode, electron beam gun, plasma electron sources.

I. INTRODUCTION

Plasma is commonly known as the fourth state of matter; it is essentially ionised gas, composed of a complex mixture of electrons, ions, and neutrals. Plasmas are generated and sustained by a balance between the generation and losses of charged particles e.g. charged particles are often generated by gas ionisation, but are also lost to electrodes.

A typical electron beam gun machine is depicted in Fig. 1, with a plasma source. Sources for electron guns have conventionally relied upon heating metals e.g. W, Ta to a few thousand K, in order to enable thermionic electron emission.

The problem of thermionic emitters is that the process intrinsically causes wear, in that material evaporates due to high temperature. Not only does this affect beam reliability during operation, but the thermionic emitter itself must eventually be replaced. On the other hand, a plasma is able to avoid material evaporation by not needing materials to be heated, offering a long-life electron source and therefore a reliable beam.

Thermionic sources are also highly sensitive to contaminating particles e.g. electronegatives from the residual vacuum, and ion back-scattering. These contaminants accelerate wear, and hence thermionic emitters require a strict vacuum environment. However, in a plasma the gas is constantly replenished, and such small contamination is unlikely to significantly alter the plasma.

II. METHODOLOGY

Previous experimental work [1] studied several important parameters for optimising extracted beam power, such as pressure, magnetic fields, and geometry. Simulation will be used to provide more detailed diagnostics to build upon this data, and help to optimise the design of the plasma electron source more efficiently. The software us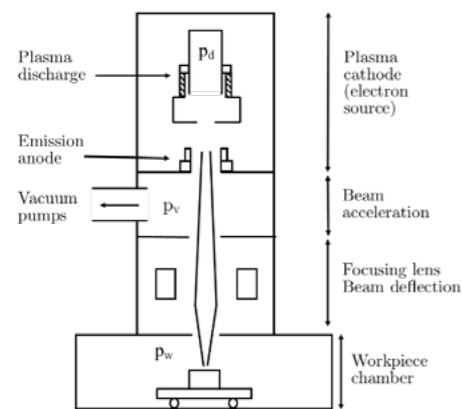ed to simulate the plasma device is XOOPIC [2], a particle-in-cell code. The magnetic field in the plasma device is generated by a permanent magnet, and this field is solved for using a finite-element magnetics solver, FEMM [3]. The magnetic field computed from FEMM is then imported into the plasma simulation.

III. RESULTS & DISCUSSION

Bennchmarking results have been obtained for the geometry in Fig.2, at a pressure of 5.8E-1 mbar. One of the important input parameters for the discharge is the secondary emission coefficient γ_{se}, which is the electron yield per ion incident on a material. Since γ_{se} is not determined experimentally here, a range of values are studied in order to help benchmark the model. The range of γ_{se} tested is based on typical values obtained from [4], and the results are depicted in Fig. 3, showing the model is a valid description of the real system.

A ring magnet is placed on the emission plate and produces a magnetic field which lies mostly along the z axis, and is concentrated in the inter-cathode region (from the end of the hollow cavity to the emission plate, Fig. 2). As depicted in Fig. 4 where the magnetic field is applied incrementally, the plasma itself also becomes concentrated in the inter-cathode region, and achieves over an order of magnitude increase in plasma density n_e. Since DC conductivity $\sigma_{dc} \propto n_e$, this results in a decreased voltage across the plasma.

External magnetic fields are known to confine charged particles via various drifts. The magnetic field in the inter-cathode region deflects particle trajectories, giving an increased path length and more opportunities for collisions. This results in increased ionisation and therefore plasma density in this region. The increase in electron density near the anode will more effectively shield the electric field from entering the hollow cavity.

IV. CONCLUSIONS
- The simulation model has been benchmarked against experiment by exploring a range of γ_{se}.
- Benchmarking results of simulations including the magnetic field agree qualitatively with experiment.
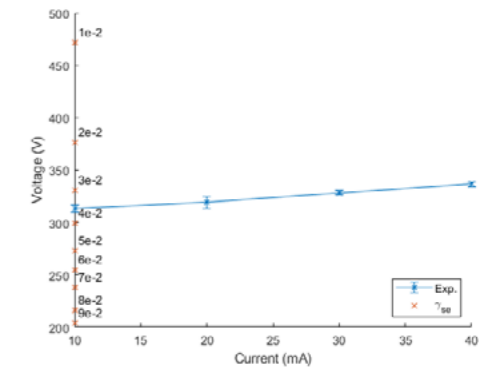
Figure 3: Comparison of experimental results with simulation, without an external magnetic field, and pressure = 5.8E-1 mbar.

V. FUTURE PLAN
Simulation:
- Breakdown simulations, studying the effect of geometry and magnetic field.
- Extension of the model to include the emission region.

Experiment:
- Construction of a Langmuir probe in order to gain more experimental diagnostics for verification with simulation.

REFERENCES
[1] Del Pozo Rodriguez, S. (2016). Investigation and optimisation of a plasma cathode electron beam gun for material processing applications (Doctoral dissertation, Brunel University London).
[2] Verboncoeur, J. P., Langdon, A. B., & Gladd, N. T. (1995). An object-oriented electromagnetic PIC code. Computer Physics Communications, 87(1–2), 199–211.
[3] Meeker, D. (2019). Finite Element Method Magnetics (FEMM).
[4] Phelps, A. V., & Petrović, Z. L. (1999). Cold-cathode discharges and breakdown in argon: surface and gas phase production of secondary electrons. Plasma Sources Science and Technology, 8(3).

Figure 1: Schematic of a typical plasma cathode electron gun (not to scale). p_d, p_v, and p_w are the pressures of the plasma discharge, vacuum, and working chamber respectively, where $p_d \gg p_v$ and $p_v \sim p_w$.
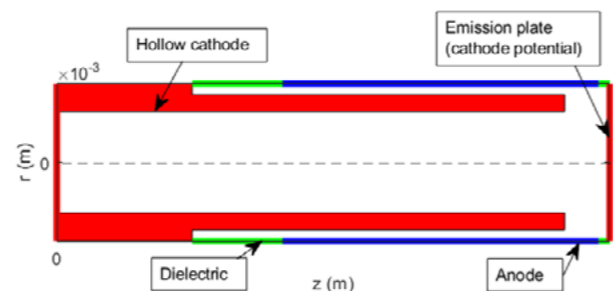

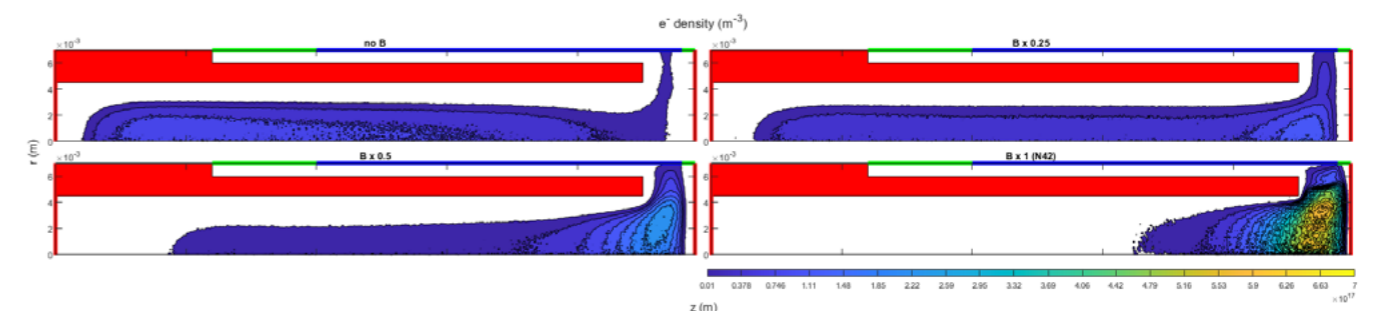**Figure 2: Axisymmetric simulation domain of the plasma discharge.**

Figure 4: Plasma density (m^{-3}) non-uniformity due to external magnetic field scaled from a N42 ring. Pressure = 1.4E-1 mbar and plasma current = 10 mA.

Chris Nyamayaro

Chris obtained his BEng and MSc in Aerospace and Mechanical Engineering at Swansea and Birmingham University respectively. As a PhD student at Lancaster University his research project explores the theoretical and practical investigation of underwater laser cutting for decommissioning applications. Chris hopes to develop underwater fibre delivered laser beam cutting technology for primarily decommissioning applications towards oil and gas and nuclear industrial sector.

Underwater laser cutting in increasing hydrostatic pressure conditions

Chris Nyamayaro[1,] Dr Ali Khan[2,] Dr Andrew Pinkerton[3,] Dr David Cheneler[4] Dr Darren Williams[5]
[1]Lancaster University, [2]TWI
3rd Year of PhD

Keywords: Underwater laser cutting, decommissioning, subsea

I. INTRODUCTION

Energy Act 2008 requires that a large proportion of the North Sea infrastructure will need to be decommissioned in the next 30 years. So far in the UK continental shelf only 88 out of 1500 installations have been decommissioned to date. With more stringent environmental legislations related to global warming and low oil prices, it's thought that decommissioning will become a priority for many companies, as the overall cost of production is no longer financially viable. This potentially likely to provide substantial decommissioning opportunities for years to come.

There is currently a selection of different Subsea Cutting Methods which could be effectively utilised for Decommissioning offshore installations. Three main competing technologies for decommissioning subsea structures are abrasive water jet, diamond wire cutting and plasma arc cutting. However, in order to couple with varied geometries and thicknesses, a single tool with flexible functionality (ease of remote deployment, operation and maintenance) and capability to cut both from outside-in and inside-out would be considered highly desirable. Fibre delivered laser beam cutting has the potential to deliver these benefits by means of cutting safer, cheaper and faster.

Also, fibre delivered underwater laser cutting has the potential to develop a system that can cut installations at extreme water depths. As the water depth increase by 10 m, the hydrostatic pressure increases by approximately 1 bar.

DESIGN/METHODOLOGY/APPROACH

In order to simulate offshore conditions a first-of-its-kind pressure vessels was designed, and manufactured by TWI Ltd. The vessel was integrated with capability to move the workpiece with 3-degrees of freedom, dynamically balance the pressure up 35bars representing depth of ~350m, provide process visual monitoring and recording capability. The system can be pressured to a desired level within minutes.

The cutting trials were carried out using a 10 kW Yb fibre laser system, with optical fibre and all associated services delivered through a prototype underwater laser cutting head capable of withstanding the hydrostatic conditions. The experiment setup is illustrated using a high-pressure vessel lid in the following Figure 1:
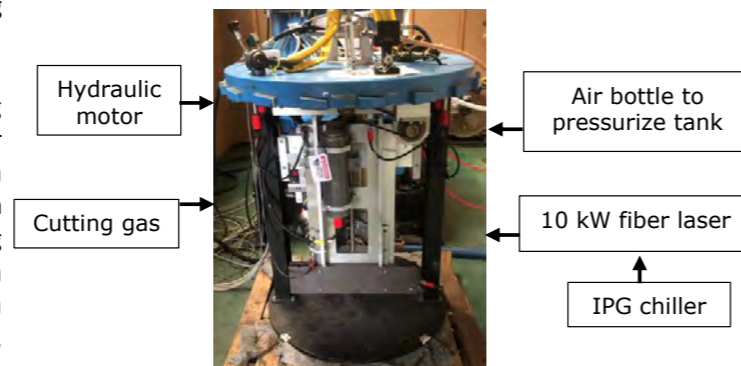

Figure 1: Experiment setup

Horizontal underwater laser cutting trials were carried out in increasing hydrostatic pressure conditions of 0, 5, 10, 15 and 20 bar in the vessel. The goal was to cut at 8 bar relative compressed air pressure to that of the vessel, which varied from 13, 18, 23 and 28 bar respectively.

A laser power of 10 kW was used to cut C–Mn steel workpieces from a thickness of 5-50 mm. The focus position was located 18 mm inside the material. All experiments were recorded using a Panasonic camera and the results were plotted.

II. FINDINGS/RESULTS

The following Figure 2 shows the maximum cut thickness with the corresponding cutting speed at different hydrostatic pressure conditions:
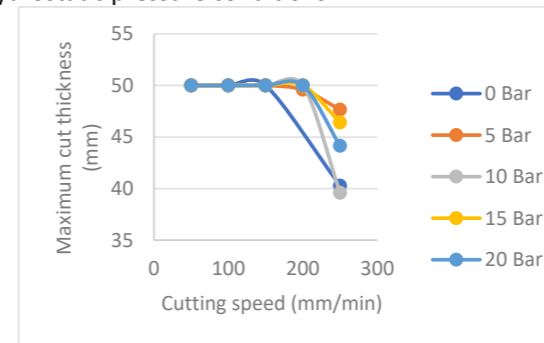

Figure 2: Maximum cut thickness with the corresponding cutting speed

Here it can be seen that a 50 mm thickness C-Mn steel workpiece can be adequately cut with a maximum cutting speed of 200 mm/min at all hydrostatic pressures. Thereafter, the maximum thickness that could be cut decreased with increase in the cutting speed for all hydrostatic pressure conditions.

For the maximum cut thickness, the dross height for every millimetre of the cut was measured using a Vernier caliper. The average dross height was calculated using Microsoft Excel. The following Figure 3 shows the dross height curves plotted at different hydrostatic pressure conditions:
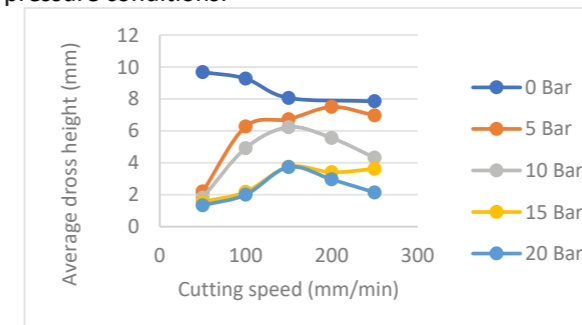

Figure 3: Average dross height with the corresponding cutting speed

As expected, the average dross height decreased with increasing cutting speed for 1 atmosphere hydrostatic pressure condition. However, the relationship between the average dross height and cutting speed at higher hydrostatic pressure conditions is unclear. At 5 and 15 bar, the average dross height increased with increasing cutting speed whilst at 10 and 20 bar, the average dross height increases with increasing cutting speed up to 150 mm/min then decreased. Figure 3 also shows that the average dross height decreases with increasing hydrostatic pressure at all cutting speeds.

The kerf width was measured 2 mm from the start and end of the cut at all cutting speeds. The measurements were taken from the top of the workpiece using a Vernier caliper. The following Figure 4 shows the average kerf width with the corresponding cutting speed:
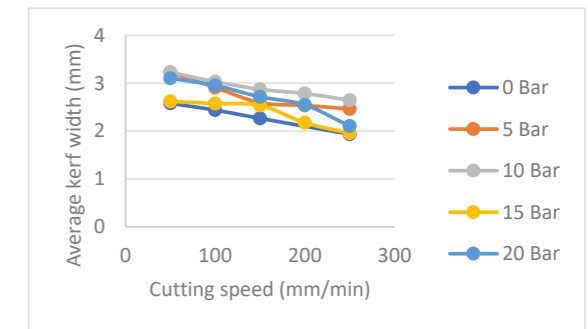

Figure 4: Average kerf width with the corresponding cutting speed

The average kerf width decreased with increasing cutting speed at all hydrostatic pressure conditions.

III. DISCUSSION/CONCLUSIONS

The following conclusions can be drawn from the hyperbaric underwater laser cutting trials:

- A maximum cutting speed of 200 mm/min was used to cut a 50 mm thick C-Mn steel workpiece at a hydrostatic pressure of 5, 10, 15 and 20 bar.
- The average dross height decreased with increasing hydrostatic pressure at all cutting speeds.
- The average kerf width decreased with increasing cutting speed at all hydrostatic pressure conditions

IV. FUTURE PLAN/ DIRECTION

- Develop an analytical model for underwater laser cutting that will be verified by experimental results
- Validate underwater gas jet expansion model with gas jet visualization experiments

V. ACKNOWLEDGEMENTS

Bowei Li

Bowei received his MSc in Mechanical Engineering from Brunel University London in 2018, after completing a BEng in Mechanical Design, Manufacturing and Automation from Xi'an University of Science and Technology. He started his PhD with Brunel University London in February 2019, and his research topic is 'Laser riveting: an innovative technique for dissimilar composite to metal joining' in collaboration with The Welding Insitute (TWI) and NSIRC. This research aims to create a dissimilar joint between composite and metal, by laser-based metal wire deposition application.

Laser riveting: an innovative technique for dissimilar composite to metal joining

Ali Khan[1], Bin Wang[2]
[1]TWI, [2]Brunel University London
2nd Year of PhD

Keywords: laser metal wire deposition, dissimilar joining, laser riveting

I. INTRODUCTION

In the transport sector, there has been a recent emphasis on the practice of 'light-weighting' in which engineers attempt to reduce the overall weight of structures in order to:

- Meet emission targets and standards as required by both national and international legislation and policy
- Improve the fuel economy of the vehicle and reduce costs for the owner
- Meet the public's environmental expectations of the sector.

The main way in which manufacturers minimise the weight of transport structures is by selecting higher strength construction materials to use. Such materials are not only metallic; there are also non-metallic materials: Carbon Fiber Reinforced Polymer Composites (CFRPs), such as PEEK, which can be used in conjunction with their metallic counterparts, to create materials that are both lightweight and tailored to their purpose. However, despite the benefits of integrating CFRPs with metallic materials, there are a number of issues relating to the manipulation and joining of these very different materials.

TWI has developed a technique it has termed 'laser riveting' which offers a quicker, cheaper, more flexible and more effective way to circumvent the limits of existing mechanical fastening techniques.

II. DESIGN AND APPROACH

The final aim of this research is to create a dissimilar joint between composite and metal. In this case, the project consists of two main research progresses: laser metal wire deposition (LMWD) to build a solid rivet on the metal substrate, and dissimilar joining to interlock composite sheet to the metal substrate. The different metals (titanium, aluminium, and steel) will be used to create dissimilar joints with CFRPs after designing and developing the experiment. Several analyses will be conducted including, but not limited, to metallurgy, strength and fatigue tests. For the numerical analysis, an ABAQUS simulation of laser riveting will be applied in this project.
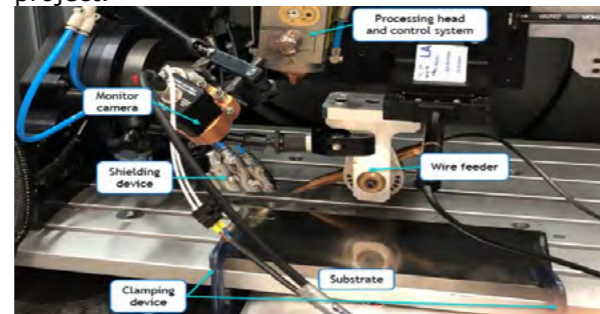

Fig 1. LMWD processing system set up.

So far, the main investigation on the first research progress, LMWD, has been completed. This focuses on the cylinder building in three areas: wettability checking, feasibility study on Ti6Al4V, and parametres control both on 304 stainless steel and AA 60601 deposition. Some trials of dissimilar joining for steel to aluminiinium have been tested and analysed at the end of this phase. LMWD experiment processing system shows in Fig 1.

In the feasibility study of cylinder building, two different shapes were explored. In both cases, because of the limited deposition rate, one single layer of material was not sufficient to build a cylinder. Thus, each cylinder was manufactured by depositing a certain number of layers onto the substrate. Two different path strategies were adopted for depositing the material in each layer: the 3-arcs and full circle path strategies.

After the processing parameteer control and improvement trials of steel deposition have been conducted, targets on the key factor of industry-productivity-time shorten. Through the processing parameters control, different deposition strategies have been designed: high speed (HS) deposition by increasing the speed and reducing the cooling time, then a new continuous deposition method (Con) developed which removed the cooling step between layers. Results are compared in the next paragraph.

III. INITIAL FINDINGS

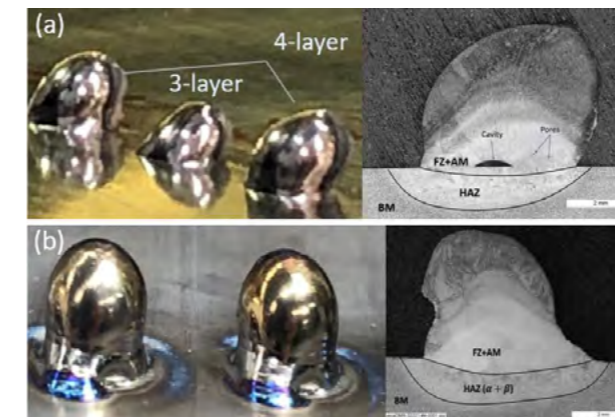*1. Feasibility check for cylinder deposition of Ti6Al4V:*

Fig 2. Multiple layers Ti6Al4V cylinder deposited by LMWD applied with (a) 3-arc path and (b) full cycle deposition path.

2. Parametre control and improvement of stainless steel cylinder deposition:
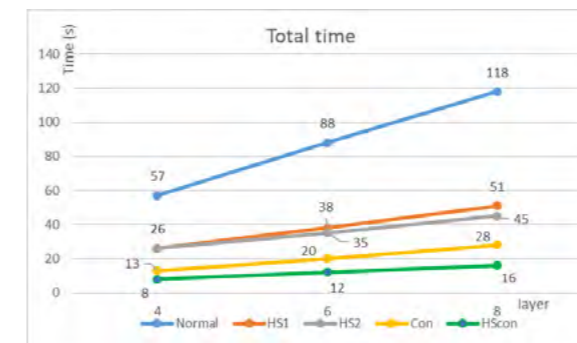

Fig 3. Total processing time results from the comparison of different deposition methods.

3. Initial trials of dissimilar joining for aluminium to steel:

Fig 4. The dissimilar joint trial of steel and alumininium plates.

IV. DISCUSSION AND CONCLUSIONS

In the preliminary stage of this research, single layer cladding and multiple layer deposition experiments were conducted using 3-arc path and full circle path strategies respectively. Both results proved the feasibility of the cylinder building method based on the laser wire deposition method in the micro-scale (circle radius from $500\mu m$ to $1.5mm$).

Although, the multiple layers were successfully implemented in the two path strategies, the results still demonstrated flaws in the single cladding, and a build angle issue while building the 3-arc path layered deposit, Fig 2(a). This issue was solved by changing deposited mass, which allowed successful deposition of proper geometry with desirable microstructure, Fig 2(b).

In the multiple layer deposition of steel trials, several deposition methods were developed by adjusting different processing parameters, which include but are not limited to, power, travel speed, cooling time and deposition path strategy. The initial feasibility trial is refered to as normal deposition (baseline), which was used as the benchmark for deposition procedures in order to reduce the processing time. These included high speed (HS 1&2) and continuous spiral deposition (CON). The outcome was a reduction in the overall deposition time by 85%, while delivering similar mechanical and metallurgical benefits.

In the development of the LMWD process, the variation of processing parameters such as shielding gas position, wire feed and retraction speed was found to be critical for build height and geometry adjustment.

V. FUTURE PLAN/DIRECTION

1. Joints development

The build process and procedures developed so far will now be taken forward to develop a disimilar joint between a composite sheet and a metal substrate. A mechanical joint performance experiment will also be carried out to discern and understand the major performance variables from the laser riveting process.

2. Evaluation of joints

After the joints are completed, results analyses, i.e., high-speed video and wettability, will be conducted to research the material's behaviour when undergoing laser riveting, in order to develop a deeper understanding of the process.

3. Numerical modelling

For some of the lab experiments, a numerical simulation will be developed and built to calibrate the results, assist the experimental investigation and better predict how the process will work under different conditions.

George Brooks

My name is George Brooks, I am a research student at TWI Ltd and Sheffield Hallam University. I joined Sheffield Hallam in 2014 on an undergraduate Aerospace Engineering degree and completed a year in industry at Knorr-Bremse Ltd as part of my studies. I represented the university competitively in badminton for 4 years and currently play cricket for Norton Oakes CC.

Investigation into the influence of Friction Stir Welding in thick section aluminium alloys.

S. Cater[1], Dr. S. Magowan[2]

[1] TWI Ltd, Wallis Way, Catcliffe, Rotherham, S60 5TZ, [2] Sheffield Hallam University, Sheffield, S1 1WB

2nd Year of PhD

Keywords: Friction Stir Welding, Aluminium, FSW, Joining

I. INTRODUCTION

Friction Stir Welding (FSW) is a solid-state joining process that in its simplest form uses a non-consumable tool with a specially designed shoulder and probe to stir material softened by friction to form a joint, such as demonstrated in Figure 1.
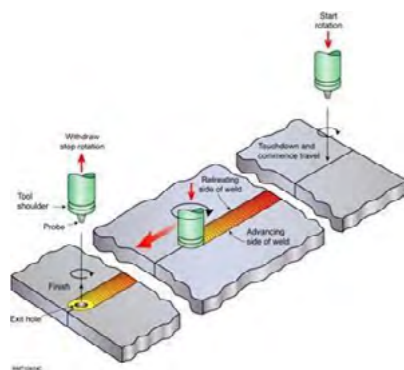
Figure 1 - Schematic of the FSW process [1].

The primary aim of the research project is to investigate the influence of welding variables on the microstructure and mechanical of welds created in thick section aluminium and thereby develop the technical and commercial benefits of the FSW process.

II. METHODOLOGY

Plates of 900x130x50mm AA5083-H111, AA6082-T651 and AA7050-T7451 were welded to the same grade of alloy by Weld-Flip-Weld (WFW-FSW) and Simultaneous Double Sided (SDS-FSW)

and subsequently tested. The composition of the alloys is presented in Table 1. Further plates of 500x130x50mm were welded using Supported Stationary Shoulder (SSS-FSW) as this technique was untested in the thickness of material, investigation into tool life was first necessary. All welds were produced using the PowerStirTM available at TWI Ltd in South Yorkshire.

Wt. %	AA5083	AA6082	AA7050
Al	94.200	97.5	90.600
Cr	0.110	0.011	0.008
Cu	0.070	0.016	1.850
Fe	0.350	0.19	0.120
Mg	4.430	0.74	1.830
Mn	0.480	0.53	0.010
Other	0.028	0.076	0.04
Si	0.240	0.92	0.054
Ti	0.017	0.010	0.058
Zn	0.075	0.007	5.290
Zr	-	-	0.140

Table 1 - Composition of alloys.

Microstructural analysis of the material included Optical Emission Spectroscopy, Energy dispersive X-ray spectroscopy (EDX), X-ray Diffraction (XRD) and Optical Light Spectroscopy (OL). Mechanical testing focused on Micro-hardness and tensile testing. In addition, energy input into the weld was calculated.

III. RESULTS & DISCUSSION

Results for the WFW-FSW in AA7050-T7451 are presented below. The weld was produced using traverse and spindle speeds of 130mm/min and 130rpm respectively. Figure 2 and Figure 3 show the macrograph and microstructure. Within the stir zone (Figure 3d, e & f) the grains are equiaxed and particles appear intergranular. Where the probes overlapped and produced a double processed region, e, the grains are much smaller. Whereas in the Heat Affected Zone (HAZ), where the heat input was sufficient to allow the precipitates and grains to grow, there are several larger grains surrounded by smaller grains.
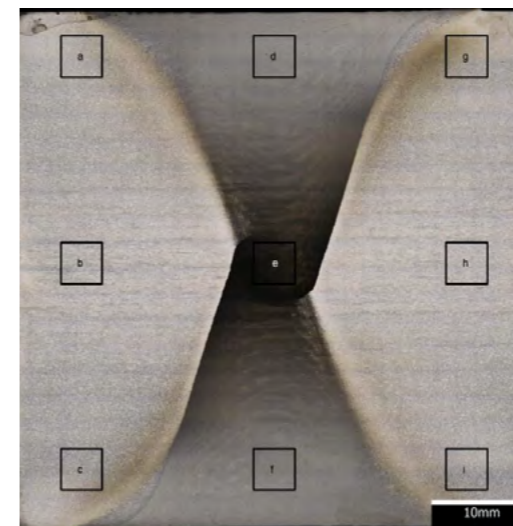

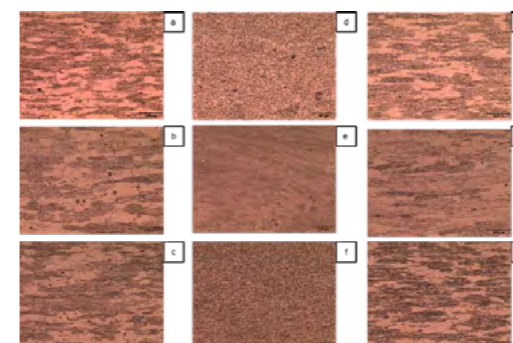Figure 2 - Macrograph of G03/04 identifying regions of microstructural analysis.

Figure 3 - Microstructure of G03/04 once etched in Krolls reagent.

The hardness of the weld, shown in Figure 4, suggests that where the Thermo-Mechanical Affected Zone (TMAZ) meets the HAZ the material retains 55% of the hardness of the Parent Material (PM). This relates to the larger grains shown in Figure 3, which were influenced by the heat from the weld. However in the stir zone there is a 70% retention in hardness compared to the PM. Although this region is hotter than the HAZ, the mechanical deformation of the grain structure by the rotating probes produces grains typically a factor of 10x small than the PM and equiaxed. This reduces the effect of the heat

input by forming more grain boundaries for the dislocations to pass through. The HAZ does not appear to extend beyond 30mm from the centre of the weld, a distance of only 10mm further than the shoulder of the tool. Compared to other FSW techniques investigated in this project, this is a much narrower HAZ.
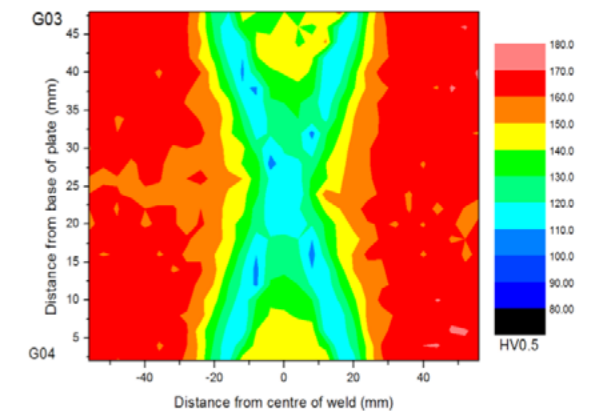

Figure 4 - Micro-hardness contour map of G03/04.

IV. CONCLUSIONS

Overall, eleven welds have been produced in 50mm thick aluminium alloys. These have been produced using Friction Stir Welding (FSW) variants; Weld-Flip-Weld (WFW-FSW), Simultaneous Double Sided (SDS-FSW) and Supported Stationary Shoulder (SSS-FSW).

The following observations have been made with regards to the microstructural and mechanical properties of the welded materials;

- Retention of ~70% hardness is observed in the stir zone but only 55% at the TMAZ/HAZ transition.
- The HAZ extends only 10mm wider than the shoulder of the tool.
- The macrograph of WFW-FSW shows a clear hourglass shape to the stir zone.
- Grains within the stir zone appear equiaxed and refined compared to the grains in the HAZ.

V. FUTURE PLAN

Future work on this project will continue the investigation into the microstructure of the welded material by conducting EBSD analysis. Full section tensile testing will be continued to provide tensile properties for the 50mm thick samples. Residual thermal stresses will be calculated using XRD analysis and further EDX mapping will be undertaken.

REFERENCES

[1] Cater, Stephen, Dick Andrews, and TWI Ltd. 2014. Fundamentals of Friction Stir Welding.

Pedro Santos IEng AWeldI
Pedro received his MSc Degree in Mechanical Engineering from the Faculty of Science and Technology at the New University of Lisbon (FCT-UNL). His MSc thesis focused on the FSW process parameter optimisation to produce tailor welded blanks for lightweight transport applications, a project sponsored by Innovate UK (LightBlank) as part of his industrial placement at TWI. His PhD is co-funded by the Industrial Members of TWI as part of the Core Research Programme and Coventry University and it focuses on the development of the Refill Friction Stir Spot Welding (RFSSW) process for lightweight aerospace applications.

Influence of tool material and design on the mechanical and microstructural

Dr João Gandra[1], Dr Anthony McAndrew[1], Prof. Xiang Zhang[2]
[1]TWI, Ltd | [2]Coventry University
3rd Year of PhD

Keywords: RFSSW, Tool material, tool design, Aluminium alloys, Lap shear strength.

I. INTRODUCTION

Refill Friction Stir Spot Welding (RFSSW) is the latest industrially relevant variant of the friction stir spot welding technologies. It provides significant advantages on aluminium joining compared to conventional single point joining technologies.

Although the welding tool plays a critical role in the RFSSW process, there is a lack of publicly available and experimental data regarding RFSSW tool design. As highlighted by other authors [1,2], the effect of different tool materials and external geometrical features on the microstructural and mechanical properties have not been widely studied.

This investigation aims to understand the influence of different tool materials and designs on the mechanical performance and microstructural properties of joints produced by RFSSW.

II. MATERIALS AND METHODS

AA2024-T3 and AA7075-T6 aerospace grade sheets with a thickness of 2 mm were used as the base material for similar material welds. Single-spot overlap welds were produced using an optimised process parameter combination selected based on previous work using TWI's Kawasaki RFSSW C-frame system.

The tool materials used in this investigation were M42 High-Speed Steel (hardened to 55 HRC) and WC-Co, coated with a diamond-like carbon coating. Physical properties are presented in Table 1.

Table 1 - Physical properties of tool materials.

	M42	WC-Co
Density [Kg/m³]	7.9	14.4
Modulus of Elasticity [kN/mm²]	200.0	580.0
Thermal Conductivity [W/m °C]	28.0	105.0

Three different RFSSW tools were produced using different tool materials and designs, as summarised in Table 2.

Table 2 - RFSSW tool materials and designs.

	Tool Material	Tool Design
Tool 1	WC-Co	Featureless
Tool 2	M42	Featureless
Tool 3	M42	Left-hand groved

Figure 1 and Figure 2 show the RFSSW tools used in this work. Shoulder and probe outer diameters are 7 and 4 mm, respectively.
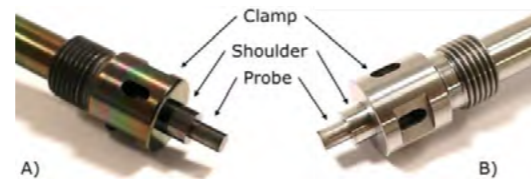

Figure 1 - Featureless RFSSW tool components: A) Tool 1 and B) Tool 2.

Figure 2 - M42 RFSSW tools components: A) Tool 2 and B) Tool 3.

Metallographic specimens were sectioned, polished and etched with Keller's reagent for microstructural analysis. Optical microscopy was conducted using an OLYMPUS GX71 microscope. Weld strength was evaluated via lap shear testing in accordance with BS EN ISO 18785-4:2018 using an INSTRON 8502 tensile machine with a displacement rate of 1 mm/min at room temperature. Three specimens were tested for each tool and alloy combination.

III. RESULTS AND DISCUSSION

Table 3 presents the lap shear strength results obtained in this investigation. All welds surpassed the shear strength requirements for resistance spot welding set by AWS D17.2/D17.2M:2013. Furthermore, Tool 3 produced joints which surpassed the strength requirements set for aluminium rivets as defined by MMPDS - 4, 2008.

Table 3 - Lap shear strength (LSS) results

	AA2024-T3	AA7075-T6
LSS minimum [kN] (AWS D17.2/D17.2M)	5,72	
LSS minimum [kN] (MMPDS-4 2008)	8,99	9,43
LSS Tool 1 [kN]	8.59 ± 0.10	9.11 ± 0.03
LSS Tool 2 [kN]	8.97 ± 0.11	8.62 ± 0.12
LSS Tool 3 [kN]	9.10 ± 0.04	10.72 ± 0.21

The presence of an external grove on the plunging component improved the weld mechanical performance on both alloys. This could be related to a more effective material mixing action and downward flow, as described in the simulations presented by Ji et al.[3]. This outcome suggests that other tool designs with external geometrical features could lead to further improvements in the mechanical performance of the weld. Based on the knowledge gathered in previous investigations [4], it was expected that a tool material with lower thermal conductivity would produce weaker welds, due to the increase in weld temperature and consequently alloy annealing. However, using different tool materials produced different outcomes on the weld mechanical properties for each alloy. Ongoing work focuses on explaining these observations.

The typical microstructure and metallurgical features of RFSSW can be observed in Figure 3.
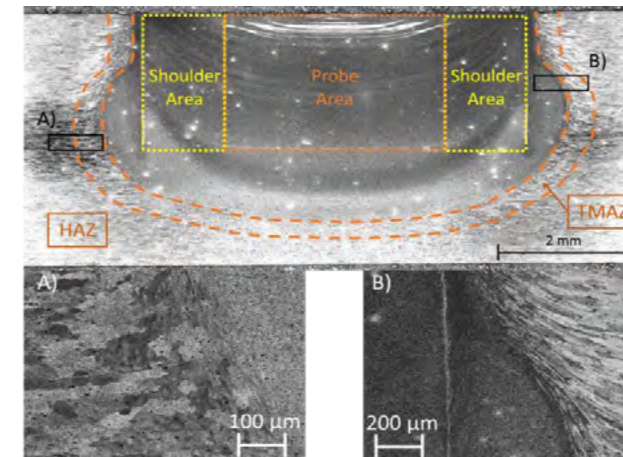

Figure 3 - AA2024-T3 RFSSW Cross-section made with Tool 3.

Fully consolidated welds were produced using all tool variants. Figure 3.A) and B) shows the hook feature (unbonded edge) and the interface between the stir zone (SZ) and the thermo-mechanical affected zone (TMAZ), respectively. The increase in downward flow of material by Tool 3 enabled an extension of the SZ as well as a reduction in the height of the hook feature. Furthermore, the hook tip is located away from the shoulder interface.

IV. CONCLUSIONS AND FUTURE WORK

Fully consolidated welds were produced using all tool design variants. Due to the geometrical features present in the plunging component of the tool 3, the increased stirring actions produced larger welded areas compared to those achieved using featureless designs.

The use of an external geometrical feature on the plunging component improved the stirring action of the tool, enhancing material consolidation and increasing lap shear strength. This promising finding suggests further research should address this topic.

Due to the different observations for each alloy, the correct choice of tool material has a significant effect on the mechanical performance of the weld properties and can lead to either a positive or negative impact. This suggests that a correct choice of tool material is a key design consideration to maximise the weld mechanical performance.

Future work will focus on determining the wear rate of the different tools when welding high strength aluminium alloys and quantify tool life expectancy. At the time of failure, the cost per weld can be determined and thus determine the most cost-effective tooling solution.

V. ACKNOWLEDGEMENTS

REFERENCES
[1] Montag, T., Wulfsberg, J.P., Hameister, H. and Maschner, R., 2014. Influence of tool wear on quality criteria for refill friction stir welding (RFSSW) process. Procedia CIRP, 24, pp.108-113.
[2] Feng, X.S., Li, S.B., Tang, L.N. and Wang, H.M., 2020. Refill Friction Stir Spot Welding of Similar and Dissimilar Alloys: A Review. Acta Metallurgica Sinica (English Letters), pp.1-13.
[3] Ji, S., Wang, Y., Li, Z., Yue, Y. and Chai, P., 2017. Effect of tool geometry on material flow behavior of refill friction stir spot welding. Transactions of the Indian Institute of Metals, 70(6), pp.1417-1430.
[4] De Sousa Santos, P., Gandra, J., McAndrew, A. and Zhang, X. (2019) "Refill friction stir spot welding parameter optimisation for transport industry aluminium alloys" in NSIRC 2019 Annual Conference.

Dimitrios Fakis
I am a PhD candidate with the Mechanical Engineering Department of Brunel University and my research is on the excitation and propagation of electromagnetic surfacewaves on structural composite substrates. I am currently stationed at the National Structural IntegrityResearch Centre and my PhD is funded by BP Ltc and TWI Ltd.

Electromagnetic characterization of carbon fiber-reinforced composites for surface wave applications

Chris Worrall[1], Mihalis Kazilas[1,2]
[1]TWI, [2]Brunel University London
3rd Year of PhD

Keywords: Composites,surface waves, microwave technology, permittivity measurement, dielectric anisotropy.

I. INTRODUCTION

Fiber reinforced composites are often found in close proximity to antennas, interacting with the near field and affecting their performance. Such is the case for conformal antennas mounted on composite panels and for radars behind composite radomes. The dielectric characterization of such materials is complicated due to the fact that composite parts usually come in the form of multi-layered structures, called "laminates", that exhibit an-isotropic characteristics due to the fiber orientation on the weave of each layer [1]. This an-isotropic behavior is further exacerbated when conductive fibers are used to reinforce the mechanical/thermal properties of the composite, as is the case for all carbon fiber composites.

II. DESIGN/METHODOLOGY/APPROACH

At microwave frequencies, while the wavelength is significantly larger than tow and the periodic features of the weave of the reinforcement fabric, weak spatial dispersion effects take place when an incident wave interacts with the composite substrate[2].

Fig. 1. Reinforcement microstructure of a carbon fiber composite laminate modelled with

Math2Market GeoDict 2020. It consists of 5 layers of plain weave carbon fiber (red: horizontal tows, black: vertical tows)

A "homogenization" approximation is thus possible and the composite can be described as an effectively continuous material with uniaxial dielectric anisotropy [3] [4]. It is also often assumed that the composite material will not have any magnetic properties (μ_r=1) [5].

A number of methods have been proposed in literature for the calculation of the complex permittivity matrix, including free space, waveguide and resonant cavity methods [6]. Nonetheless, making an accurate assumption on the wavelength inside the composite material is often not possible, which in turn creates difficulties with methods that utilize resonant effects, where the thickness of the material is crucial.

For that purpose, a number of carbon fiber reinforced composite samples were manufactured in this work and their complex permittivity was measured. The free space method was used with composite panel samples placed on a holder perpendicularly between a set of the pyramidal horn antennas. The distance between each horn and the sample was selected to be 10 times the wavelength so that the incident wave on the sample surface is approximately a planar wave. A TRL (Transmission-Reflect-Line) calibration was implemented to move the reference plane of the incident wave at the location of the sample and thus clear the measured signal from reflections [7]. The resulting reflectance value were subsequently used to calculate the frequency and material dependent complex permittivity values and the caracteristic coefficients of surface wave propagation.
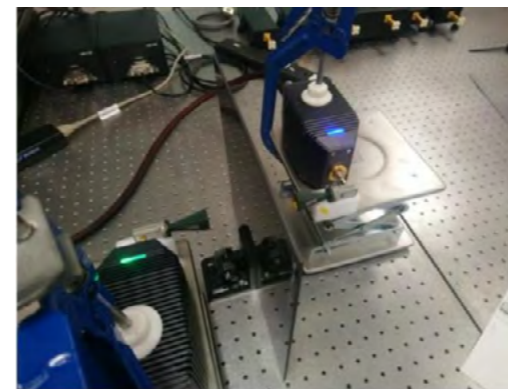

Fig. 2. Photo of the experimental setup, showcasing the carbon fibre composite sample, the pyramidal horn antennas and the holder used.

III. FINDINGS/RESULTS

As frequency increases and the wavelength becomes comparable to features of the internal structure of the composite part, spatial dispersion becomes more significant and resonant effects start taking place inside the composite. There is therefore a transition from an effectively continuous medium to what could essentially be described as an artificially dielectric metamaterial characterised by a complex permittivity tensor[6].
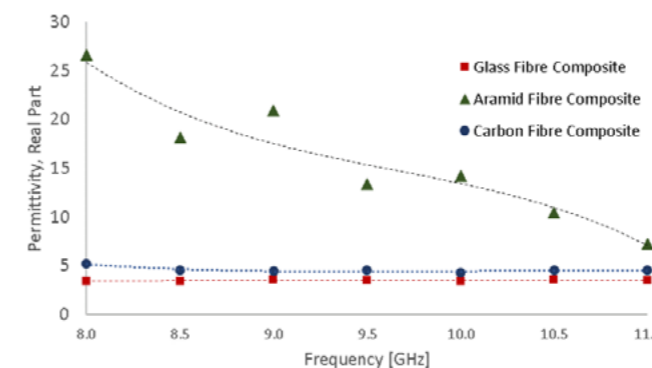

Fig. 3. Measured permittivity values for different types of composite materials (real part).
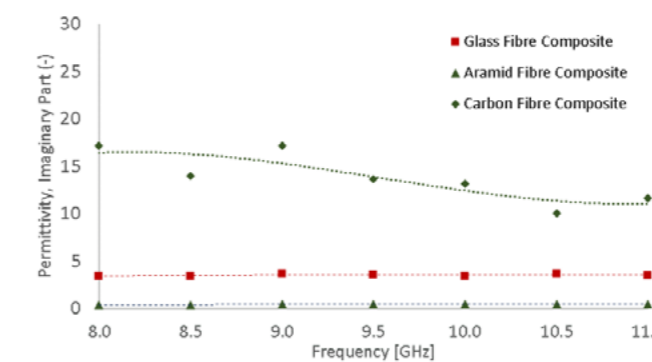

Fig. 4. Measured permittivity values for different types of composite materials (imaginary part, inverted sign).

The surface wave propagation coeffients can be calculated using the resulting complex permittivity

values for a hypothetical surface wave propagating along the inteface between two semi-infinite media, air (medium I) and a composite material (medium II).
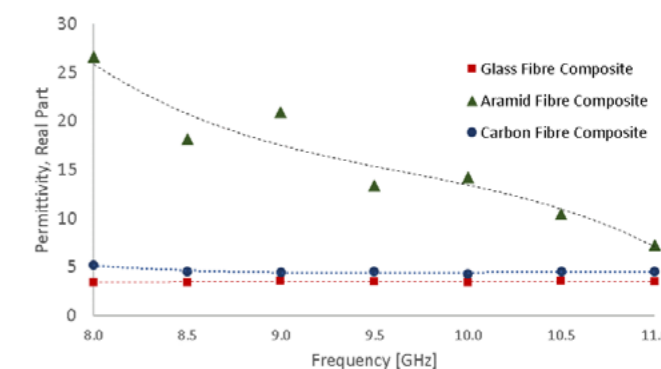

Fig. 3. Measured permittivity values for different types of composite materials (real part).

IV. DISCUSSION/CONCLUSIONS

Due to the significant variations in weave types, tow dimensions and fiber conductivity, this behavior and the frequency at which this transition occurs per composite type has not been well documented, but this phenomenon is expected to have severe effects on antenna applications such as aerospace or automotive conformal antennas directly mounted on composite panels.

V. FUTURE PLAN/DIRECTION

Future work will be focused on the investigation of the properties of additional composite types and laminate configurations, and experimental evaluation of a surface wave communication system that would consist of more intricate intrface geometries and improved surface wave excitation antennas and tranceivers.

REFERENCES

[1] D. Chung, Carbon Composites: Composites with Carbon Fibers, Nanofibers, and Nanotubes, Elsevier, 2016.

[2] C. Simovski, Composite Media with Weak Spatial Dispersion, Jenny Stanford Publishing, 2018.

[3] V. N. Peshlov, "MODELS OF MULTILAYER ANTENNA RADOMES WITH ANISOTROPICMATERIALS," in First European Conference on Antennas and Propagation, 2006.

[4] Valda P. Levcheva, "Characterization and Modeling of Microwave Absorbers in the RF and Antenna Projects," Telfor Journal, vol. Vol. 1, no. No. 2, pp. 57-61, 2009

[5] Reza Zoughi, "Permittivity Characteristics of Kevlar, Carbon Composites, E-Glass, and Rubber (33% Carbon) at X-Band (8–12 GHZ)," in Review of Progress in Quantitative Nondestructive Evaluation, Boston, MA, Springer, 10B, pp. 1431-1436.

[6] P. I. DAnkov, "Dielectric Anisotropy of Modern Microwave Substrates," University of Sofia, Faculty of Physics, Bulgaria.
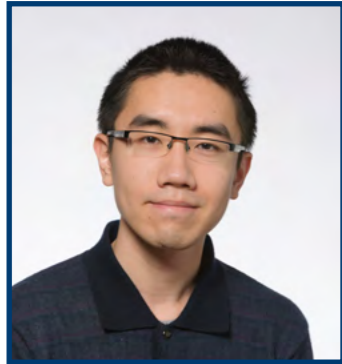
Changyi Yu
Changyi Yu is a third year PhD student currently researching on 'The Effect of Insufficient Homogenization of Carbon Black During the Extrusion of Polyethylene Pipes on Butt Fusion Joint Integrity'. Changyi has started his PhD in January 2018 with Coventry University and TWI Ltd. Changyi graduated with first class honours in Polymer Science and Technology MSc from Loughborough University in 2017 and graduated in Polymer Material and Engineering BEng from Beijing University of Chemical Technology in 2016.

Effect of insufficient homogenization during the extrusion of polyethylene pipes on butt fusion joint integrity

Dr Amir Khamsehnezhad[1], Dr Mike Troughton[1], Prof Xiang Zhang[2]
[1]TWI, [2]Coventry University
3rd Year of PhD

Keywords: polyethylene, windows, butt fusion joint, mechanical properties

I. INTRODUCTION

High-density polyethylene (HDPE) is wldely used in pipe applications because of the lower cost and higher resistance to chemical corrosion and biological attack compared with metallic materials [1]. PE100 is a new generation of HDPE with improved mecanical performance brought by applying short chain branching and bimodal molecular weight distribution [2]. Carbon black (CB) is one of the most widely used additives in PE pipe due to its low cost and absorption of UV which contributes to the resistance of HDPE pipes against photo degradation [3].

During the extrusion of HDPE pipes, fine particle additives like CB tend to agglomerate and in addition to this the high molecular weight part of PE100 tends to self-segregate and float in the molten low molecular weight part due to significant viscosity difference between these two [4]. Insufficient homogenisation during in-line extrusion of black HDPE pipes has been observed as white striations within the pipe, called windows. Previous work at TWI [5] and by Deveci et al. [6] has shown that butt fusion (BF) welds in PE pipes containing windows can have reduced short-term integrity.

The main objective of this current project is to determine the relationship between the extent of windows and the mechanical performance of the BF joints in order to determine the maximum level of windows that does not affect the joint integrity.

II. METHODOLOGY

Butt fusion welding was conducted on five sets of 110mm SDR5 PE100 pipes made on a laboratory extrusion line with different levels of windowing (Table 1).

Before carrying out the welding, a procedure for quantifying the level of windows in the pipe was developed, which involved cutting a ribbon with a thickness of 250 ± 50µm and a length equal to the whole pipe circumference from the pipe end. A segment of 20mm × pipe thickness was cut from the highest windowed region in the ribbon. Each segment was photographed and a 10 × 10mm suqare was cropped from the photo to perform image analysis, based on a greyscale threshold (60) to quantify the window concentration (Figure 1).

Table 1 Variation of PE pipes with different level of windowing

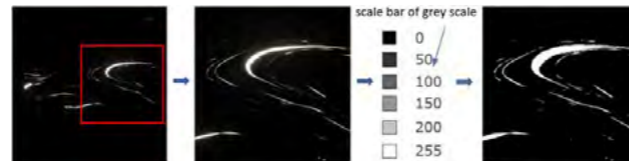| Pipe No.	Windows level
Pipe 1	No windows
Pipe 2	High
Pipe 3	Medium
Pipe 4	Low
Pipe 5	High (extruded with breaker plate)

Figure 1. The image analysis process for window quantification

Following the welding trials, waisted tensile specimens were machined from the welds according to BS EN 12814-7 [7] and the energy to break the weld was calculated. The specimen geometry and their position around the circumference of the joint are given in Figure 2 and Figure 3, respectively.
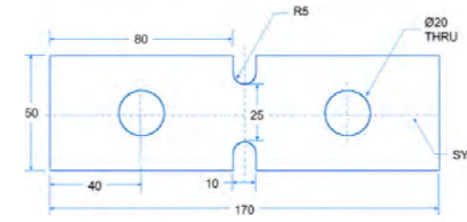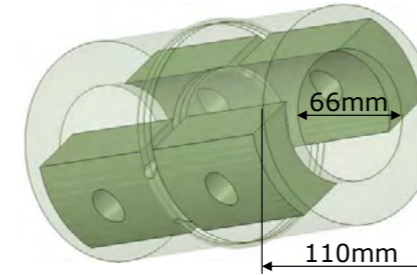

Figure 2. Waisted tensile specimen geometry

Figure 3. Location of the waisted tensile specimens in BF joints made in HDPE pipe samples

III. RESULTS

Representative images of the 10mm × 10mm analysis areas from Pipes 2 to 5 are shown in Figure 4 and the average window percentage (AWP) for each pipe type is given under the respective image. Pipe 1 contained no windows.

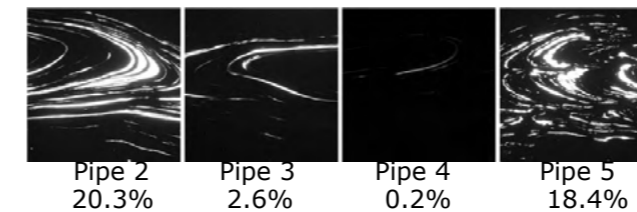| Pipe 2	Pipe 3	Pipe 4	Pipe 5
20.3%	2.6%	0.2%	18.4%

Figure 4. Window percentage of each set of pipe

Figure 5 shows the mechanical properties of the joints. The average energy to break of the joints dropped significantly from 318J to 79J with increasing levels of windows and the average extension at break decreased from 27mm to 9mm.
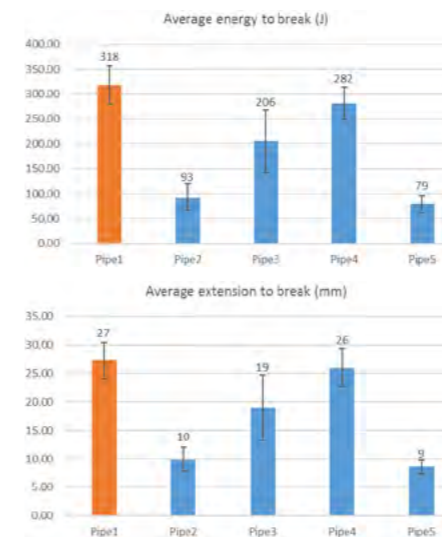

Figure 5 Mechanical properties of the BF joints from each set of pipes.

The average energy to break per cross-sectional area of each pipe set was calculated and plotted against the log of AWP (Figure 6) in order to find the critical window level that does not affect the BF joint integrity. The highest value of energy to break per cross-sectional area from all of the specimens that fractured in a brittle mode (427 KJ/m²) was selected as the critical energy level. The corresponded critical window level was 0.5%.
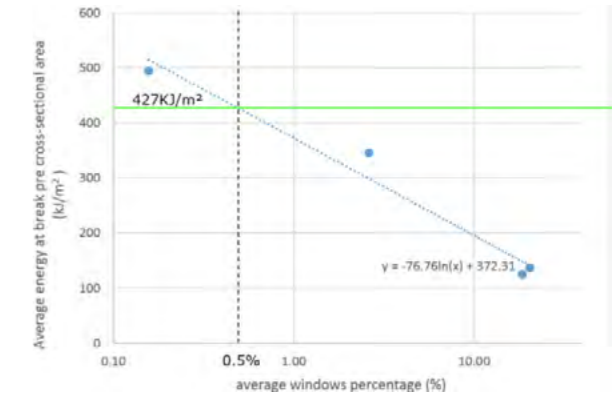

Figure 6. Plot of average energy to break per cross-sectional area values of the BF joints from Pipes 2 to 5 versus logarithmic AWP values

IV. CONCLUSIONS

The significant reduction of the average energy to break and average extension at break of the BF joints with increasing levels of windows indicate that the presence of windows has a significant effect on the short-term integrity of the BF joints made using these pipes. The critical level of windows in the pipe that does not affect the short-term integrity of BF joints was determined to be 0.5%.

V. FUTURE PLAN

Additional welds from commercial in-line extruded PE pipes will be carried out to determine whether welds from commercially-available pipe containing windows have data points on the same energy to break per unit area vs log (window percentage) as Pipes 1 to 5. Further mechanical tests will be carried out to determine the effect of windows on long-term performance of the BF joints made in these pipes.

REFERENCES

[1] Basavaraju C, Naujock D. Safety Evaluation by the Office of Nuclear Reactor Regulation. Relief Request No. 06-CN-003, Catawba Nuclear Station, Duke Energy Carolinas, LLC, United States Nuclear Regulatory Commission, Washington, DC. 2008.
[2] Pircheraghi G, Sarafpour A, Rashedi R, Afzali K, Adibfar M. Correlation between rheological and mechanical properties of black PE100 compounds-Effect of carbon black masterbatch. eXPRESS Polymer Letters. 2017 Aug 1;11(8).
[3] Deveci S, Antony N, Eryigit B. Effect of carbon black distribution on the properties of polyethylene pipes-Part 1: Degradation of post yield mechanical properties and fracture surface analyses. Polymer Degradation and Stability. 2018 Feb 1;148:75-85.
[4] Heidemeyer P, Pfeiffer J. Special requirements on compounding technology for bimodal polyolefines and their industrial application. InMacromolecular Symposia 2002 May (Vol. 181, No. 1, pp. 167-176). Weinheim: WILEY-VCH Verlag GmbH.
[5] Troughton M. Insufficient Homogenization During Extrusion of PE Pipes - Windows and Their Effect on Butt Fusion Joint Integrity. PE100+ Association Advisory Board Meeting. 2018 June 7.
[6]Deveci S, Antony N, Nugroho S, Eryigit B. Effect of carbon black distribution on the properties of polyethylene pipes part 2: Degradation of butt fusion joint integrity. Polymer degradation and stability. 2019 Apr 1;162:138-47.
[7] BS EN 12814-7. Testing of welded joints of thermoplastics semi-finished products- tensile test with waisted test specimens. British Standards Institution, London, UK. 2002

Faranak Bahrami
Faranak completed her BEng (Hons) and MSc in Biomedical Engineering at the University of Surrey. Faranak is currently completing her Engineering Doctorate (EngDoc) in Micro and Nano Materials and Technologies at the University of Surrey and Adhesives, Composites and Sealants section at TWI. Faranak's project is sponsored by EPSRC, University of Surrey, TWI Core Research Programme, and Horizon 2020.

Thermally assisted piercing: assessment of its impact on mechanical properties of perforated composites.

Dr C.M. Worrall[1], Prof S.L. Ogin[2], Dr M. Oldfield[2], Prof J.F. Watts[2]
[1]TWI, [2]University of Surrey
4th Year of PhD

Keywords: Thermoplastic composite, Perforation, Thermally Assisted Piercing, Mechanical properties

I. INTRODUCTION

Perforated metal panels are currently used in many industries and applications including sound-absorbing engine components, leading-edge anti-icing, and blast protection systems. Due to the increasing demand for weight reduction, the aerospace industry, in particular, is trying to increase its exploitation of composite materials. Composite parts can be manufactured to near-net-shape with minimum wastage of material; however, there is often a need for further machining. Creating holes for assembly amounts to approximately 90% of the aerospace industry's requirements for composites machining [1]. Perforation of composite materials is currently carried out using conventional machining techniques, such as drilling and abrasive water jet cutting. However, these techniques cut the load-bearing fibres and reduce the efficiency of the composite around the holes. This project is funded by TWI's Member companies and aims to exploit the benefits of thermoplastic composite materials for perforated structures; it is a further development of the Thermally Assisted Piercing (TAP) process [2, 3], an innovative technique applied to mechanical fastening. In this technique, the thermoplastic composite is heated above its melting point and a pin is pushed into the material. Since the matrix is molten, the fibres are free to move around the pin. In previous work [3], the effects of varying the process parameters on a single 6mm diameter hole generated by the TAP process were studied. Strength improvements of up to 11% and 21% were found for pierced specimens compared with drilled specimens for open-hole tension and compression loading, respectively.

II. APPROACH

A multiple-piercing rig has been designed with the potential of piercing a thermoplastic composite structure with one hundred 2mm diameter holes simultaneously (see Fig1). The rig allows creating a variety of perforation patterns.
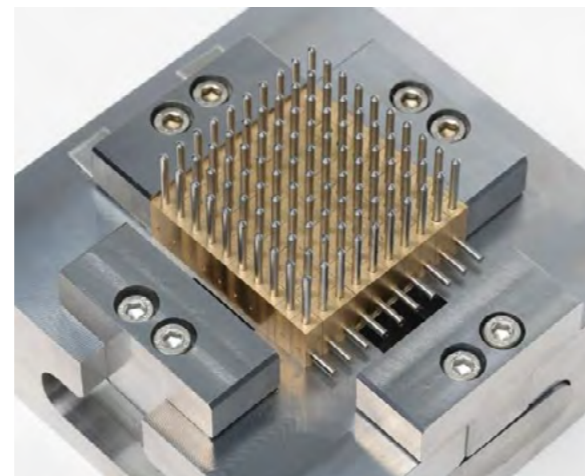
Fig1. Multiple Piercing rig

Test coupons were made of Carbon fibre reinforced Polyamide (CF/PA12) laminates with a nominal fibre volume fraction of 55%. The layup of the laminates was [0/90]8S.

To understand the effect of the multiple thermally assisted piercing technique on the composite materials, various mechanical tests and NDT techniques were used. The coupons were divided into three groups to aid comparison: Unperforated (UP), and Perforated: Pierced (P), and Drilled (D).

III. RESULTS

Table 1 and Table 2 show a summary of results for open-hole tensile (OHT) and open-hole compression strength (OHC), respectively.

Table 1. OHT test results for unperforated, pierced, and drilled coupons.

	Unperforated	Pierced	Drilled
σ_{Max} (MPa)	328 ± 49	233 ± 34	274 ± 23

Table 2. OHC test results for unperforated, pierced, and drilled coupons.

	Unperforated	Pierced	Drilled
σ_{Max} (MPa)	648 ± 77	658 ± 79	555 ± 38

The mechanical test results indicated that pierced coupons have higher average strength under tensile loading. However, the compression test results proved otherwise.

IV. DISCUSSION/CONCLUSIONS

Results of the mechanical testing revealed two different behaviours of the pierced perforated composites. Under tensile loading, the OHT tests showed the pierced composite specimens to have a strength similar to the unperforated coupons and a significantly higher strength that the drilled equivalents. This was to be expected, and was one motivation behind using the TAP method to make holes. No fibres are cut when making the holes, allowing more of the fibres to carry the tensile stresses, even allowing for the stress concentration factor initiated by the hole. If this beneficial effect is continued in larger test panels containing an array of pierced perforated holes (not a simple line as investigated in this project) then the perforation using TAP offers significant benefits and impetus to increase the adoption of composites and exploit their advantages, in applications currently dominated by metals. However, when loaded under compression, the behaviour is different. The OHC strengths determined were lower than those obtained from the unperforated test coupons, and also slightly lower than the drilled specimens.
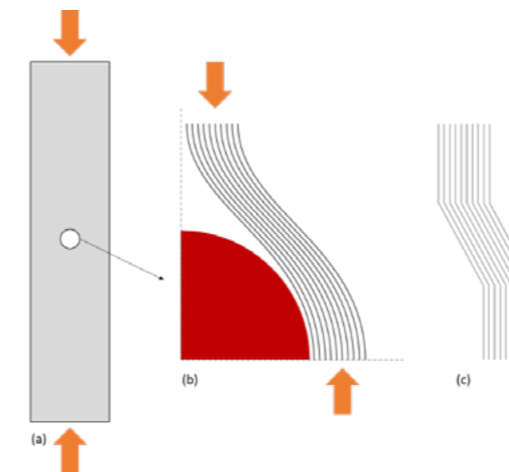
Figure 2. OHC tests: (a) OHC test geometry, (b) Longitudinal fibres displaced around the hole, (c) Kink failure under axial compressive stress.

The compressive failure behaviour of continuous aligned fibre composites is sensitive to local changes in fibre orientation, or fibre waviness, which can cause fibre buckling. The piercing process displaces the fibres around the pin (Figure 2.b. The changes in the fibre orientation do not have a significant effect under tensile loading of the coupon, however, under the compressive loading, they can act as an initiation for a local kink failure (Figure 2.c). Optical microscopy of the OHC tested pierced coupons demonstrated the kink band which can explain the lower failure strength of the pierced coupon, relative to both the unperforated and the drilled.

Figure 3. Optical microscope image of a pierced coupon tested under OHC loading.

The reduction in OHC strength measured may suggest that the use of the TAP process does not have any benefits if the application is dominated by compressive loading. However, if the application experiences mainly tensile loading the TAP technique can still be beneficial. Such an application may be in blast protection systems.

V. ACKNOWLEDGEMENT

REFERENCES
[1] Richardson M (2012) 'Know the Drill', Aerospace Manufacturing 7(59), June 2012, MIT Publishing Ltd., UK.
[2] Brown N.W.A (2016). 'Development of a Thermally-Assisted Piercing (TAP) Process for Introducing Holes into Thermoplastic Composites'. EngD Thesis, University of Surrey, Guildford.
[3] Brown N, Worrall C, Ogin S and Smith P (2015) 'Investigation into the mechanical properties of thermoplastic composites containing holes machined by a thermally-assisted piercing (TAP) process'. Advanced Manufacturing: Polymer & Composites Science, 1(4), pp.199-209, 2015.

Marie-Salome Duval-Chaneac
Post-graduate research student with the university of Southampton, within the Physical science faculty and part of the Materials and Engineering Research Group. Under the supervison of Dr. Nong Gao, Prof. Pilippa Reed and Dr. Raja Khan. Sponsored by EPSRC and LRF.

Effect of post thermal treatments on microstructure and mechanical properties of multiple materials fabricated by 3D printing.

Dr Raja Khan[1], Dr Nong Gao[2], Prof. Philippa Reed[2]
[1]TWI, [2]University of Southampton
2nd Year of PhD

Keywords: Multiple Material Additive Manufacturing (MMAM), Fatigue, Heat treatment, Inconel 718, 316L stainless steel, multi-material, additive manufacturing (AM)

I. INTRODUCTION

Multiple material additive manufacturing (MMAM) allows the production, in a single operation, of components with varying functional materials integrated into specific design locations. Targeting properties such as high temperature resistant alloy, as Inconel 718 (IN718) and highly corrosion resistant 316L stainless steel, combined to produce key components in systems with extreme environments such as gas and oil industries, or pharmaceutical production line. However, these types of materials normally require specialised post manufacture heat treatments to optimise their mechanical properties and ensure their structural integrity.

II. DESIGN/METHODOLOGY/APPROACH

In this study, layered structure combining Inconel 718 (IN718) and 316L austenitic stainless steel have been fabricated by MMAM, and the effect of heat treatment on the microstructure and mechanical properties of these specimens has been studied. Single edge notched bend (SENB) specimens of bi-layer and four alternated layers were built horizontally, both IN718 and 316L layers were produced using the same set of process parameters. A specific heat treatment strategy including an annealing stage followed by a rapid cooling and a single stage ageing was applied in order to allow precipitation strengthening to occur in IN718, while limiting the formation of detrimental phases in the 316L region and at the transition zone between the two alloys.

Microstructure of both as-built (AB) and heat-treated (HT) bi-layers specimens were studied using SEM, EDS, and EBSD. First, the microhardness was measured across bi-layer specimens, then tensile properties of each material were characterised separately, finally fatigue tests were performed on the combined material system under three point bending configuration. Crack growth was investigated on single edge notched bend samples, through the dissimilar interface, with increasing and at constant crack tip stress intensity factor in order to discriminate the magnitude of the shielding/anti-shielding effect of the interface, in as-built and heat treated condition.

III. FINDINGS/RESULTS

It was found that, compared with the as-built specimens, the yield strength and ultimate tensile strength after heat treatment increased by 11% and 22% for IN718, and decreased by 31% and 5.2% for 316L. At the dissimilar material interface an inter-diffusion zone with a width of 145μm was observed and the presence of some Laves phases and carbide formation was found in this region.

The effect of dissimilar material properties on crack propagation has been studied. The crack growth rate increased by a factor of three when transition from hard IN718 layer to soft 316L layer (anti-shielding effect) in the as-built specimen, and reciprocally the influence of the more compliant 316L layer in multi-material specimen showed a decrease in the overall crack propagation rate by effectively shielding crack propagation at the second interface.

IV. DISCUSSION/CONCLUSIONS

The effect of grain misorientation on crack propagation has been found as a main factor affecting crack propagation in the as-built L-PBF. Whereas the yield stress difference between IN718 and 316L after heat treatment is larger, its effect on crack propagation is more significant. The transition from the soft 316L layer towards hard IN718 layer, should display shielding and effectively delay the overall crack propagation rate.

V. FUTURE PLAN/DIRECTION

Further work on material strengthening and shielding effect will be continued, and enhancement of fatigue lifetime in multiple-material layered specimens will be investigated further.

PhD research bringing new products to market - Teletest, a device for NDT inspection of metallic pipes, made possible thanks to multiple PhD research projects at TWI. Photo: TWI Ltd

Stephen Cullen

Stephen is a highly motivated engineering professional with a Master's degree in Energy Engineering from the University of Huddersfield. His research currently focuses on the discipline of directed energy deposition, a process of additive manufacturing. Study includes geometry assessment, and how thermally induced distortion influences the outcome of the components being produced by this manufacturing method. Stephen has taken a keen interest in all things engineering from a young age, and has always been industrious, results driven and focused. He enthusiastically embraces new tasks and is a driver for modernisation.

Effects of laser power and surface thickness on thermally induced distortion of laser deposited In-718 flanges

Prof. L. Blunt[1], Dr. P. Bills[1], Dr. C. Hauser[2]
[1] School of Engineering, The University of Huddersfield, [2]TWI Technology Centre Yorkshire
2nd Year of PhD

Keywords: Laser metal deposition; additive manufacturing; porosity; thermally induced distortion; In-718

I. INTRODUCTION

Deemed one of the more adaptable additive manufacturing (AM) processes, directed energy deposition (DED) allows for fabrication of metallic parts directly from computer aided design (CAD) data [1]. A blown powder discipline of the AM process, currently being employed to produce large near net functional 3D shapes and structures. The established cladding process behind DED has been adapted utilising a layering method to allow for complex geometries to be formed. DED allows for flexibility within the system to conduct component repairs and production on a larger scale to the order of above 1m^3. In combination with its reduced lead times [1] when compared to conventional subtractive machining, the use of DED reduces waste, having up to 80% nozzle efficiency in some cases. Therefore the volume/mass of material used is nearer to the volume/mass of the final built component, and thus optimises material usage/waste in the production process, reducing its carbon footprint [2]. The DED discipline uses the generated heat from a laser beam energy source, creating a melt-pool on the surface of a metallic component or substrate. Fine metallic powder is then fed into the melt-pool forming a solidified deposition that becomes fusion bonded to the preceding layer beneath it [3]. In combination with controlled laser beam movements and mapped geometry through CAD software, the solid metal part is built one layer at a time. Computer numerical control (CNC) of the laser and powder injection nozzle axis gives a freedom of motion that is greatly exaggerated from that of a powder bed process. Although advantageous in its use, using DED does lead to new challenges, where there are large knowledge gaps in understanding of the geometrical, mechanical and microstructural properties of the components being produced. This, in turn brings into question the DED part durability and functional predictability whilst in service. The cyclical heating and re-heating of deposited material generates large temperature gradients within the deposited material during manufacture, effecting the geometrical and mechanical behaviour. These temperature gradients have been seen to induce thermal distortion and residual stresses in components [4]. Factors shown to have the most bearing on geometrical, metallurgical and mechanical properties of the deposited material are those parameters that require forefront consideration when processing. These include: laser beam power, scanning velocity and powder flow rate, all directly effecting the energy density [5]. For the remit of this study laser power will be the focus. The nickel-based alloy Inconel 718 will be the subject material for this study. Such alloys, known for their excellent oxidation, corrosion, fatigue and creep resistance, are becoming widely used in applications of AM constructed jet engine casings, nuclear reactors, turbine blades/components [6,7] and in the petrochemical industry, all of which require large components for heavy industry.

II. METHODOLOGY

Twelve test specimen cylinders were additively manufactured using the Trumpf DMD 505 machine. Using the 1.8kW CO2 laser, each cylinder was constructed with a single spiral pathway as a vertical build, built from a cylindrical billet. Each cylinder was then rotated through 90° to allow for deposition of a flange, as another vertical spiralling build around the circumference of the cylinder. To determine the effect of laser power on the lamination of weld tracks and topographical deviation, the power percentage for the laser was varied for each deposited flange, with a spread taken to show if any pertinent trends emerged. Using electrical discharge machining (EDM), sections were cut from the flange of each sample at 90° increments of one another, inclusive of the weld interface between cylinder and flange, for further investigation. Sections cut from the specimens measured approximately 20mm ±0.05 in width. For distortional analysis on interface thickness, three cylinders were subsequently manufactured at the optimum wattage (840W, as seen through metallography) using a variance in cylinder wall thickness to determine the effect of deviation from the CAD model against the single cylinder builds.

III. RESULTS

Initial analysis of the X-ray computed tomography (X-CT) demonstrated large amounts of delaminating between deposited tracks of samples produced with low power, high power samples showing a near, fully dense structure with few pores and potential porosity occurring. As the power decreases, samples start illustrating degradation of the weld fusion, thus the trend that decreasing the laser power increases the amount of porosity and inclusions. The porosity analysis of the X-CT is illustrated on a colour gradient from small to large using blue to red respectively (Fig.2).
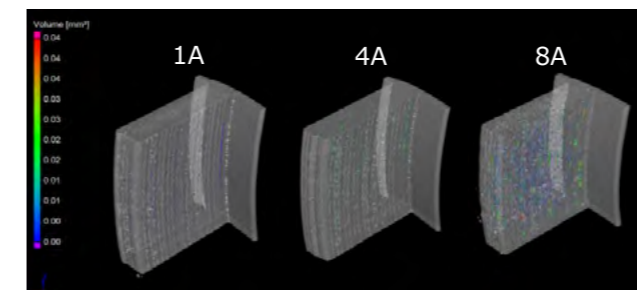

Fig 2. XCT samples 1A, 4A and 8A showing increase in porosity and inclusions

Further investigations depict that the defects within the samples follow the path of deposition, showing that the laser energy has influenced the quality of the material through the path of the deposited track. The frequency of porosity and inclusions trend directly to the laser path and energy alterations. The density of the samples increased with the increase in laser power. As the range of laser energy gave little shape deformation, further samples were produced to see the effect of increased cylinder thickness on this deformation. Using the Hexagon Romer RS3 arm, it was possible to map the cloud point data onto existing CAD files used in the production of the samples. There can be seen a continuing reduction of the distortion through the spread of samples analysed. Approximately a magnitude of 10° distortion at the cylinder top was noted as the maximum, where specification tolerances would undoubtably have failed on a commissioned component.

IV. DISCUSSION/CONCLUSIONS

This study illustrates that laser energy plays a crucial part in the AM process where component integrity is concerned. The effects of reducing the laser energy on the deposited tracks show an increase in the amount of porosity and inclusions found within the samples analysed. The presence of such defects would bring into question the structural and mechanical integrity of a finished components, compromising functionality. As measured by the metallography sections, the layer size is also decreased with the decrease in laser power, thus effecting the efficiency of the process where larger builds will subsequently require more build time. The distortion at the weld interface showed minimal difference through the course of the laser power used, but was ultimately eliminated with the increase of wall thickness.

REFERENCES

[1] Ghosal, P., Majumder, M., & Chattopadhyay, A. (2018). Study on direct laser metal deposition. Materials Today: Proceedings, 5(5), 12509-12518. doi: 10.1016/j.matpr.2018.02.232

[2] Abdulrahman, K., Akinlabi, E., & Mahamood, R. (2018). Laser metal deposition technique: sustainability and environmental impact. Procedia Manufacturing, 21, 109-116. doi: 10.1016/j.promfg.2018.02.100

[3] Mahmood, R. M. (2016). Laser Metal Deposition Process. 3D Printing, 172–182. https://doi.org/10.4018/978-1-5225-1677-4.ch009

[4] Mukherjee, T., Manvatkar, V., De, A., & DebRoy, T. (2017). Mitigation of thermal distortion during additive manufacturing. Scripta Materialia, 127. https://doi.org/10.1016/j.scriptamat.2016.09.001

[5] Shim, D. S., Baek, G. Y., Seo, J. S., Shin, G. Y., Kim, K. P., & Lee, K. Y. (2016). Effect of layer thickness setting on deposition characteristics in direct energy deposition (DED) process. Optics and Laser Technology, 86, 69–78. https://doi.org/10.1016/j.optlastec.2016.07.001

[6] V.A. Popovich, E. B. (2017). Functionally graded Inconel 718 processed by additive manufacturing: Crystallographic texture, anisotropy of microstructure and mechanical properties. Materials and Design, 441-449.

[7] Tresa M. Pollock, S. T. (2006). Nickle-Based super alloys for advanced turbine engines: chemistry, microstructure and properties . Journal of Propulsion and Power , 361-374.

[8] Aerospace specification materials Inc. . (2020). Special Metals INCONEL® Alloy 718. Retrieved from http://asm.matweb.com/: http://asm.matweb.com/search/SpecificMaterial.asp?bassnum=NINC34

(N.B. Please see main paper for figure/table references.)

Helen Elkington
I am a second year PhD student based at TWI Yorkshire, and Sheffield Hallam University where I originally went to to study a Masters in Mechanical Engineering.

Direct energy deposition with laser – the dffect of process parameters on metallurgical and mechanical properties

Dr. Carl Hauser[1], Dr. Stephen Magowan[2], Dr. Quanshun Luo[2]
[1]TWI, [2]Sheffield Hallam University
2nd Year of PhD

Keywords: direct energy deposition with laser, microstructure, mechanical properties, Inconel 718

I. INTRODUCTION

Direct energy deposition with laser (DED-L) uses a laser as a heat source to melt metal in powder form to create components. There are numerous process parameters involved within this process which can be altered, with multifaceted relationships between these and the properties of the deposited material [1]. This research looks into the effect of certain process parameters on the metallurgical and mechanical properties of Inconel 718 in its as-deposited state.

II. METHODOLOGY

A Trumpf 505 DMD system was used to manufacture all test specimens of Inconel 718. Work was split into three phases of investigation. Phase 1 examines the differences present between planes of a single build. Phase 2 investigates the effect of using different build deposition directions for identical geometries (an oblong block) and process parameters. Phase 3 looks into the effect of using two deposition directions within a single build.

Test specimens were subject to both metallurgical and mechanical analysis. This included optical light microscopy, scanning electron microscopy and energy dispersive X-ray analysis. Mechanical testing consisted of tensile testing followed by fractography and microhardness testing.

III. RESULTS

Phase 1 found anisotropy to be present within the test specimen, and this was also true of Phase 2 and Phase 3 DED-L builds. Columnar grain growth was observed within the sample, with each deposited track clearly visible under the microscope. This columnar growth was also present in Phase 2 and Phase 3 test specimens.

Phase 2 results indicate that the direction used to build a part with regards to the parts geometry affects final properties, this is likely to be due to its influence on heat build-up during the deposition process. Under high magnifications (>50x) on the optical light microscope, differences were revealed in grain structures between the two build directions used (Figure 1).
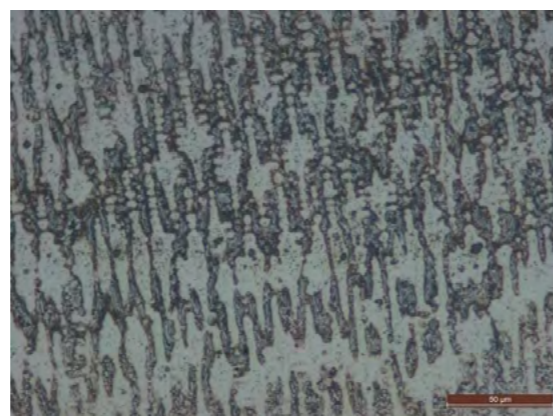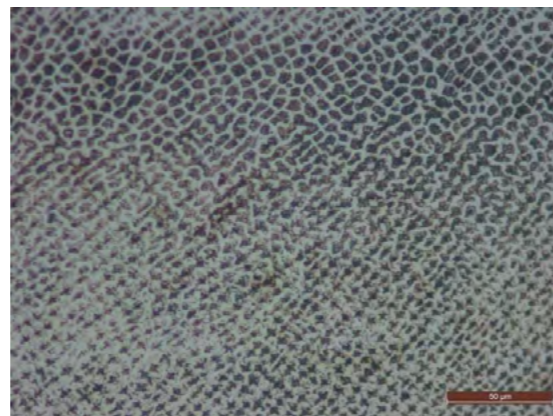
Figure 1. The different microstructures observed in horizontal (long length parallel to substrate, top image) and vertical (long length perpendicular to substrate, bottom image) samples within Phase 2.

Phase 3 results indicate that when using more than one deposition direction within a part, the interface is not be detrimental to mechanical properties. The interface where the two deposition directions meet is visibly clear under the microscope.

Scanning electron microscopy backscatter images observed elemental segregation within test specimens. Energy dispersive x-ray analysis revealed Nb to be the predominant segregating element (Figure 2).
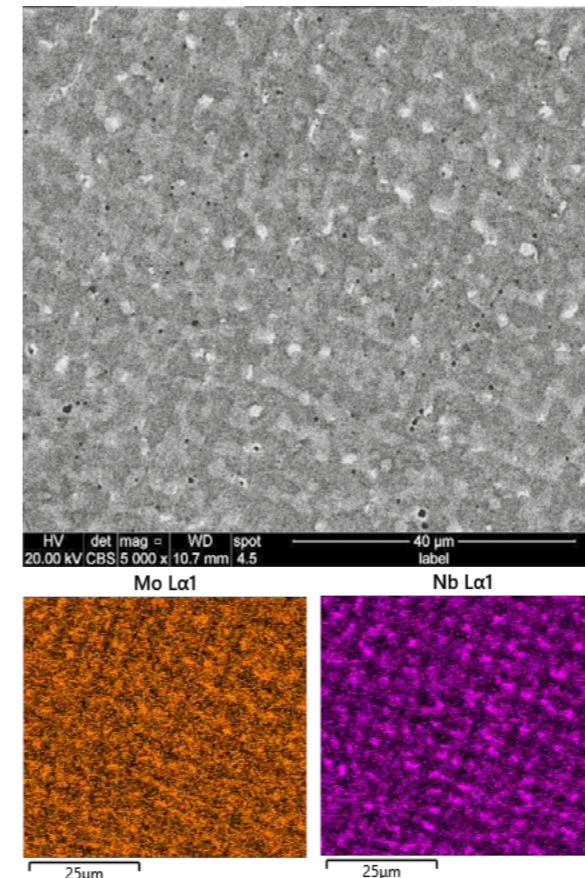
Figure 2. A backscatter image of one of the test specimens (top) and the elemental maps of Mo and Nb (bottom).

Examination of fracture faces for all tensile specimens observed no presence of oxidation and two distinct regions to be visible. Cleavage facets, coarse intergranular regions and the presence of microvoid coalescence could be seen.

IV. DISCUSSION AND CONCLUSIONS

The columnar growth present in all samples can be attributed to the repetitive heat cycling, causing the Inconel 718 to grow coarser and in a columnar manner as subsequent layers of material are deposited. It is possible that some grains will have extended the full length of the DED-L part, agreeing with Li et al. [2] that columnar grains can grow the length of an entire DED-L part. This results in fewer grain boundaries and thus will have a negative effect on the yield strength of the part, as according to the Hall-Petch equation.

The difference between microstructure in Phase 2 horizontal and vertical samples is attributed to the differences in heat build-up during the DED-L process, as the vertical samples have less cooling time between subsequent layers.

The elemental segregation of Nb is likely to have been detrimental to the mechanical properties of the Inconel 718 test specimens [3].

Fracture faces showed no presence of "cup and cone" ductile failure mechanism. The cleavage facets and coarse intergranular regions are indicative of brittle fracture, whilst the presence of microvoid coalescence indicates ductile failure. It is likely that the intergranular region propagated first resulting in the visible cleavage facets, and once the remaining ligament was small enough, the specimen was torn apart in a ductile manner.

V. FUTURE PLAN

To further this work, three key process parameters which influence the heat within the DED-L process will be examined. These have been identified as laser power, laser scan speed and powder feed rate. These will be used within a Taguchi Design of Experiments, with three levels for each process parameter. Ranges for these will be determined based on previous work using Inconel 718 on the Trumpf 505 DMD system.

REFERENCES

[1] Segerstark, A., Andersson, J., & Svensson, L. (2014). Review of laser deposited superalloys using powder as an additive. 8th International symposium on superalloy 718 and derivatives, 393-408.

[2] Li, J., Luo, Z., Guan, X., Zhou, X., Brochu, M., & Zhao, Y. (2018). A novel microstructure simulation model for direct energy deposition process. Solid Freeform Fabrictaion Symposium, 1737-1750.

[3] Manikandan, S., Sivakumar, D., & Kamaraj, M. (2019). Welding the Inconel 718 Superalloy. Elsevier.

Vishal Vats

I am a materials engineer, currently working on the PhD. project 'hexavalent chromium in welding fumes'. I am in my second year of PhD. at Teesside University and sponsored by TWI. I obtained my bachelor's degree in Mechanical Engineering from Annamalai University (India) in 2014 and then earned a scholarship from the Government of India, to pursue my Master's in Materials Engineering from National Institute of Technology Karnataka, Surathkal (India) in 2015. After completing my Master's in 2017 I joined Indian Institute of Technology, Gandhinagar as Junior Research Fellow for the Project titled 'Nanocrystalline substituted cobalt based metal oxides for oxygen evolution reaction'. My interests are electrochemistry, Corrosion science and welding engineering

An investigation on feasibility of using FTIR for Cr (VI) analysis in welding fumes

Geoff Melton[1], Dr Venkatesan V. Krishnan[2], Prof Meez Islam[2]
[1]TWI, [2]Teesside university
2nd Year of PhD

Keywords: Hexavalent Chromium, Welding fumes, FTIR,

I. INTRODUCTION

The issue of occupational exposure to welding fumes, deleterious to welders, has gained considerable urgency, since last year, when HSE (UK) issued a safety alert to industries (in Feb 2019) requiring them to minimise exposure of their workers to welding fumes [1]. Current Long-term exposure limit (8-hr TWA reference period) for Cr(VI), are 0.025 mg/m^3.[2] Airborne hexavalent Chromium (Cr [VI]) compounds, generated during arc welding is a known human carcinogen [highly toxic due to its ability to oxidize biomolecules, notably DNA[3]] whilst Cr (III) which is not harmful, is usually in condensed phase. The Na^+ and K^+ ions present in the welding electrodes are known for forming Cr (VI) compounds during welding.

$$2Na + Cr + 2O_2 \rightarrow Na_2CrO_4$$

$$2K + Cr + 2O_2 \rightarrow K_2CrO_4$$
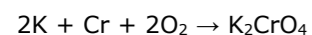
The presence of both +3 and +6 oxidation stage of chromium in welding fumes makes it difficult to analyse the correct amount of Cr (VI) in welding fumes. The current analytical methods used to determine Cr (VI) percentage in welding fumes are always being challenged as these methods involve wet chemistry. The most common procedure for Cr (VI) analysis is via extraction of air filtered particulate samples with sulfuric or nitric acid. Extraction is followed by spectrophotometric analysis of the magenta chromogen which is formed by the reaction of Cr (VI) with 1,5-diphenylcarbazide (DPC) in strongly acidic solution.

During analysis there are chances of redox reactions oxidising Cr (III) to Cr (VI) and reducing Cr (VI) to Cr (III). The divalent iron [Fe(II)] which is most likely to be present in the welding fumes works as reducing agent for Cr (VI); also the manganese dioxide which too is likely to be present in welding fumes may react with Cr (III) and oxidise it to Cr (VI) during the course of hot alkaline extraction of insoluble Cr (VI) compounds in welding fumes. The effect of pH on the distribution of chromium between trivalent and hexavalent oxidation state in presence of iron is described by the equation below.

$$Cr(OH)_3 + 5OH^- + 3Fe^{3+} \rightleftarrows CrO_4^{2-} + 4H_2O + 3Fe2^+$$
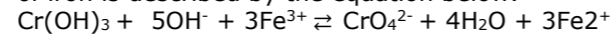
To avoid these redox reactions during the analytical analysis of Cr (VI) possibilities of using new methods to analyse Cr (VI) in welding fumes need to be explored. One of these new methods which has not been explored is Fourier Transform Infrared Spectrometry (FT-IR). FT-IR does not involve any wet chemistry so there are no chances of redox reaction, which interfere with the present analysis methods because of the complex mixture of welding fumes.

II. FINDINGS/RESULTS

To investigate the possibility of using FT-IR for analysis, the welding fumes were collected by performing Metal active gas (MAG) welding on mild steel bars with a 92% Argon and 8% Carbon Dioxide mixture as shielding gas. The consumable used was mild steel solid wire which has less chromium compared to a stainless steel filler wire. A mild steel filler wire was chosen instead of stainless steel as the fumes formed due to mild steel have less chromium in them, and it will enable the usage of FT-IR for tungsten inert gas (TIG) welding too, as the Cr (VI) content in the TIG welding is hard to determine due to generation of lesser fumes and much less Cr (VI) - similar to mild steel and hence fumes from TIG welding are not being tested for Cr(VI) analysis.

After collecting the fume samples by the method described in ISO 15011-1, these were analysed by Perkin Elmer FT-IR which has an ATR (Attenuated Total Reflection) probe attached. Along with the fume sample reference potassium dichromate sample was also analysed to see if the spectra of welding fumes contain any dichromates (and establish a location for the absorption bands for Cr (VI)). To get clear peaks fumes were tested with the different parameters of FT-IR and finally optimized at a probe resolution of 4cm^{-1}.
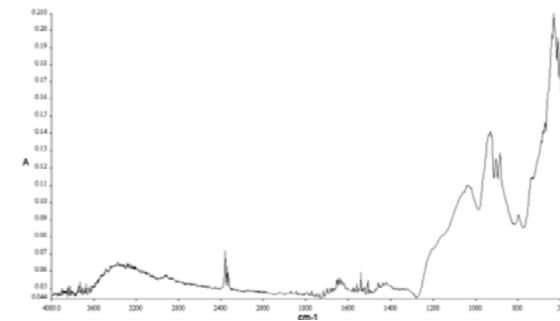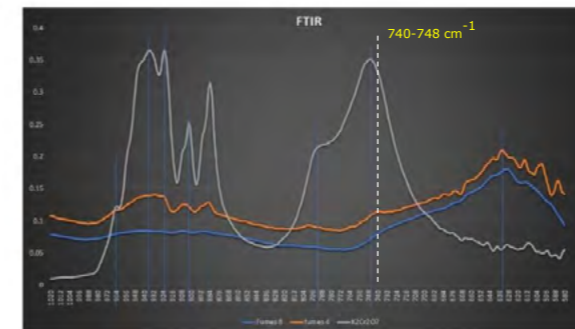

Fig.1 FT-IR spectra of welding fumes at 4cm^{-1} resolution

Fig.2 FT-IR spectra of welding fumes at 4cm^{-1} resolution (orange); 8cm^{-1} resolution (blue); and Potassium Dichromate (white).

III. DISCUSSION/CONCLUSIONS

Fume compositions from welding mild steel have been reported earlier [4], and were identified to be compounds of Fe, Mn, Cr, Ni and Cu. The other important point to consider is that most of the welding fumes originate from consumables and not from the welded base material and as a result it is always important to investigate the filler material composition. In this work, the electrode used was mild steel and its typical composition contains C (0.1%), Si (0.8%), Mn (1.3), and Iron. Previous FTIR data on chromates and dichromates shows peaks in the region of 900cm^{-1} to 700cm^{-1} [5,7,8] and these peaks were also reflects in our sample analysis which is shown in fig.1. Since the fume samples in this work was from mild steel Cr(VI) levels were perhaps low, but there is evidence of absorption bands peaks wavelength of 900cm^{-1} to 700cm^{-1} which might be due to the functional group of $Fe_2O_4^{2-}$, which overlaps chromates peaks in the region of 720 cm^{-1} to 840 cm^{-1}[6,7,8,9].

The FT-IR spectra was segregated into the various peak regions, and then analysed. The peaks in the initial results (fig.2), show the presence of functional group such as MnO_3^{2-}, MnO_4^{2-}, SiF_6^{2-}, $Fe_2O_4^{2-}$, SiO_4^{4-}. These functional group peaks are due to the bending vibrations and stretching of molecules due to the energy provided by infrared. MnO_3^{2-} and MnO_4^{2-} can be characterised by a sharp peak between 860 cm^{-1} to 890 cm^{-1}, SiF_6^2 peak is present between 610 cm^{-1}– 640 cm^{-1} and $Fe_2O_4^{2-}$ peaks overlaps the chromates and dichromats which may be challenge to differentiate when analysing stainless steel fumes.

These preliminary results confirms that the FT-IR can be a promising technique to study the composition of the welding fumes and the chemical structure of the welding fumes can be easily determined through FTIR. The second phase of the study is to find out how we can use the FT-IR for the quantitative analysis of the welding fumes.

IV. FUTURE PLAN/DIRECTION

Plans include quantification of welding fumes, by looking at welding fumes from different consumables such as stainless steel electrodes and establishing a standard procedure for Cr (VI) analysis by FTIR. It is also planned to carry out more FT-IR analysis by changing the depth of penetration and work on Beer's law for qualitative analysis of welding fumes. Another focus area is to investigate the possibility of analysing TIG welding fumes by FT-IR as they cannot be analysed by UV-Vis spectrometry because of low sample size.

Along with FT-IR analysis work is in progress towards understanding the mechanism of Cr (VI) formation in welding fumes and the methods to mitigate them.

REFERENCES

[1] https://www.twi-global.com/media-and-events/press-releases/2019/uk-health-and-safety-executive-issues-welding-safety-alert
[2] EH40/2005 Workplace exposure limits
[3] Ashley, Kevin, et al. "Sampling and analysis considerations for the determination of hexavalent chromium in workplace air." Journal of Environmental Monitoring 5.5 (2003): 707-716.
[4] Blair, A. J., and D. A. Pantony. "Inorganic analysis in organic solvents: Spectrophotometric determination of chromium following a chromatographic separation." Analytica Chimica Acta 14 (1956): 545-552.
[5] Nyquist, Richard A., and Ronald O. Kagel. Handbook of infrared and raman spectra of inorganic compounds and organic salts: infrared spectra of inorganic compounds. Vol. 4. Academic press, 2012.
[6] Kimura, S. "Investigations on chromium in stainless steel welding fumes." (1980).
[7] Hallam, H. E. "Infrared and Raman spectra of inorganic compounds." Royal Institute of Chemistry, Reviews 1.1 (1968): 39-61.
[8] Miller, Foil A., and Charles H. Wilkins. "Infrared spectra and characteristic frequencies of inorganic ions." *Analytical chemistry* 24.8 (1952): 1253-1294.
[9] Vogel, Christian, et al. "Thermal treatment of chromium (III) oxide with carbonates analysed by far-infrared spectroscopy." Applied spectroscopy 69.10 (2015): 1210-1214.

Ahmed Teyeb

Ahmed joined has a master degree in instrumentation and measurements. He joined Brunel University as a researcher and member of power Ultrasonic team, in Brunel Innovation Centre from March 2017, and started his part-time Phd in April 2018. Ahmed's research background is in instrumentation, data acquisition and sensors' development. He is working on projects dealing with electronics development andpower ultrasonic for cleaning and material processing.

Investigation of the use of ultrasonic power for the improvement of manufacturing processes

Tat-Hean Gan[1], Wamadeva Balachandran[2]
[1]TWI, [2]Brunel University London
2nd Year of PhD

Keywords: Ultrasonic waves, manufacturing, composites, nanoparticles, agglomeration

I.   INTRODUCTION

Novel materials processing techniques nowadays allow the production of parts with high mechanical properties that were beyond those of previous techniques. The reinforcement of composite materials with micro and nanoparticles has attracted the attention of several researchers. This type of reinforcement makes it possible to substantially improve the properties of the materials against a considerable reduction in weight. This is particularly useful in applications where mass reduction is critical, such as automotive, aerospace, nuclear and renewable energy.

However, the quality of those parts produced with manufacturing processes involving a solidification phase requires further improvement, mainly regarding the size of the grains, the poor distribution of the particles, the agglomeration of certain additives, etc.

The use of power ultrasounds during the liquid phase has shown high potential for solving this, as it helps to homogenise the material, refine grains, prevent agglomerations and improve the mechanical properties.

The goal of this project is to investigate the use of power ultrasonic (hundreds of watts) for material refining and nanoparticles dispersion inside liquid phase material during manufacturing processes. The main focus is on the processes used for the manufacturing of composite laminates with fibre reinforcements (CFRP and GLARE), with nanoparticles (Grpahene and Carbon nanotubes).

II.   DESIGN/METHODOLOGY/APPROACH

The proposed research includes a preliminary FEA study of ultrasonic waves propagation in laminate composites. The models help to prove that ultrasonic waves are propagating to a sufficient depth within the manufactured parts, and to determine and optimize ultrasonic processing parameters for manufacturing process. The wave propagation depends obviously on the attenuation properties of the materials, the number and types of layers, interlayer acoustic impedance, fibre orientation in composites, etc.

COMSOL Multiphysics is used to run the simulations. It allows conduct different numerical analysis i.e. frequency domain, time domain, modal analysis.

Models for wave propagation in multilayer composites were simulated at a range of frequencies varying from 20 kHz to 60 kHz. Results were obtained for impedance which allows to confirm the resonant frequency of the transducer. Distribution of total displacement was also observed at the resonant frequency and was compared with the different configurations.

Integration of kinetic energy at each frequency was considered. To quantify the impact of the ultrasonic processing, it is necessary to study the variations of elastic energy through the whole media.

At resonant frequency, high levels of displacement with node and antinode regions were observed closer to contact site as seen in Fig. 1.
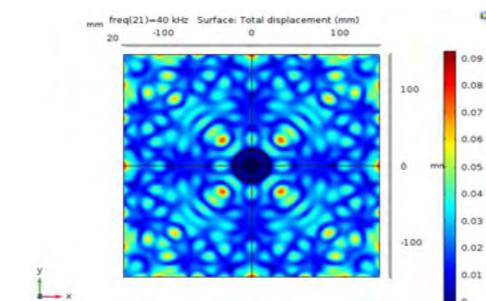
Fig.1. Displacement in Glare 3 sample

The validation of the outcome of ultrasonic processing is achieved by the manufacturing and the testing of a set of composite samples that covers relevant parameters. The design of experiments allowed us to propose an optimal testing matrix that covers the parameters and that will reveal how the ultrasound will help to improve the Nano dispersion in composites. CFRP and GLARE samples, with and without nanoparticles, were manufactured, using Oven, autoclave curing and res_____nd without ultraso__

Fig.2. Autoclave setup with US transducers

III. FINDINGS/RESULTS

The experimental validation of numerical models is achieved using 3D laser vibrometry of surface composite out of plane vibration, animated with ultrasonic power transducers from one side of the plates.
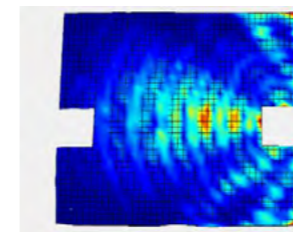
Fig.3. 3D laser vibrometry

The waves propagating through the composites are compared to the output obtained from the numerical model. Preliminary experimental tests consist in an analysis of the out of plane surface vibration following the propagation of an ultrasonic wave. High power ultrasonics were successfully applied to improve the manufacturing of CNT enhanced GLARE and Graphene enhanced CFRP panels. The samples were prepared with UD prepreg and nanoparticles veils, using oven curing method. The resulting samples showed:

-Improvement of the surface quality of the samples processed with Ultrasounds, confirmed by visual inspection.

-Reduction of grains size and improvement of microscopic structure of the materials. This was confirmed by SEM tests.

IV. DISCUSSION/CONCLUSIONS

Preliminary tests were conducted to study the applicability of ultrasonication to improve the manufacturing of CFRP and GLARE composites. Numerical study was conducted to study the propagation of the ultrasonic waves through plates, using the piezoelectric transducers for the selection of appropriate transducer. Numercial results were validated using a controlled experiment and this behavior has been studied using the 3D laser Doppler Vibrometer. After the validation of the numerical model, this can be used to conduct a parametric study for further optimization of the process.High power ultrasonics were successfully applied to improve the manufacturing of CNT enhanced GLARE and Graphene enhanced CFRP panels. The samples were prepared with UD prepreg and nanoparticles veils, using oven curing method. The resulting samples showed:

Improvement of the surface quality of the samples processed with Ultrasounds, confirmed by visual inspection.

Reduction of grains size and improvement of microscopic structure of the materials. This was confirmed by Sem tests.
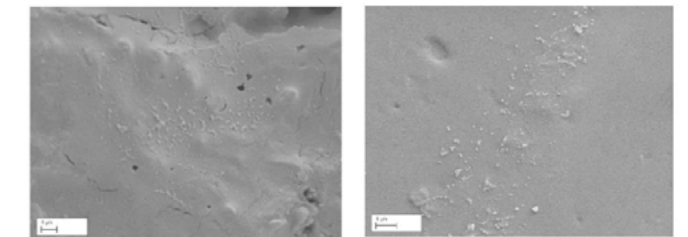
High power ultrasonic waves applied during the manufacturing of composite laminates involving the use of nanoparticles improve the homogenization of this material, and help preventing nanoagglomerations.

V.   FUTURE PLAN/DIRECTION

- Manufacturing of full testing matrix

- Destructive and non-destructive evaluation of - manufactured samples

- Numerical model refinement

- Parametric study, optimisation, and iterative improvements

VI. ACKNOWLEDGEMENT

References

[1] Qi Gao et al, Effects of ultrasonic vibration treatment on particles distribution of TiB2 particles reinforced aluminium composites, Materials Science & Engineering A (2017).
[2] Ajit D. Kelkar et al, Boron nitride nanoparticle enhanced prepregs: A novel route for manufacturing aerospace structural composite laminate, Materials Chemistry and Physics (2016).

Alessandro Sergi

Alessandro obtained his MSc degree in Mechanical Engineering at the University of Calabria (Italy) in May 2017. He started his PhD with the University of Birmingham in January 2018. His research is focused on powder hot isostatic pressing (P-HIP) of high temperature materials, including nickel-based superalloys, refractory metals and nickel-based metal matrix composites (MMCs).

Powder got isostatic pressing of IN625: influence of atomisation route on microstructure and mechanical properties

R.H.U. Khan[1], M.M. Attallah [2]
[1]TWI, [2]University of Birmingham
2nd Year of PhD

Keywords: IN625, powder atomisation routes, powder characterisation, P-HIP, microstructure, prior particle boundaries, mechanical properties

I. INTRODUCTION

Powder hot isostatic pressing (P-HIP) is an advanced manufacturing process capable of producing near to net-shape complex parts. To achieve powder consolidation, a metallic container, commonly called a canister, is filled with powder and then hot isostatically pressed (HIPed) using a temperature around 0.7 Tm (melting temperature) and a pressure ranging from 100 to 200 MPa [1]. P-HIP has many advantages when compared to conventional manufacturing processes for the production of high value parts. The main one is the reduction in buy-to-fly ratio, with very little secondary machining. If compared to casting, P-HIP material's microstructure is free from elemental segregation, with a fine isotropic grain structure, which ultimately reduces the scatter band in the mechanical properties [1]. On the other hand, the major limitation associated with P-HIP of nickel-based superalloys is how to control and/or eliminate the formation of a continuous network of oxides, carbides and oxycarbides detrimental phases at or around the prior particle boundaries (PPBs). These PPBs act as crack initiation sites, leading to poor ductility, fatigue life and fracture toughness of the P-HIP nickel-based, superalloy material.

The main scope of this study is to gain a comprehensive understanding of the influence of powder atomisation types on the microstructure, such as generation of PPBs and consequently on the mechanical properties of HIPed IN625. To this end, four different powder atomisation production routes have been investigated including argon, nitrogen, plasma and water atomisation (AGA, NGA, PA, WA, respectively). The first part of the work was focused on a detailed analysis of the powder characteristics including chemical analysis, flowability, density (apparent, tap and packing), morphology and particle size distribution. In addition, to have a better understanding of the surface chemistry of the powders, X-ray photoelectron spectroscopy (XPS) analysis was also carried out on all four IN625 powders. During the second part, microstructural differences between the four HIPed IN625 powders were assessed. Finally, mechanical properties of the four HIPed IN625 powders were determined to see any difference in the tensile, Charpy impact data compared to wrought alloy.

II. METHODOLOGY

Powder morphology was assessed using a scanning electron microscopy (SEM). Chemical analysis was performed using inductively coupled plasma optical emission spectroscopy (ICP OES) and LECO systems. Semi-quantitative analysis of the surface chemistry of the powders was performed using X-ray photoelectron spectroscopy (XPS) technique. The particle size distributions (PSDs) of all four powders were calculated by laser diffraction, using Malvern Mastersizer 3000. The packing density was determined using Copley JV 2000.

Four cylindrical canisters (Ø50mm x 185mm) with 2mm wall thickness were fabricated, helium leak checked, filled, de-gassed, crimped and HIPed (1160°C/120MPa/4h) using the EPSI HIP system. After HIPing, four samples were extracted using the electrical discharge machine (EDM) cutting method. The microstructure of the samples was characterised using SEM, energy-dispersive X-ray spectroscopy (EDX) and electron backscattering diffraction analysis (EBSD). Furthermore, three samples from each HIPed canister were extracted for tensile and Charpy impact tests performed according to ASTM E8/E8M-16a and ASTM E23-18 respectively.

III. RESULTS

1. Powder Characterisation - One of the key results outlined in the chemical analysis is the difference in oxygen levels between the four different atomisation routes. In particular, chemical analysis revealed that WA powders showed an oxygen level of 7100ppm, which is far above the requirements. The oxygen level of NGA powders is lower but still above the required range, while, PA and AGA have the lowest levels of oxygen within the standard requirements. This is further confirmed by XPS depth profiles (Figure 1), which show a consistent difference of oxygen concentration on the surface of the four powders.
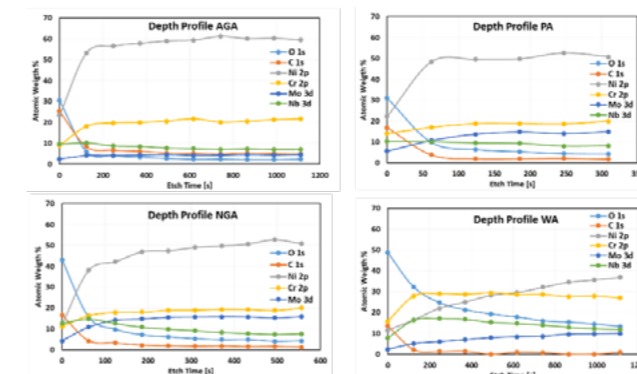

Figure 1. XPS depth profiles of four IN625 powders

2. Microstructure and Mechanical Properties - Figure 2 shows fully dense HIPed microstructure of all four IN625 powders. NGA and especially WA HIPed powders' microstructure dominated with a strong network of PPBs, which can be directly linked to the amount of oxygen present in these powders.
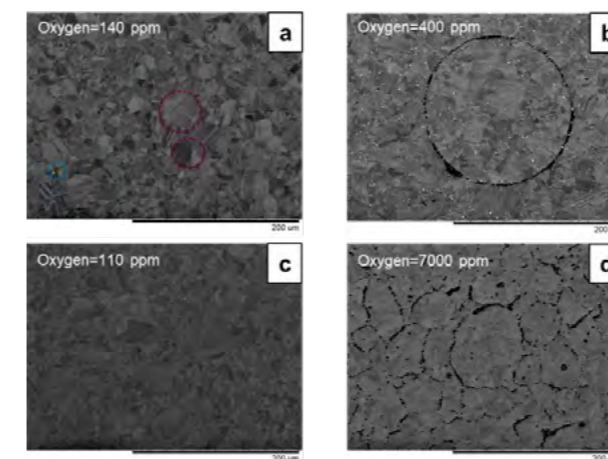

Figure 2. SEM of as-HIPed microstructure of IN625: (a) AGA; (b) NGA; (c) PA; (d) WA

The mechanical properties of the four HIPed powders is reported in Table 1. Tensile properties of NGA, AGA and PA are higher than the minimum specification for wrought IN625, while WA has lower levels of strength and ductility. On the other hand, only HIPed PA powder has shown Charpy absorbed energy (J) similar to wrought IN625.

Table 1. Room temperature mechanical properties of as-HIPed IN625 vs wrought IN625

	0.2% YS [MPa]	UTS [MPa]	El [%]	Absorbed energy [J]
Wrought [2]	414	827	30	66
AGA	521 ±1.2	918 ±13.0	29.7 ±5.6	53 ±0.5
NGA	467 ±4.6	948 ±4.6	30.4 ±2.6	34 ±0.6
PA	462 ±2.0	908 ±2.3	41.3 ±1.3	64 ±0.5
WA	419 ±1.9	517 ±6.2	4.5 ±0.4	4.0 ± 0.0

IV. CONCLUSIONS

Powder atomisation production method plays a crucial role in the microstructure and mechanical properties of HIPed IN625. In particular, XPS analysis outlined the presence of an outer oxide layer which is responsible for the formation of PPBs. The mechanical properties of HIPed IN625 are highly influenced by the microstructural features such as PPBs. In fact, PA and AGA, with the lowest amount of PPBs, showed the best mechanical properties. HIPed PA powder showed mechanical properties similar to wrought IN625.

V. FUTURE WORK PLAN

Future work will focus on understanding the influence of heat treatment on the microstructure and mechanical properties of HIPed IN625 material. Furthermore, high temperature tensile tests will be performed on as-HIPed, HIPed and heat treated IN625.

VI. ACKNOWLEDGEMENTS

REFERENCES
[1] Atkinson, H.V. and S. Davies, Fundamental aspects of hot isostatic pressing: An overview. Metallurgical and Materials Transactions A, 2000. 31(12): p.2981-3000.
[2] www.specialmetals.com Inconel alloy 625. Special Metals Corporation, 2013. 1-18.

Shuang Yan
Shuang is a PhD student jointly funded by TWI NSIRC and the University of Nottingham. She is a member of the Numerical Modelling & Optimisation (NMO) group at TWI and the Composites group at the University of Nottingham. Before joining TWI she obtained her Master's degree in Earthquake Engineering from University College London. Before then, she graduated from the University of Nottingham with first class in Civil Engineering. Her research focus on the simulation of composites curing and the development of deep learning based surrogate model.

Multi-phase multi-physics predictive modelling in composites forming

Shuang Yan[12], Savvas Triantafyllou[3], Philippe Bastid[1], Dimitrios Chronopoulos[2] Tyler London[1] [1]TWI, [2]University of Nottingham, [3]National Technical University of Athens
2nd Year of PhD

Keywords: composites, void formation, pore-pressure cohesive zone, curing simulation

I. INTRODUCTION

In the the aerospace industry, high-fidelity fibre reinforced composites structures are typically manufactured using prepregs. For components with irregular geometric features, such as curved thick sections, air can be easily entrapped during the lay-up procedure. These air pockets or voids are defects where damage initiates eventually leading to delaminations and hence compromising the expected performance of the final product. Despite the significant amount of research porosity is not yet fully understood due to the inherent uncertainties stemming from the manufacturing process itself.

II. DESIGN/METHODOLOGY/APPROACH

This work presents a multi-phase, multi-physics (MP^2) modelling framework for composites forming in the presence of manufacturing defects.

This MP^2 framework aims to simulate the formation of entrapped air pockets during prepregs lay-up and the evolution of residual stresses through the autoclave cure cycle. In addition, structural performance is evaluated through fatigue analysis, capturing the crack initiation and propagation. Air pockets entrapped at ply interfaces are explicitly modelled using a pore-pressure cohesive zone approach. This method has been widely used to simulate hydraulic fracture, while first implemented in predicting voids formation by Seon et al[1]. The curing process integrates the air-solid interaction. This leads to a fully coupled thermal-chemical-mechanical problem that is solved using Abaqus coupled pore fluid diffusion and stress analysis.

III. FINDINGS/RESULTS

Results indicate that the presence of voids alters the heat transfer path from the exterior to the interior, causing significant variations in the degree of curing, especially in thick sections. Voids also result in uncertainties in cure shrinkage and thermal expansion/contraction, leading to non-uniform residual stresses and distortion. The fatigue analysis also shows the crack initiation from the edge of the air pockets, bringing structural failure forward.

IV. DISCUSSION/CONCLUSIONS

This modelling framework includes the simulation of the composites life cycle from the lay-up preparation to the performance evaluation, based on the necessary justifications on porosity distribution, dominant mechanisms during various stages of the cure cycle, and fracture/degradation mode etc. While some mechanisms are not considered in this framework, such as debulking, the purpose of this work is to illustrate the multi-phase, multi-physics modelling approach in Abaqus. This work quantitatively assesses the significance of voids in altering the curing process and the resulting effect on structural integrity

V. FUTURE PLAN/DIRECTION

Instead of executing time-consuming FE model in iterative design phase, a deep-learning based surrogate model will be developed to provide rapid, yet accurate predictions, for any design variations in geometrical features or processing characteristics.

ACKNOWLEDGEMENTS

REFERENCES

[1] Seon, G., Nikishkov, Y., Makeev, A., & Ferguson, L. (2020). Towards a digital twin for mitigating void formation during debulking of autoclave composite parts. Engineering Fracture Mechanics, 225, 106792.

The fundamental research conducted by PhD students at NSIRC covers a range of technologies and industries, including aerospace, oil and gas, renewable energy and automotive to name a few.
Photo: TWI Ltd

TWI
Innovation Network

FACILITATOR AND HUB FOR TECHNOLOGY DEVELOPMENT AND INNOVATION

INNOVATION ACCELERATION STRATEGIC PLANS

TECHNOLOGY FOCUS

- Foresight review
- Product innovation
- Trending subjects
- CPD courses
- Technology development
- Marketplace strategies

ROADMAPPING

- Technology mapping
- Ideas generation
- Concept development
- Idustrial targets
- Trends analysis
- Roadmap canvas
- SWOT analysis
- Future development focus
- Value chain analysis
- Key Performance Indicators (KPIs)

UNLOCKING OPPORTUNITIES

- Key partner matching
- TWI Innovation Network (TWIIN):
  - Innovation Centres
  - Technology Acceleration Programmes (TAPs)
  - Private Technology Innovation Partnerships (PTIPs)
  - Access to TWI Industrial Members and SMEs
- Dissemination and marketing
- Events management
- Innovation consultancy

FUNDING SUPPORT

- Technology innovation management
- Proposal management and delivery
- Consortium management
- Ideas development
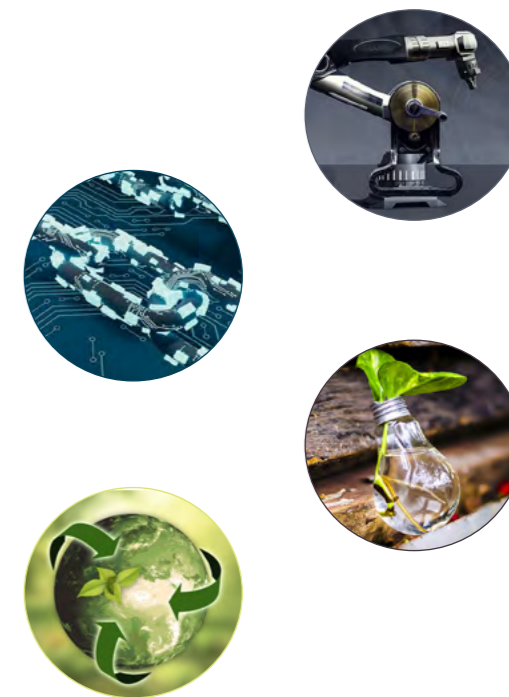- Investment and financing

#COLLABORATEANDINNOVATE